

University of Memphis

University of Memphis Digital Commons

---

Electronic Theses and Dissertations

---

1-1-2019

**MODIFIED ELECTROSPUN CHITOSAN GUIDED BONE  
REGENERATION MEMBRANES FOR STIMULATING  
OSTEOGENESIS AND ANGIOGENESIS**

Vishnu Priya Murali

Follow this and additional works at: <https://digitalcommons.memphis.edu/etd>

---

**Recommended Citation**

Murali, Vishnu Priya, "MODIFIED ELECTROSPUN CHITOSAN GUIDED BONE REGENERATION MEMBRANES FOR STIMULATING OSTEOGENESIS AND ANGIOGENESIS" (2019). *Electronic Theses and Dissertations*. 2936.

<https://digitalcommons.memphis.edu/etd/2936>

This Dissertation is brought to you for free and open access by University of Memphis Digital Commons. It has been accepted for inclusion in Electronic Theses and Dissertations by an authorized administrator of University of Memphis Digital Commons. For more information, please contact [khgerty@memphis.edu](mailto:khgerty@memphis.edu).

MODIFIED ELECTROSPUN CHITOSAN GUIDED BONE REGENERATION  
MEMBRANES FOR STIMULATING OSTEOGENESIS AND ANGIOGENESIS

by

Vishnu Priya Murali

A Dissertation

Submitted in Partial Fulfillment of the

Requirements for the Degree of

Doctor of Philosophy

Major: Biomedical Engineering

The University of Memphis

December 2019

Copyright © 2019 Vishnu Priya Murali

All rights reserved

## **DEDICATIONS**

I want to dedicate this dissertation to my mother and father, without whom I would not have had this opportunity to pursue my dream. They have always been there for me and have supported me in every decision that I have made. Words can never express how much they mean to me. Thank you, Mom and Dad for everything!

## ACKNOWLEDGEMENTS

First and foremost, I want to extend my sincerest gratitude to my advisor, Dr. Joel D. Bumgardner, who has given me this opportunity to pursue doctoral degree and supported me throughout my dissertation with his knowledge whilst allowing me the room to work in my own way. I also owe my deepest gratitude to my research committee. Their input and expertise have been extremely helpful in my pursuit of this doctoral degree. The guidance they have shown is invaluable as I move forward with my future endeavors.

I would like to thank Dr. Yongmei Wang and Caleb Gallops from the department of chemistry, UM, for their valuable inputs on molecular modeling, which was a totally new and different field for me. My sincere thanks to Dr. Buddington, Donny Ray, Dr. Najib Ghadri, Dr. Jim Christian and his residents for their help with the animal studies, which was a crucial part of my dissertation. I would like to thank Dr. David Brand for providing me the access to the Micro-CT facility for analyzing my samples and Dr. Anastasios Karydis for his valuable inputs about the analysis. I would like to extend my warmest gratitude to Dr. Jayakumar Rangasamy and A. Siva Shanmugam, from Amrita University, India, for getting me started on this research path, mentoring me during my master's and playing a crucial part in completion of this dissertation as well.

I would like to thank my lab mates for their support and guidance throughout my research. Their inputs, advice and help in conducting the experiments were timely and very useful towards the completion of my work. Last but not the least, my heartfelt thanks to my loving sister Dr. Lakshmi Priya Murali and my best friends Priyadarshan Sundararaju, Vivardhini Veerakumar and Supraja Srihari for their endless love, support and motivation that kept me going through my dissertation. Thank you for being there with me through my ups and downs.

## **PREFACE**

The purpose of researching a guided bone regeneration (GBR) membrane was to try and overcome the limitations of currently used GBR membranes and improve their bioactivity to enable faster bone healing. With the rise in the number of implant surgeries being performed every year, there is an increasing need to develop effective membranes in order to heal grafted bone faster to reduce any undue complications due to graft failure.

### **Manuscripts:**

#### **Chapter 2: Modified Electrospun Chitosan Membranes for Controlled Release of a Potential Osteogenic Agent**

Planned submission to: Journal of Controlled Release (November 2019)

#### **Chapter 3: Simvastatin Loaded Electrospun Chitosan Guided Bone Regeneration Membranes to Stimulate Osteogenesis**

Planned submission to: Journal of Dental Research (December 2019)

#### **Chapter 4: Evaluating Angiogenic and Osteogenic Potential of Magnesium Incorporated Chitosan Membranes for Promoting Bone Growth: Preliminary Study**

Looking at potential IP options

## ABSTRACT

Guided bone regeneration (GBR) membranes are commonly used to maximize bone healing/regeneration by protecting bone grafted sites from invasion by soft tissues. Electrospun chitosan membranes modified by short chain fatty acids (Acetic anhydride (AA), butyric anhydride (BA) and hexanoic anhydride (HA)) or with tBOC (tert-Butyloxycarbonyl group) have many characteristics including retention of nanofiber structure, occlusive to soft tissues and osteoconductive properties *in vivo* that are important for GBR applications. The high surface area of the nanofiber structure of the membranes provides opportunity for the local delivery of osteogenic or angiogenic agents for enhancing their healing and bone regeneration properties. The objective of this research was to fabricate modified electrospun chitosan membranes capable of controlling the release of an osteogenic (Simvastatin, SMV) and angiogenic (magnesium) agent and evaluate their bioactivity for GBR applications in a series of *in vitro* and *in vivo* experiments. Electrospun chitosan membranes with different modifications were fabricated that enabled the controlled release of loaded/incorporated agents. SMV was released faster by AA and tBOC modified membranes than BA and HA modified membranes. SMV loaded membranes prevented soft tissue infiltration into the defect site and promoted better bone healing than non-loaded membranes in a rat calvarial defect model. A slow release of high SMV dose showed better bone healing than fast release of high or low dose. Membranes incorporated with magnesium were capable of stimulating angiogenesis *in vitro*. The AA modified membranes released more magnesium and thereby showed better angiogenesis than HA modified membranes. Osteogenic and angiogenic potential of our drug loaded chitosan membranes was successfully demonstrated. Since angiogenesis plays an important role in the bone healing process, future studies with dual

loading of SMV and magnesium might prove useful in enhancing the ability of these membranes to stimulate better/faster bone regeneration.



## TABLE OF CONTENTS

<b>LIST OF TABLES .....</b>	<b>xi</b>
<b>LIST OF FIGURES .....</b>	<b>xii</b>
<b>Chapter 1: Introduction .....</b>	<b>1</b>
<b>Chapter 2: Modified Electrospun Chitosan Membranes for Controlled Release of a Potential Osteogenic Agent .....</b>	<b>14</b>
2.1. Introduction .....	14
2.2. Materials & Methods.....	16
2.2.1. Materials .....	16
2.2.2. Electrospinning.....	17
2.2.3. Post-spinning treatment .....	17
2.2.4. SEM.....	18
2.2.5. ATR-FTIR .....	18
2.2.6. Water contact angle measurement.....	19
2.2.7. Elemental analysis .....	19
2.2.8. SMV loading & release study.....	20
2.2.9. Computation of Hansen solubility and Flory-Huggins parameter ( $\chi_{1,2}$ ) of SMV with chitosan and differently modified chitosan .....	21
2.2.10. Cell culture .....	22
2.2.11. Cell viability .....	23
2.2.12. Cell mineralization studies .....	23
2.2.13. Statistical analysis.....	24
2.3 Results .....	25
2.3.1. SEM.....	25
2.3.2. ATR-FTIR .....	25
2.3.3. Water contact angle measurements .....	26
2.3.4. Elemental analysis .....	27
2.3.5. SMV release study.....	28
2.3.6. Determination of solubility and Flory-Huggins parameter ( $\chi_{1,2}$ ) of SMV with chitosan and differently modified chitosan.....	30
2.3.7. Cytotoxicity evaluation of SMV.....	33
2.3.8. ALP activity and mineralization of W-20-17 cells in the presence of SMV.....	34

2.4. Discussion .....	36
2.5. Conclusion.....	41
References .....	42
<b>Chapter 3: Simvastatin Loaded Electrospun Chitosan Guided Bone Regeneration Membranes to Stimulate Osteogenesis.....</b>	<b>50</b>
3.1. Introduction .....	50
3.2. Materials & Methods.....	52
3.2.1. Materials .....	52
3.2.2. Electrospinning.....	52
3.2.3. Post-spinning treatment .....	53
3.2.4. SMV loading & release study.....	53
3.2.5. Cell culture .....	54
3.2.6. Cell viability assay to monitor membrane toxicity.....	55
3.2.7. Cell responses to SMV loaded chitosan membranes.....	55
3.2.8. Experimental animal model.....	57
3.2.9. Tissue processing, micro-CT and histologic evaluation.....	59
3.2.10. Statistical analysis.....	60
3.3. Results .....	61
3.3.1. SMV release study.....	61
3.3.2. Cell viability assay.....	61
3.3.3. In vitro osteogenic evaluation of SMV loaded membranes .....	62
3.3.4. Membrane endotoxin levels, animal surgery and clinical observations.....	65
3.3.5. Histological evaluation of membrane degradation and biocompatibility.....	67
3.3.6. Micro-CT analysis for new bone formation .....	71
3.4. Discussion .....	74
3.5. Conclusion.....	81
References .....	83
<b>Chapter 4: Evaluating Angiogenic And Osteogenic Potential of Magnesium Incorporated Chitosan Membranes for Promoting Bone Growth: Preliminary Study .....</b>	<b>89</b>
4.1. Introduction .....	89
4.2. Materials & Methods.....	92
4.2.1. Materials .....	92
4.2.2. Synthesizing MgP-NP .....	92

4.2.3. Fabricating Mg incorporated chitosan membranes .....	93
4.2.4. Characterization of MgP-NP and membranes .....	95
4.2.5. In vitro Mg release profile .....	95
4.2.6. Endothelial cell cultures .....	95
4.2.7. Bone cell cultures .....	96
4.2.8. Statistical analysis.....	97
4.3. Results .....	97
4.3.1. Characterization of MgP-NP and Mg incorporated chitosan membranes .....	97
4.3.2. Mg release from membranes .....	99
4.3.3. Cell viability and tube formation assay using HUVECs .....	100
4.3.4. Cytocompatibility and osteogenic potential of membranes .....	102
4.4. Discussion .....	104
4.5. Conclusion.....	109
References .....	110
<b>Chapter 5: Conclusions .....</b>	<b>116</b>
<b>Chapter 6: Future Work .....</b>	<b>121</b>
<b>BIBLIOGRAPHY .....</b>	<b>122</b>
<b>APPENDIX 1 .....</b>	<b>137</b>
<b>APPENDIX 2.....</b>	<b>140</b>
<b>Aporoval Form : University of Memphis IACUC (rat studies)</b>	

**LIST OF TABLES**

**Table 2-1:** Water contact angle measurement of differently modified membranes. Each value represents mean  $\pm$  standard deviation (n=4).....27

**Table 2-2:** Elemental analysis of original chitosan, as-spun chitosan and modified chitosan.....28

**Table 2-3:** Percentage cumulative release of SMV from thick membranes after 28 and 91 days of elution..... 30

**Table 2-4:** Estimated Hansen Solubility Parameters for SMV, hydrolyzed SMV and chitosan with different modifications.....31

**Table 2-5:** Hansen solubility differences and polymer-drug interaction parameters at 310K.....32

**Table 3-1:** The 95% confidence intervals of inflammatory response scores of AA and HA membranes with and without SMV in 5mm rat calvarial defect model. Each value represents the confidence interval and (mean).....71

**Table 3-2:** Micro-CT results for bone healing with membranes in 5 mm rat calvarial defects at 4 and 8 weeks. Each value represents mean  $\pm$  standard deviation of % new bone formed in the defect area (new bone volume/total volume). \* represents significantly different from corresponding blank; **a** represents significantly different from week 4. (data within parenthesis shows the mean %bone fill of HA50 membranes at week 8 if one HA50 membrane value that was less than (median -1.5IQR), is neglected from the analysis).....73

**Table 4-1:** Composition of 1L test SBF containing 5X more Mg ions.....93

**Table 4-2:** EDS results showing the weight percent of magnesium and phosphorous in the particles and membranes. Each value represents mean  $\pm$  std dev (n=4).....97

**Table 4-3:** EDS results of membranes after 5 days of elution showing weight percent of magnesium left in the membranes.....99

## LIST OF FIGURES

- Figure 2-1:** Images show micrographs of (A) as-spun membrane (B) AA-treated membrane (C) BA-treated membrane (D) HA-treated membrane and (E) TEA-tBOC-treated membrane.....25
- Figure 2-2:** ATR spectra of chitosan powder, as-spun chitosan, showing the TFA peaks and modified chitosan showing the disappearance of TFA peaks and addition of methyl groups.....26
- Figure 2-3:** Graphs show cumulative release over time for thick membranes treated with either fatty acids or tBOC and loaded with (a) 500 $\mu$ g, (b) 250 $\mu$ g, (c) 100 $\mu$ g and (d) 50 $\mu$ g. The AA and tBOC membranes released higher amounts of drug than BA and HA treated membrane. Each value represents the mean  $\pm$  SD (n=6).....29
- Figure 2-4:** Schematic of unmodified and modified chitosan after tBOC and fatty acid treatments. The degree of substitution was assumed to be 1 for all the modifications. The tBOC groups attach to amine group of the polymer and the fatty acids react with hydroxyl group.....31
- Figure 2-5:** Flory-Huggins interaction parameter ( $\chi_{1,2}$ ) of SMV and hydrolyzed SMV with chitosan and differently modified chitosan. Hydrolyzed SMV had more interaction with the polymer than the unhydrolyzed lactone form. The drug was more soluble in the BA and HA modified chitosan than the AA and tBOC modified polymer.....32
- Figure 2-6:** Graph shows cell viability expressed as a percentage compared to 0ng/ml SMV controls for increasing doses of SMV. Each value represents the mean  $\pm$  SD (n=4).....33
- Figure 2-7:** The effect of SMV on induction of alkaline phosphatase (ALP) activity in W-20-17 cells in regular media (a) and BMP-2 media (b). Each value represents the mean  $\pm$  SD (n=4). \* indicates significant difference between the experimental group and the TCP (tissue culture plastic) group for that time point (p<0.05).....35
- Figure 2-8:** Calcium assay to determine the amount of calcium deposited by the cells in the presence of different concentrations of SMV in regular media (a) and BMP-2 media (b). Each value represents the mean  $\pm$  SD (n=4). \* indicates significant difference between the experimental group and the control group for that time point (p<0.05).....36
- Figure 3-1:** Surgical procedure for implanting chitosan membranes on rat calvaria. (a) surgical site was shaved and cleaned; (b) a midline incision in the skin over the cranium was made; (c) underlying soft tissue and periosteum were incised and reflected to expose the calvaria; (d & e) two 5mm defects were made diagonally on either side of the mid suture; (f) one drug loaded and one non-drug loaded membrane was placed on top of each defect and secured in place using a suture; (g) the periosteum and skin were sutured up and the defects left to heal for 4 or 8 weeks..58
- Figure 3-2:** *In vitro* release profiles of SMV from AA treated chitosan membranes over a 4 week period. The cumulative release (a) and daily release (b) amounts of SMV were determined using a HPLC method at 236nm. Initial amount loaded in the membranes was 10 $\mu$ g. Each value represents the mean  $\pm$  standard deviation (n=4).....61
- Figure 3-3:** Cell viability of W-20-17 cells grown in the presence of different membranes and expressed as % viability as compared to cells grown on tissue culture plastic. Each value represents the mean  $\pm$  SD (n= 4 per each group). \* denotes significant difference among groups at a given

time point ( $p < 0.05$ ). The horizontal line represents 70% cell viability, which is the minimum viability required to be supported by a device to be cytocompatible, according to ISO standard...62

**Figure 3-4:** ALP activity by W-20-17 cells in regular medium (a) and 25ng/ml BMP-2 medium (b). AA0, AA10, HA0 and HA50 membranes were evaluated for their osteogenic potential and compared with controls. Each value represents the mean  $\pm$  SD (n= 4 per each group) \* represents significant difference between membrane group and control.  $p < 0.05$  was considered to be statistically significant.....63

**Figure 3-5:** OCN expression by W-20-17 cells in the presence of AA and HA loaded and non-membranes grown in regular or BMP-2 medium. Each value represents the mean  $\pm$  SD (n= 4 per each group). \$ represents significant difference between regular and BMP-2 media groups.....64

**Figure 3-6:** Calcium assay to quantify the amount of calcium deposited on W-20-17 cells in regular osteogenic media (a) and 25ng/ml BMP-2 supplemented osteogenic media (b). AA0, AA10, HA0 and HA50 membranes were evaluated for their osteogenic potential and compared with controls. Each value represents the mean  $\pm$  SD (n= 4 per each group). \*represents significant difference between membrane group and control; \$ represents significant difference between day 21 vs day 14 for corresponding groups.  $p < 0.05$  was considered to be statistically significant.....65

**Figure 3-7:** Representative Alizarin red S staining of the well plates after 21 days of mineralization study. All the BMP-2 groups stained darker than the regular media groups.....65

**Figure 3-8:** Representative image of a 4 week defect covered with AA membrane. New bone appeared to grow along the defect edges. Early degradation of AA membranes caused soft tissue infiltration at the defect site. Insets show (a) membrane infiltrated with monocyte and fibroblasts and (b) granulation tissue formation at the defect site. M indicates the membrane region; NB indicates new bone formed; DE indicates defect edge.....67

**Figure 3-9:** Representative image of a 4 week defect covered with HA membrane showing bone bridging and minimum soft tissue infiltration at the defect site. Insets show (a) new bone formed across the defect (b) PMNs surrounding the membrane as part of the foreign body response. M indicates the membrane region; NB indicates new bone formed; DE indicates defect edge.....68

**Figure 3-10:** Representative image of an 8 week defect covered with AA membrane showing new bone formation along the edges and dense connective tissue at the defect site. Inset shows complete resorption of the membrane and presence of connective tissue at the membrane site. M indicates the membrane region; NB indicates new bone formed; DE indicates defect edge.....69

**Figure 3-11:** Representative image of an 8 week defect covered with HA50 membrane showing bone bridging across the defect site. Insets show (a) minimum inflammatory response to HA membranes and (b) monocytic infiltration into the membranes and new bone forming along the membranes. M indicates the membrane; NM indicates new formed; DE indicates defect edges... 70

**Figure 3-12:** Representative micro-CT images of 5mm rat calvarial defects after 4 and 8 weeks of membrane implantation.....74

**Figure 4-1:** Representative SEM images of particles (A) showing uniform spherical morphology; AA cospun and HA cospun (B& C) showing nanofibrous structure and AA-SBF and HA-SBF (D & E) showing the salt deposits on the membrane surface.....97

**Figure 4-2:** Release of Mg from (A) Cospun membranes and (B) SBF treated membranes. Low levels of magnesium were detected in the cospun membranes. AA-SBF membranes released much higher Mg than HA-SBF membranes on day1. Each value represents mean  $\pm$  std dev (n=4).....98

**Figure 4-3:** Cell viability assay with MgP-NPs (a) and Mg membranes (b) showed no cytotoxicity to the cells. Each value represents mean  $\pm$  standard deviation with n=4.....99

**Figure 4-4:** Quantifying the number of meshes formed by HUVECs in the presence of different MgP-NP concentrations (A). Each value represents mean  $\pm$  standard deviation with n= 4. Representative images of *in vitro* tube formation by different MgP-NP concentrations (B). Increased particle concentration demonstrated increased angiogenic potential. \* indicates significantly different than cells (p<0.05).....100

**Figure 4-5:** Quantifying the number of meshes in each membrane groups (A). Each value represents mean  $\pm$  standard deviation with n= 4. Representative images of *in vitro* tube formation by different membranes (A). Mg incorporated AA membranes showed more angiogenic potential than HA membranes. \* indicates significantly different than cells (p<0.05).....101

**Figure 4-6:** Cytocompatibility of Mg loaded membranes with W-20-17 cells in indirect culture. None of the groups showed any toxic effects towards the cells. Each value represents mean  $\pm$  std dev (n=4). \* indicates significantly different from control at the given time point.....102

**Figure 4-7:** ALP activity of W-20-17 cells in the presence of conditioned media from different membrane groups. ALP activity of membrane groups was not significantly different from the control group. Each value represents mean  $\pm$  standard deviation with n = 4. \* indicates significantly different from control at the given time point.....103

**Figure A2:** SEM images of HA (a) and AA (b) membranes loaded with 50 $\mu$ g SMV.....140

## **Chapter 1**

### **Introduction**

Every year over five million dental implants are placed in the United States, out of which more than half require bone-grafting procedures (Gaviria, Salcido, Guda, & Ong, 2014). This number is expected to double in the near future, not only in the US but worldwide. Main causes for this increase are aging population and success of implant therapies (Gaviria et al., 2014). Bone grafting is generally performed in patients with bone loss due to cranio-maxillofacial injuries from assaults, motor vehicle accidents, domestic violence, periodontal diseases and/or dental implant procedures. 70% of the facial injuries are caused by assaults and at least 10% of the fractured facial bones result due to domestic violence (Thaller & McDonald, 2004). In the Iraq and Afghanistan conflicts, close to 30% of the injuries affected the craniomaxillofacial region, out of which 40% were severe open mandibular fractures requiring extensive grafting (Lew, Walker, Wenke, Blackbourne, & Hale, 2010; Zachar et al., 2013). Such injuries often result in complications of masticatory function, speech and altered aesthetics that affect health and ability to function in society. Current reconstructive techniques for these injuries and diseases employ auto-, allo- or synthetic bone grafts depending on patient condition, availability and clinician preference (Finkemeier, 2002; Mauffrey, Barlow, & Smith, 2015). Autografts, the gold standard, have the advantage of being non-immunogenic and are the most widely used type of bone graft. They are however limited by donor site morbidity and their availability, especially in defects that are larger than 4cm (De Long Jr et al., 2007; Finkemeier, 2002). Allografts have less osteogenic potential as compared to autografts and involve the risk of immune rejection and infection transmission (De Long Jr et al., 2007; Finkemeier, 2002). Other graft material like bone cement fillers, ceramics, synthetic bone grafts, etc. are frequently susceptible to failure due to



high incidence of delayed or non-union of the defect site (De Long Jr et al., 2007; Finkemeier, 2002; Mauffrey et al., 2015).

A major obstacle to efficient bone grafting procedures is the invasion of epithelial/fibrous tissues into graft sites, which grow faster than the healing bone (Taba Jr, Jin, Sugai, & Giannobile, 2005). This results in inadequate bone tissue regeneration and requires additional interventions to overcome it. Guided bone regeneration (GBR) membranes are commonly used to augment healing by covering and protecting bone grafted spaces during the bone regeneration process and preventing soft tissue migration into the grafted site (Taba Jr et al., 2005). Currently a wide range of non-resorbable and resorbable GBR membranes are used to prevent soft tissue infiltration and promote osseous tissue formation. Non-resorbable membranes commonly used are made of polytetrafluoroethylene (PTFE). Three types of PTFE membranes commercially available are expanded PTFE (e-PTFE), high density PTFE (d-PTFE) and titanium-reinforced e-PTFE (Ti-e-PTFE) (Gentile, Chiono, Tonda-Turo, Ferreira, & Ciardelli, 2011). e-PTFE membranes are reported to be effective in clinical studies, confirming their biocompatibility and ability to promote significant bone regeneration (S. Zhao, Pinholt, Madsen, & Donath, 2000; Zwahlen et al., 2009). These membranes however require second surgery for removal and their stiffness may cause soft tissue dehiscence exposing the membranes to bacterial infection (Becker, Becker, Handelsman, Ochsenein, & Albrektsson, 1991; Buser, Bragger, Lang, & Nyman, 1990; Tempro & Nalbandian, 1993). d-PTFE membranes are reported to prevent bacterial infection due to their less porous structure which inhibits bacterial colonization on the membranes (Bartee, 1995; Bartee & Carr, 1995). Ti-e-PTFE membranes are reported to show superior regenerative capability than conventional e-PTFE membranes and also provide good

mechanical support to overlying soft tissue, preventing them from collapsing into the defect site (Lindfors, Tervonen, Sándor, & Ylikontiola, 2010). Their mechanical stability also allows surgeons to easily place the membrane under flaps with minimal dissection and flap reflection (Jovanovic & Nevins, 1995; Lindfors et al., 2010). However, the second removal surgery disrupts the healing at the graft site in some cases and causes further complications (Aurer & Jorgić-Srdjak, 2005).

Cross-linked and uncross-linked collagen and poly-lactic-co-glycolic acid (PLGA) based membranes are biodegradable and thus do not require second surgeries. Commercially available collagen membranes include Bio-Gide® (Geistlich) and BioMend® (Zimmer). Bio-Gide® membranes are based on xenogenic collagen Type I from porcine skin. They were reported to stimulate osteoblastic differentiation within 14 days of implantation (Taguchi et al., 2005). Their compact structure prevents epithelial cell and soft tissue migration and protects the graft site thus allowing the surrounding bone cells to migrate into the site to heal the defect (Gentile et al., 2011; Taguchi et al., 2005). BioMend® membranes fabricated from bovine Achilles tendon, showed partial effectiveness in clinical studies, with successful regeneration dependent on the site and size of the defect (Maksoud, 2001; Sela, Kohavi, Krausz, Steinberg, & Rosen, 2003). In one such study, the presence of bacterial infection at the graft site led to premature degradation of the membrane causing exposure of the grafted site (Sela et al., 2003). However, in another implant procedure with no infection, using these membranes with the graft material resulted in better bone formation as compared to cases where only the graft material was used (Maksoud, 2001). These collagen membranes also have a perceived risk of disease transmission to humans from animal-derived collagen (Gentile et al., 2011). A number of PLGA based membranes have

been used in the clinics for GBR membrane application with varying degrees of effectiveness (Gentile et al., 2011). These membranes often result in inflammation, foreign body reactions and cytotoxicity because of acidic degradation products (Meinig, 2010; Turri et al., 2016).

Regardless of composition, GBR membranes are reported to suffer as high as 50% rates of complications due to exposure, infection and low bone regeneration (Tal, Kozlovsky, Artzi, Nemcovsky, & Moses, 2008). Thus, there is a need to overcome the limits of current GBR materials and develop membranes that are able to provide effective barrier function and have a synergistic adjunctive effect on stimulating bone regeneration, especially in large bone grafted sites.

Chitosan, a polycationic polysaccharide derived from biopolymer chitin, has a structure similar to hyaluronic acid, an essential component of the extracellular matrix (ECM). It has many advantages over currently used materials for GBR applications, such as, controllable non-toxic degradation properties, ability to stimulate wound healing and osteoconductivity (Khor, 2001; Xu, Lei, Meng, Wang, & Song, 2012). Its ability to dissolve in dilute acids allows it to be easily fabricated into various forms like hydrogels, electrospun membranes, sponges, films, pastes, etc. making it a widely investigated tissue engineering scaffold and a drug delivery vehicle (Ali & Ahmed, 2018; Balagangadharan, Dhivya, & Selvamurugan, 2017; Noel, Courtney, Bumgardner, & Haggard, 2008; J. J. Wang et al., 2011; Xu et al., 2012). Chitosan films, sponges and membranes have been investigated for GBR applications (Kuo, Chang, Chen, & Kuan, 2006; Ma et al., 2016; Park et al., 2006; Park et al., 2000; Yeo et al., 2005). Kuo et al. demonstrated that chitosan films gelled with sodium hydroxide NaOH, and films cross-linked with sodium triphosphate and sodium sulphate, were able to stimulate bone formation in rat calvaria better

than controls (empty defects) (Kuo et al., 2006). The films remained intact and prevented soft tissue infiltration. However, prolonged presence of the construct at the defect site hindered the bone healing process (Kuo et al., 2006). Ma et al. developed chitosan films, which stimulated bone formation similar to a commercially used collagen membrane (BioGide®) but was not effective at limiting soft tissue infiltration (Ma et al., 2016). Chitosan sponges fabricated by Park et al. stimulated bone formation in rat calvaria by 4 weeks but showed early degradation of the scaffold causing fibrous tissue infiltration into the defect site (Park et al., 2006). Chitosan wet-spun non-woven membranes were evaluated in canine one-wall intra-bony mandibular defects (Yeo et al., 2005). They regenerated larger amounts of bone than biodegradable collagen membranes (Biomesh®, SamyangCo.) while having comparable soft tissue attachment and barrier function (Yeo et al., 2005). Although these studies were promising, these chitosan constructs did not offer all of the advantages of nano fabricated membranes.

Porous nanofibrous membranes are fabricated by the process of electrospinning. Electrospinning has gained much attention in the last decade due to its versatility in spinning a wide variety of polymeric fibers (Demir, Yilgor, Yilgor, & Erman, 2002; Duan et al., 2006; Ohkawa, Cha, Kim, Nishida, & Yamamoto, 2004; Yang, Qin, & Wang, 2008). The process uses a high voltage electric field to produce electrically charged jets from polymer solution or melts, which on drying by means of evaporation of the solvent produce nanofibers. The highly charged fibers are field directed towards the oppositely charged collector, to collect the fibers (Subbiah, Bhat, Tock, Parameswaran, & Ramkumar, 2005). The fiber diameter and to some extent, the pore size, can be modulated by changing parameters like the viscosity of the solution, the choice of solvent, the voltage, the distance between the solution and collector plate, the rate at which the

solution flows towards the collector plate, etc. (Beachley & Wen, 2009; Haider, Haider, & Kang, 2018). The process also depends on the ambient temperature and relative humidity (Beachley & Wen, 2009; Haider et al., 2018).

The advantage of electrospun nanofibrous chitosan membranes are that they resemble the native fibrous structure of the ECM which supports cell growth and provide increased surface area for drug delivery (Bhattarai, Edmondson, Veisoh, Matsen, & Zhang, 2005; Z. Chen, Wang, Wei, Mo, & Cui, 2010; Jayakumar, Prabakaran, Nair, & Tamura, 2010). Studies have demonstrated the ability of electrospun chitosan membranes to facilitate new bone formation in critical size bone defects (Bavariya et al., 2014; Norowski Jr et al., 2015; Shin et al., 2005; Yeo et al., 2005). The nanofiber structure with its porosity allows communication between the osseous and epithelial tissue compartments and allows the exchange of nutrients and ions while remaining cell occlusive (Turri et al., 2016). This would prevent the resorption of the underlying bone graft while stimulating bone regeneration. Shin et al. demonstrated that while electrospun chitosan membranes facilitated more new bone formation in critical-sized bone defects than controls (empty defects), they showed significant fragmentation by 8 weeks post implantation (Shin et al., 2005).

A major problem with electrospun chitosan membranes is that they often swell and lose the nanofibrous structure when placed in aqueous environment (Sangsanoh & Supaphol, 2006). Trifluoroacetic acid (TFA) is one of the most commonly used solvents for electrospinning chitosan as it provides the adequate viscosity for the polymer solution to be pulled into

nanofibers. TFA salts formed due to this processing, make the membranes extremely hydrophilic, thereby causing them to swell in an aqueous environment. Neutralization and cross-linking techniques have been used to overcome this. A Commonly employed neutralization technique involves soaking the nanofibrous membranes in solutions of sodium hydroxide, sodium carbonate, or ethanol (Correia et al., 2014; Sangsanoh & Supaphol, 2006; Sencadas, Correia, Areias, et al., 2012; Sencadas, Correia, Ribeiro, et al., 2012). Sangsanoh et al. investigated sodium hydroxide and sodium carbonate neutralization techniques and reported partial success with sodium hydroxide but were able to demonstrate good fiber retention with sodium carbonate treatment (Sangsanoh & Supaphol, 2006). Others have used ethanol and have demonstrated good fiber retention but with decreased fiber diameter (Correia et al., 2014; Sencadas, Correia, Areias, et al., 2012; Sencadas, Correia, Ribeiro, et al., 2012). Cross-linkers like glutaraldehyde, ultra-violet light (UV), genipin, etc., have been investigated to improve the mechanical stability of these membranes (Aini et al., 2012; Austero, Donius, Wegst, & Schauer, 2012; Bavariya et al., 2014; Mi, Tan, Liang, Huang, & Sung, 2001; Norowski Jr et al., 2015; Norowski, Mishra, Adatrow, Haggard, & Bumgardner, 2012; P. A. Norowski et al., 2012; Schiffman & Schauer, 2007; Zhang, Hu, Zhu, & Liu, 2013). After cross-linking with glutaraldehyde, chitosan membranes became insoluble in aqueous solutions but had increased fiber diameter and a decreased Young's modulus (Schiffman & Schauer, 2007). Zhang et al. showed that chitosan membranes irradiated with UV had decreased swelling in aqueous conditions and twice the tensile strength as the pristine chitosan membranes (Zhang et al., 2013). UV cross-linked chitosan membranes also showed good cytocompatibility with mesenchymal stem cells (MSC) (Tsai, Chen, Li, Lai, & Liu, 2012). Natural cross-linker, genipin has also been investigated widely for stabilizing chitosan membranes (Austero et al., 2012; Bavariya et al.,

2014; Mi et al., 2001; P. Norowski et al., 2012; P. A. Norowski et al., 2012). Genipin was successfully cospun with chitosan solution to form nanofibrous membranes (Austero et al., 2012). Addition of genipin stabilized the nanofibrous structure in aqueous solutions without influencing the fiber diameter. A comparative study of genipin cross-linked and glutaraldehyde-cross-linked chitosan membranes showed an improved cytocompatibility, improved ultimate tensile strength, lowered swelling ratio and slower degradation rate of genipin cross-linked membranes (Mi et al., 2001). Bavariya et al. and Norowski et al. demonstrated good cytocompatibility and effective barrier function of genipin cross-linked membranes *in vitro* and *in vivo*, respectively, with superior degradation rates compared to commercial collagen membrane (Bavariya et al., 2014; Norowski Jr et al., 2015). Though these techniques maintained the nanofibrous structure and improved the stability of the membranes to some extent, they were brittle and lacked the handleability desired by clinicians (Bavariya et al., 2014; P. Norowski et al., 2012; Park et al., 2006; Shin et al., 2005). These membranes also lost their mechanical properties and original structure upon prolonged exposure to physiological environment (Shin et al., 2005).

Recently, novel post-spinning treatments for removing these TFA salts and protecting the nanofibrous structure of the membrane has been investigated by Su et al. and Wu et al. (Su et al., 2016; Wu, Su, Tang, & Bumgardner, 2014). One of the techniques involved a Triethylamine (TEA) in acetone wash step followed by blocking chitosan's amino groups by tBOC groups (from di tert butyl dicarbonate) in tetrahydrofuran (THF) solution (Su et al., 2016). The TEA/Acetone step removes the TFA salts from the polymer while in the tBOC-THF step the amino groups are blocked by reaction with tBOC. The tBOC groups increase the hydrophobic

character of the fibers which prevents the fiber from swelling in aqueous environment. This technique stabilized the nanofibrous structure of the membranes for upto 4 weeks in aqueous environment (Su et al., 2016). These membranes showed good biocompatibility with bone cells *in vitro* (Su et al., 2016). They had a higher tensile tear strength than a commercial polylactic acid membrane (GUIDOR®) and supported bone growth *in vivo* similar to a commercial collagen membrane (BioMend® Extend, Zimmer), while preventing soft tissue infiltration into the defect site (Su et al., 2016). Another technique developed by Wu et al. involved grafting fatty acid groups to the hydroxyl groups on the outside of the chitosan fibers to create a hydrophobic wrap to prevent fiber swelling during water rinsing steps to remove the TFA ions (Wu et al., 2017; Wu et al., 2014). Butyrylated chitosan membranes showed decreased swelling in aqueous solution, doubling in suture pull out strength and decreased degradation as compared to non-modified membranes (Wu et al., 2017). *In vitro*, these membranes showed excellent biocompatibility with fibroblasts (Wu et al., 2017; Wu et al., 2014). When tested in a rodent model, they showed significant bone formation and effective barrier function similar to a commercially available collagen membrane (Wu et al., 2017). The nanofibrous structure of the membranes makes them an attractive option in drug delivery applications. The increased surface area of the porous nanostructure is thought to retain the drug within the membranes for longer time, thereby enabling a sustained release of the drug. Previously nanofibrous membranes made of polymers like PLGA, polylactic acid, polyvinyl alcohol, collagen, gelatin, hyaluronic acid, etc. have been used to deliver a wide a range of therapeutics for tissue regeneration, wound healing and antimicrobial treatments (C.-H. Chen, Chen, Shalumon, & Chen, 2015; D. W. Chen et al., 2012; Jo et al., 2015; Lee & Kim, 2016; X. Li, Kanjwal, Lin, & Chronakis, 2013; Park et al., 1997; Thacharodi & Rao, 1996). Though some studies also evaluated chitosan nanofibrous



membranes for drug delivery applications, retention of their nanofibrous structure for the entire duration of drug release was not reported.

While GBR membranes have been made bioactive through the addition of therapeutics such as bone morphogenetic protein-2 (BMP-2) to augment healing of bone grafted sites, dosing and release profiles of BMP-2 are not optimal and have been implicated in adverse reactions such as ectopic bone formation, bone/tooth root resorption and ankylosis (Choi et al., 2002; Seeherman, Wozney, & Li, 2002). These are also associated with high therapeutic costs (Choi et al., 2002; Seeherman et al., 2002). To circumvent these drawbacks, we propose to locally deliver a drug called simvastatin (SMV). This drug belongs to the statin class of pharmaceuticals and has been reported to promote bone growth and healing after local delivery, by antagonizing TNF- $\alpha$  inhibition of BMPs, inhibiting osteoclastic activity and improving angiogenesis, a critical factor in regenerating large bone defects (Sakoda et al., 2006; Takenaka et al., 2003; Yamashita et al., 2008). Early human studies reported a positive association between systemic statin use and reduced risk of hip fracture as well as increased bone density (Funkhouser, Adera, & Adler, 2002; P. S. Wang, Solomon, Mogun, & Avorn, 2000). Osteogenic differentiation of human periodontal ligament stem cells cultured with SMV was enhanced as evidenced by elevated expression of osteogenic markers such as alkaline phosphatase, bone sialoprotein, and BMP-2 (B. j. Zhao & Liu, 2014). Furthermore, SMV was shown to promote osteoblastic differentiation by stimulating vascular endothelial growth factor (VEGF) expression in osteoblasts and reducing osteoclastic activity, both of which lead to improved osteogenesis (Maeda, Kawane, & Horiuchi, 2003). Studies also report the anti-inflammatory and antimicrobial properties of SMV that may

play an important role in cases where infection may interfere with the bone healing process (Jerwood & Cohen, 2007; Sakoda et al., 2006).

In recent years much attention has been focused on local delivery strategies of SMV to allow adequate dosage at the desired site and avoid systemic side effects such as liver toxicity and myositis (Hung & Yeung, 2000; Jody, 1997). Locally delivered SMV is reported to positively influence bone regeneration in the treatment of periodontal diseases, maxillary sinus augmentation and enhance osseointegration around dental implants (Gouda, Helal, Ali, Bakry, & Yassin, 2018; Nyan et al., 2014; A. Pradeep et al., 2012; A. R. Pradeep & Thorat, 2010; Priyanka et al., 2017). Bone regeneration was also higher when SMV was delivered locally in defects of calvaria, mandible and tibial osteotomy animal models (Jiang et al., 2013; Mundy et al., 1999; Nyan et al., 2009; Qi et al., 2013; Stein et al., 2005; Wong & Rabie, 2003; Xue et al., 2019). Qi et al. investigated the effects of SMV locally applied from calcium sulfate (CS) combined with an MSC sheet on fractured tibial healing in rats. At 8 weeks, complete bone union was obtained in the CS/SMV/MSC sheet group and partial bone union was obtained in CS/SMV and CS/MSC groups, whereas no bone formation was seen in groups without SMV (Qi et al., 2013). Wong et al. showed small but significant amount of bone formation in rabbit parietal bone defects that were treated with SMV-loaded collagen sponges, within 14 days post implantation (Wong & Rabie, 2003). Xue et al. demonstrated *in vivo* bone formation stimulated by locally delivering SMV via chitosan nanoparticles in rat calvaria (Xue et al., 2019). In general, these studies report cancellous bone volume and higher bone formation rates when SMV was locally delivered to the defect sites. Though these studies reveal a positive osteogenic potential of locally delivering this

drug to the defect site, the ideal daily release profile and/ or the release kinetics of SMV to stimulate good bone healing is still not clear.

Frequently, grafted defect sites are susceptible to failure due to high incidence of delayed and/or non-union of the defect site (De Long Jr et al., 2007; Mauffrey et al., 2015). This is commonly caused due to lack of vascularization in the grafted implant (Mauffrey et al., 2015). Vascularization is critical in bone healing not only for the transport of oxygen and nutrients to the defect site but also to transport MSCs stem cells to facilitate bone regeneration (Stegen, van Gastel, & Carmeliet, 2015). There has been a close connection between angiogenesis and osteogenesis in the process of bone repair (Carano & Filvaroff, 2003; Stegen et al., 2015). The currently used gold standard for promoting angiogenesis is the use of VEGF, which has disadvantages similar to BMP-2. This includes supraphysiological dosing required for effective response, enhanced tumorigenicity, higher therapeutic costs, etc. To overcome this, magnesium is thought to an effective alternative. Several studies have demonstrated the angiogenic as well as osteogenic potential of magnesium (Laurant & Touyz, 2000; Liu, Yang, Tan, Li, & Zhang, 2014; Maier, Bernardini, Rayssiguier, & Mazur, 2004; Staiger, Pietak, Huadmai, & Dias, 2006; N. Zhao & Zhu, 2015). Magnesium stimulates nitric oxide production in endothelial cells which stimulates their proliferation (Cooke & Losordo, 2002; Maier et al., 2004). VEGF is known to stimulate angiogenesis using a similar mechanism (Cooke & Losordo, 2002). Magnesium stimulates endothelial proliferation and migration, enhances the mitogenic response to angiogenic factors and attenuates bacterial endotoxin-induced inflammatory response in a dose-dependent manner (Maier et al., 2004). Mg doped bioglass showed good angiogenic potential when tested *in vitro* with Human Umbilical Vain Endothelial Cells (HUVEC) (Priya et al.,

2016). Yegappan et al. reported good osteogenic and angiogenic property of carrageenan hydrogels loaded with Mg-based nanoparticles (Yegappan et al., 2019). Mg alloys are also increasingly being used in metallic implants application due to their improved mechanical biological activities (Bondarenko et al., 2014; N. Li & Zheng, 2013).

With the increase in the number of grafting procedures performed every year, there is a rising need for developing more effective GBR strategies. The membranes proposed in this work will have a large impact in augmenting craniomaxillofacial and dental bone regeneration, by locally delivering novel, less expensive pro-osteogenic and pro-angiogenic therapeutics via state of the art electrospun chitosan membranes. Our ability to stimulate osteogenesis along with angiogenesis can be effectively used in treating large segmental defects as well, since these mainly fail due to lack of vascularization.

### **Hypothesis:**

The hypothesis for this study is: electrospun chitosan-based GBR membranes loaded with SMV will prevent soft tissue infiltration into the defect site and promote bone regeneration.

Incorporating magnesium in these membranes is hypothesized to stimulate vascularization, which would improve the bone healing process. The objectives associated with this study are (1) control the release of SMV from chitosan membranes (2) identify optimal dosing and release pattern of SMV from chitosan membranes that would promote osteogenesis *in vitro* and in established rat calvarial defect model and (3) fabricate, characterize and evaluate magnesium incorporated chitosan membranes for angiogenic potential *in vitro*.

## Chapter 2

# Modified Electrospun Chitosan Membranes for Controlled Release of a Potential Osteogenic Agent

### 2.1. Introduction

Chitosan, derived from a natural polymer, chitin, is a linear chain polysaccharide made of N-acetyl glucosamine and glucosamine units. Chitosan has been investigated for a wide range of biomedical applications due to its excellent biocompatibility, controllable degradation and ability to be manufactured into various forms like films, beads, hydrogels, sponges and particles, etc. [1-4]. Chitosan can be electrospun to produce membranes with fiber diameters in the nano-scale range that mimic the nanofibrous structure of the natural extracellular matrix (ECM) [5]. The ability to mimic the natural nanofibrous structure of the ECM is advantageous for supporting growth and proliferation of cells important to tissue engineering/regeneration strategies [5-7]. Another advantage of the nanofibers created by the electrospinning process is the increased surface area for loading and delivering therapeutic agents [8-10]. Because of this combination of degradability and nanofiber structure, electrospun chitosan membranes (ESCM) are investigated for a number of tissue regeneration and drug eluting tissue scaffold applications including dental and orthopedic [1, 2, 7, 11-17].

Trifluoroacetic acid (TFA) is one of the most commonly used solvent for electrospinning chitosan as it provides adequate viscosity for the polymer solution to be pulled into nanofibers [18, 19]. However, TFA forms a salt with the amino groups on the chitosan polymer during the spinning process and must be removed. Two strategies have been developed to remove the salts

without compromising the nanofiber structure or deteriorating the mechanical properties of the ESCM (13,22). One of the techniques involves a Triethylamine (TEA) wash to remove the TFA ions, followed by blocking of chitosan's amino groups on the surface of the fibers with tBOC groups (di tert butyl dicarbonate) to prevent amine protonation that can lead to swelling in aqueous environments [17]. Another technique developed by Wu et al. involves grafting fatty acid groups to the hydroxyl groups on the outside of the chitosan fibers to create a hydrophobic wrap that would prevent fiber swelling during water rinsing steps to remove the TFA ions [20]. The fatty acids can be subsequently removed with alkali as desired to regenerate the native ESCM [20]. The TEA/tBOC and the FA-modified chitosan membranes demonstrated the ability to maintain the nanofibrous structure in aqueous environments as compared to alkali based treatments used to remove TFA salts, while maintaining good mechanical, degradation and cytocompatibility properties [17, 20]. Both types of membranes have shown promise for regenerating bone in guided bone regeneration applications in rodent models [17, 20, 21].

While GBR membranes have been made bioactive through the addition of therapeutics such as bone morphogenetic protein-2 (BMP-2) to augment healing of bone grafted sites, dosing and release profiles of BMP-2 are not optimal and have been implicated in adverse reactions such as ectopic bone formation, bone/tooth root resorption and ankylosis [22, 23]. These are also associated with high therapeutic costs [22, 23]. To circumvent these drawbacks, we propose to locally deliver a drug called simvastatin (SMV). Recently, SMV was reported to possess good osteogenic property [24-29]. This drug belongs to the statin class of pharmaceuticals and is used in clinics for anti-cholesterol treatment. SMV has been reported to promote bone growth and healing after local delivery, by antagonizing TNF- $\alpha$  inhibition of BMPs, decreasing osteoclast

activity and improving angiogenesis [30-33]. Studies also reported a positive association between statin use by elderly patients and reduction in the risk of hip fracture [34, 35]. SMV has shown to induce osteogenic differentiation of bone marrow stromal cells, increasing the alkaline phosphatase (ALP) activity and osteocalcin and osteopontin production [26, 36, 37] in vitro and better bone healing in vivo [38, 39]. SMV is also reported to possess anti-inflammatory and anti-microbial properties that may play a critical role in the tissue regeneration process [31, 40].

This study investigated the potential of adding SMV to tBOC or FA-modified chitosan membranes for the purpose of increasing bioactivity of chitosan GBR membranes for bone regeneration. The modified membranes were characterized for morphology, degree of modification and hydrophobic behavior. This study examined effects of different levels of loading and membrane modifications for controlling release of SMV from the membranes. Molecular modeling was used to evaluate the interaction between the differently modified chitosans and SMV to understand the mechanism of drug release. Different concentrations of SMV were tested on mouse stromal cells to identify effects of dosing on ALP production and in vitro mineralization.

## ***2.2. Materials & Methods***

### ***2.2.1. Materials***

Chitosan with 71% DDA and 311 kDa was purchased from Primex. TFA, dichloromethane (DCM), pyridine, fatty acids, tetrahydrofuran (THF), TEA, Acetone, tBOC were bought from Sigma and Fisher. SMV was purchased from Cayman Chemicals. Reagents

for HPLC were HPLC grade and bought from Fisher. W-20-17 cells were obtained from ATCC and cultured as per ATCC instructions. Reagents for cell culture were bought from Fisher.

### *2.2.2. Electrospinning*

Chitosan membranes were fabricated by electrospinning in an in-house spinning setup, as described previously [2, 11, 17, 20]. Briefly, a 5.5% (w/v) chitosan (71% DDA, MW: 311.7kDa) solution was made in 70% TFA and 30% DCM, loaded into 10 ml syringe with a 20-gauge blunt needle and electrospun at 27 kV using a syringe pump onto an aluminum foil covered plate rotating at ~ 8.4 rpm. To ensure better handle ability, each membrane was made with either 10- or 30-ml solution (three 10ml volumes of chitosan solution spun consecutively) to produce 13cm diameter membranes approximately  $0.3 \pm 0.1$  mm or  $0.7 \pm 0.1$  mm thick, respectively. The electrospinning apparatus was housed inside a ventilated box which was vented to the fume hood. The apparatus was operated at room temperature and at 40 to 60% humidity.

### *2.2.3. Post-spinning treatment*

The ESCMs were treated to remove TFA salts using the TEA/tBOC or FA methods as previously described [17, 20]. Briefly, for the TEA/tBOC treatment, membranes were immersed in 10% (v/v) TEA/acetone solution for 24 hours under mild stirring, washed twice with acetone, and then placed in a tBOC/THF (0.1g/ml) solution for 48hours at 600C<sup>-</sup> under mild stirring. After 48 hours, membranes were washed three times with acetone and then dried between nylon meshes and paper towels [17].

For the FA treatment, as-spun membranes were first punched into small 1cm diameter discs and soaked in a pyridine-fatty acid anhydride (v/v) (50-50) solution at 5mg/ml for 1.5



hours. Next, the membranes were washed by gentle stirring in 1L MQ water ( $18\text{M}\Omega@25^\circ$ , Integral 15, Millipore) for 72 hours to remove the unreacted and excess reagents. The water was changed every 24 hours for 3 days, after which the membranes were freeze-dried. The fatty acids used in this study are acetic (AA), butyric (BA) and hexanoic (HA). These fatty acids were chosen based on a previous study where BA (number of carbons in the fatty acid chain,  $n=4$ ) modified chitosan membranes showed good cell attachment and GBR application [20, 21]. Here, a slightly smaller (AA;  $n=2$ ) and slightly longer (HA;  $n=6$ ) chain fatty acids were evaluated not to significantly affect the biocompatibility of the membranes.

#### 2.2.4. SEM

Membranes were examined under SEM (Nova NANOSEM 650 FEI™) before and after the TEA/tBOC and fatty acid treatments to determine the effects on fiber size and morphology. Three samples of as-spun and treated membranes from three different ESCM were examined at four different regions. Parameters used for the measurement were 5000X magnification, 5kV and a spot size of 3.0.

#### 2.2.5. ATR-FTIR

ATR Spectra were collected to evaluate the extent of TFA salt removal by the treatments and attachment of tBOC and fatty acid groups to the chitosan polymer chain. The spectra were collected using FT-IR spectrometer, Frontier (Perkin-Elmer). Three samples of as-spun and treated membranes were scanned from  $500\text{cm}^{-1}$  to  $4000\text{cm}^{-1}$  for 16 times.

### 2.2.6. Water contact angle measurement

Water contact angles of modified chitosans were determined using a VCA optima measurement machine (AST products, INC, USA). 5 $\mu$ L of water droplets were placed carefully onto the membrane surfaces, and the photographs of the droplets were recorded by a digital camera. The contact angles were calculated by the goniometry software of VCA OptimaXE. For each modification, four different membranes were tested at three different regions.

### 2.2.7. Elemental analysis

Elemental analysis was carried out to evaluate the extent of modification of the membrane by the tBOC or FA molecules based on the carbon to nitrogen ratio (C/N). C/N of the chitosan would change with modification since the modifying groups will add more carbon to the polymer. The analysis was carried out by Atlantic Microlabs, (Norcross, GA, USA) using Perkin-Elmer Model 2400 series II autoanalyzer. The samples were also analyzed to detect any residual amount of TFA salts left after the treatments. Each sample was vacuum dried and analyzed in duplicate.

The actual C/N number ratio of original chitosan used in this study was calculated by the atomic weight % obtained by elemental analysis, using the following equation:

$$\frac{n_o(C)}{n_o(N)} = \frac{C\%/12.011}{N\%/14.0067} = \frac{6.68}{1} \quad (1)$$

The degree of modification (DM), x is defined as the number of tBOC or FA group per chitosan/chitin monomer unit, and calculated using the atomic weight % of modified chitosan obtained from elemental analysis by the following equation:

$$\frac{n_m(C)}{n_m(N)} = \frac{C\%/12.011}{N\%/14.0067} = \frac{6.68+px}{1} \quad (2)$$

Where C% and N% are weight percentage of carbon and nitrogen, and p is the number of carbon atoms in the substituted groups (specifically, p value for tBOC, acetyl, butyryl, and hexanoyl groups is 5, 2, 4, and 6, respectively).

### 2.2.8. SMV loading & release study

SMV release study was performed using 1 cm discs of the TEA/tBOC-, AA-, BA- and HA-modified membranes and each was tested at two different thicknesses; a thin (~0.3mm thick) or thick (~0.7mm) membrane thickness. Four different amounts of SMV- 500, 250, 100, 50µg - were loaded onto the membranes. These amounts were chosen as representative of the wide range of concentrations tested previously in studies which showed significant osteogenic potential [28, 41-43]. SMV at 500 and 250µg, 100 and 50µg were used as representative for high and low dose respectively. Membranes were disinfected by rinsing in 70% ethanol and drying under UV light for one hour. Since SMV is insoluble in aqueous solvents, stock of SMV solution was made in 200 proof ethanol (non-denatured) and loaded onto the membranes passively. The volume of SMV stock added onto the membranes was kept to a minimum to ensure complete absorption by the membranes. Membranes were left to dry for 20 to 30 minutes before placing them in 48-well plates and adding 0.5 ml of PBS. PBS was replaced every day for the first week and then every other day till day 28. The study was continued till day 91, with samples being collected weekly after 28 days. The collected samples were stored at -20°C for further analysis. There were 6 membranes/treatment/thickness/loading amount. An isocratic HPLC method was used to analyze the amount of SMV released from the membranes. SMV was detected at 236 nm

using a UV-VIS detector, a solvent phase of 0.1% TFA: acetone (30:70) and injected at a flow rate of 1ml/min [44]. The amount of sample injected was 10 $\mu$ l and was detected using a Hypersil GOLD column (dim-150 X 4.6mm) with a particle size of 5 $\mu$ m (ThermoScientific™), heated to 30°C. Since SMV is insoluble in aqueous solvents, standards were made in PBS-ethanol (1:1) solutions. To maintain consistency between samples and standards, the samples were also diluted with ethanol that was spiked with SMV. The spike SMV was added to compensate for any drug loss during dilution, which might result in negative values. SMV readily hydrolyzes when in aqueous environment, giving rise to three separate HPLC peaks for SMV hydroxy-acid, lactone form, and dimer form. Area under these three peaks were added and used to calculate the total concentration of SMV in the eluates.

### *2.2.9. Computation of Hansen solubility and Flory-Huggins parameter ( $\chi_{1,2}$ ) of SMV with chitosan and differently modified chitosan*

Molecular modeling was carried out using Hansen Solubility Parameters in Practice (HSPiP) software version 5.1.08 to determine the Hansen Solubility parameters (HSP). These parameters account for dispersion forces ( $\delta_D$ ), dipolar intermolecular forces ( $\delta_P$ ) and hydrogen bonding ( $\delta_H$ ) [45]. The sum of these squared parameters is the squared total solubility parameter  $\delta_T$  (3).

$$\delta_T^2 = \delta_D^2 + \delta_P^2 + \delta_H^2 \quad (3)$$

The solubility parameters for any two chemical species (i.e., drug and polymer) can be used to calculate the Flory-Huggins interaction parameter ( $\chi_{1,2}$ ) according to Equation 4, where

$V_{m,1}$  is the molar volume of the drug,  $R$  is the ideal gas constant and  $T$  is the absolute temperature [45].

$$\chi_{1,2} = \frac{V_{m,1}}{RT}(\delta_{T2} - \delta_{T1})^2 = \frac{V_{m,1}}{RT}\Delta\delta_T^2 \quad (4)$$

For non-polar compounds like chitosan, Hansen proposed using  $A_{1,2}$  (5) in place of  $\Delta\delta_T^2$ , which was generally found to provide more accurate predictions of  $\chi_{1,2}$  for a wider range of systems [45]. The value  $A_{1,2}$  is the sum of squared differences of each parameter with weights of  $\frac{1}{4}$  applied on the polar and hydrogen bond parameters. By using  $A_{1,2}$  in place of  $\Delta\delta_T^2$ , Equation 4 can be rewritten as Equation 5. Therefore, the Flory-Huggins interaction parameter between SMV and polymer are calculated using Equation 6 [45].

$$A_{1,2} = (\delta_{D2} - \delta_{D1})^2 + \frac{1}{4}(\delta_{P2} - \delta_{P1})^2 + \frac{1}{4}(\delta_{H2} - \delta_{H1})^2 \quad (5)$$

$$\chi_{1,2} = \frac{V_{m,1}}{RT}A_{1,2} \quad (6)$$

A detailed explanation of this molecular modeling is provided in the appendix 1.

#### 2.2.10. Cell culture

W-20-17, ((W-20 clone 17] (ATCC<sup>®</sup> CRL-2623<sup>™</sup>)), preosteoblast mouse bone marrow stromal cells, were grown and maintained in Dulbecco's Modified Eagle media (DMEM) supplemented with 10% FBS and 50 $\mu$ g of penicillin, 50 $\mu$ g of streptomycin, and 100 $\mu$ g of neomycin (PSN) (Gibco<sup>™</sup>, Molecular Probes<sup>™</sup>). Cells were cultured in T75 flasks (Nunc<sup>™</sup> EasyFlask<sup>™</sup>, vented) and placed in an incubator supplied with 5% CO<sub>2</sub> at 37°C. The culture

media was changed every two days and the cells were passed when the flask reached 80-90% confluency. Cells used for cell culture experiments were between passage number 4 and 7.

#### *2.2.11. Cell viability*

Cells were seeded in 96 well plates at  $1 \times 10^4$  cells/well and allowed to attach overnight. On following day, media containing different concentrations of SMV was added to the well plates. Each concentration was tested in quadruplicates. Media with no drug was used as the control (TCP-tissue culture plastic). After 24 and 72 hours, the drug toxicity was analyzed by measuring cell viability using CellTiter-Glo® Luminescent Cell Viability Assay (Promega Corporation) according to manufacturer's protocol.

#### *2.2.12. Cell mineralization studies*

Cells were seeded in 48 well plates at  $1 \times 10^4$  cells/well with complete DMEM (DMEM supplemented with 10% FBS and 1% PSN) and left to attach overnight. On next day, complete medium was replaced either with osteogenic media (complete DMEM supplemented with 5mM beta-glycerophosphate and 50µg/ml ascorbic acid) and non-toxic concentrations of SMV (referred hereafter as regular media) or osteogenic media with 25ng/ml BMP-2 (BMP-2 medium) and non-toxic concentrations of SMV. The concentration of SMV added to the medium were 75-600ng/ml. To examine the potential interactions between SMV and BMP-2, SMV medium was spiked with 25ng/ml BMP-2 (SMV-BMP-2 media). The cell culture media were completely replenished every two days. After 1, 7, 14 and 21 days, the media were removed, and the cells were lysed by adding 300µl of molecular grade water to each well and freeze-thawing the plates three times. The cell lysates were used to measure double stranded DNA and ALP activity of the

cells. Double stranded DNA was measured using a Quant-iT PicoGreen assay kit, from Invitrogen and the ALP activity was measured using a QuantiChrom™ alkaline phosphatase assay kit (DALP-250) from BioAssay Systems. The activity of cells was then normalized to double stranded DNA (dsDNA) (ng/ml) and expressed as IU/ng DNA. Additional plates were made for day 14 and 21 to carry out the calcium deposition assay. After the designated time points, medium was completely removed from the wells and the cell layers were carefully washed twice with 500µl of warm PBS. To each well, 500µl of 0.5N acetic acid was added to each well and the plates were placed on a rotary shaker (Belly Dancer™, Strovall, life science Inc., Greensboro, NC, USA) at moderate speed for 24hours to solubilize the deposited calcium. On next day, the entire well content was transferred to labelled microcentrifuge tubes and frozen at -20°C until ready to assay. A calcium reagent set (Pointe Scientific, Inc), based on o-cresolphthalein method, was used to measure the amount of calcium deposited in each group.

### 2.2.13. Statistical analysis

All data are presented as mean ± standard deviation, except the molecular modeling data. Significant differences in cytotoxicity of SMV concentration, and *in vitro* bioactivity analyses were analyzed by one-way ANOVA test followed by post-hoc analysis. The differences in groups and experimental time points at any time were considered significant if  $p < 0.05$ .

## 2.3 Results

### 2.3.1. SEM

All membranes exhibited smooth fibers with diameters in the nano-range in scanning electron micrographs (Figure 2-1). The as-spun membranes (1A) had fibers around 200-300nm, which did not change significantly after the treatments (1B-E). SEM images of SMV loaded membranes also did not show significant changes in the fiber diameter (Appendix 2).

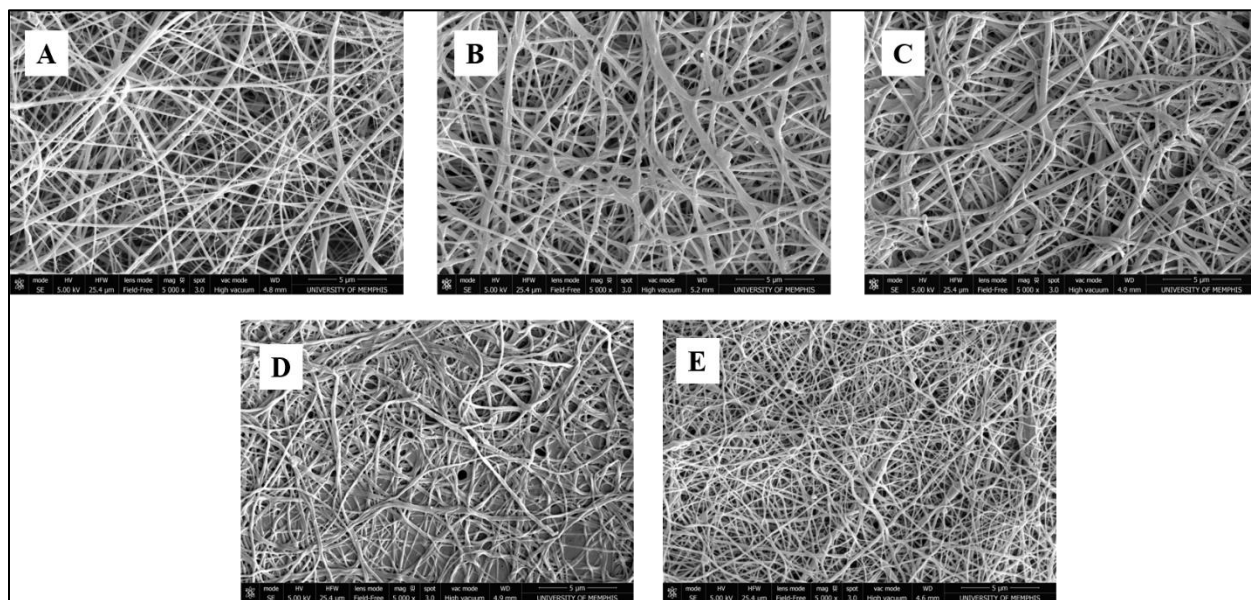


**Figure 2-1:** Images show micrographs of (A) as-spun membrane (B) AA-treated membrane (C) BA-treated membrane (D) HA-treated membrane and (E) TEA-tBOC-treated membrane.

### 2.3.2. ATR-FTIR

ATR spectroscopy was used to analyze the change in the chemical structure of chitosan after the different treatments. Figure 2-2 shows the spectra of as-spun chitosan membrane and membranes after post-spinning treatments. The broad peak between  $3100$  and  $3500\text{cm}^{-1}$  represents the inter- and intra-molecular hydrogen bonding of the  $-\text{NH}_2$  and  $-\text{OH}$  stretching



vibration of chitosan molecules [20]. The absorption peak around  $1750\text{cm}^{-1}$  represents the acyl ( $\text{C}=\text{O}$ ) group, which confirms the acylation reaction. The peaks between  $2750$  and  $3000\text{cm}^{-1}$  represent asymmetrical and symmetrical bending vibrations of the methylene groups, which increased in intensity with increasing FA chain lengths. The ester  $\text{C}=\text{O}$  stretch around  $1700$ - $1750\text{cm}^{-1}$  did not show up in the spectrum of tBOC modified membrane as it selectively reacts with the amine groups of chitosan. The transmittance peaks at  $720$ ,  $802$  and  $837\text{cm}^{-1}$  representing TFA salts were not seen in the treated membranes, confirming the removal of TFA salts.

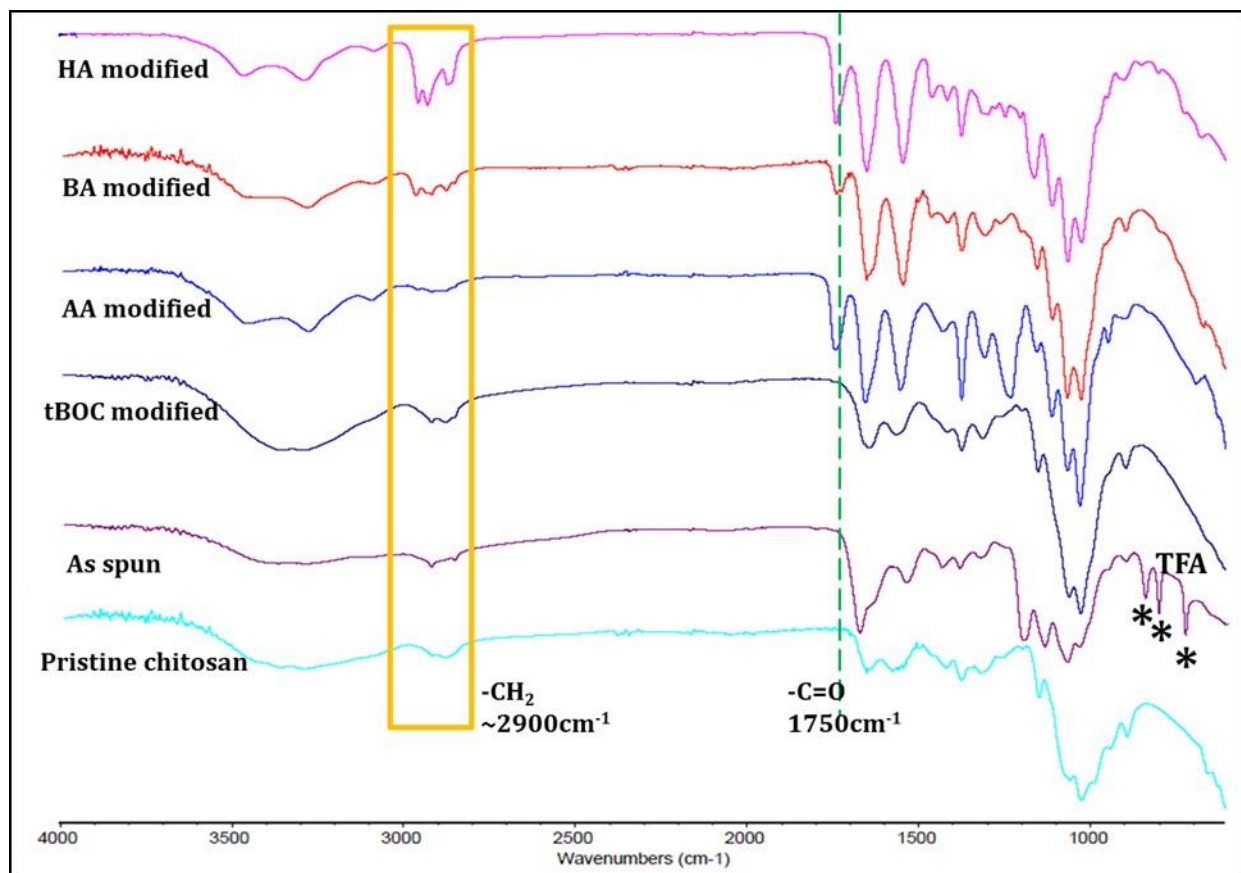


**Figure 2-2:** ATR spectra of chitosan powder, as-spun chitosan, showing the TFA peaks and modified chitosan showing the disappearance of TFA peaks and addition of methyl groups.

### 2.3.3. Water contact angle measurements

The measurements of water contact angles for differently modified chitosan is represented in Table 2-1. Among all the treatments, tBOC modified membranes were the most

hydrophobic ( $119.3^\circ \pm 17.4^\circ$ ). For the fatty acid treated membranes, as the fatty acid chain length increased the membranes became more hydrophobic. The AA membranes were least hydrophobic, and the HA were most hydrophobic.

**Table 2-1:** Water contact angle measurement of differently modified membranes. Each value represents mean  $\pm$  standard deviation (n=4)

<b>Membrane modification</b>	<b>Water contact angle (<math>^\circ</math>)</b>
AA	$59.3 \pm 8.2^a$
BA	$73.3 \pm 5.4^b$
HA	$94.3 \pm 8.5^c$
tBOC	$119.3 \pm 17.4^d$

Superscripts indicate statistically different groups,  $p < 0.05$

#### 2.3.4. Elemental analysis

The absence of F in the elemental analysis data indicated there was no residual TFA salts left in the membranes after the post spinning treatments (Table 2-2). The degree of modification (DM) of the fatty acids or the tBOC groups was calculated based on the C/N ratio from elemental analysis and equation 3. The maximum DM per chitin/chitosan monomer unit for the short chain fatty acids was 2 since there are two reactive -OH groups on each unit. For the AA and BA modified chitosan, the degree of substitution was 1 and for the HA membrane it was between 1 and 2. For the tBOC membrane, the theoretical maximum DS is 0.71 (DDA) as only the chitosan unit has an -NH<sub>2</sub> group to react. The DM of tBOC modified chitosan was calculated to be 0.40.

**Table 2-2:** Elemental analysis of original chitosan, as-spun chitosan and modified chitosan.

	Elements	Original chitosan	As-spun	tBOC	AA	BA	HA
Atomic wt%	C	39.8	33.38	42.3	42.11	48	56.56
	H	6.99	5.42	6.93	6.84	7.07	7.87
	N	6.95	4.68	5.7	5.58	5.27	4.12
	F	0	14.5	0	0	0	0
Atomic number ratio	C/N	<b>6.68<sup>a</sup></b>	<b>8.32</b>	<b>8.65</b>	<b>8.80</b>	<b>10.62</b>	<b>16.01</b>
DM			<b>0.82<sup>b</sup></b>	<b>0.40</b>	<b>1.06</b>	<b>0.99</b>	<b>1.56</b>

a. theoretical  $n_0(C)/n_0(N)$  is 6.58 for DDA 71% chitosan.

b. as-spun membrane includes TFA salt.

### 2.3.5. SMV release study

Amount of SMV released out of the membranes mainly depended on the type of membrane treatment. Thickness of the membranes did not have significant effect on drug release. Representative cumulative release graphs of thick membranes are shown in Figure 2-3. For all loadings and thicknesses, AA and tBOC membranes exhibited significantly higher initial burst release levels of SMV than the other two treatments. There was no difference in the release between the BA and HA modified membranes. For all loadings, AA and tBOC membranes released 10-15 $\mu$ g/ml SMV on day 1, whereas the other two membrane groups released less than 5 $\mu$ g/ml. Amount of drug released from the membranes decreased till day 7, after which all the membranes released  $\sim$ 1 $\mu$ g/ml per day. For HA membranes, the initial loading amounts did not seem to influence the release amount, as all the membranes released only around 20 $\mu$ g by the

end of 28 days. The BA membranes also had a similar release pattern, however, 500 $\mu$ g SMV loaded BA released more than other BA loaded membranes.

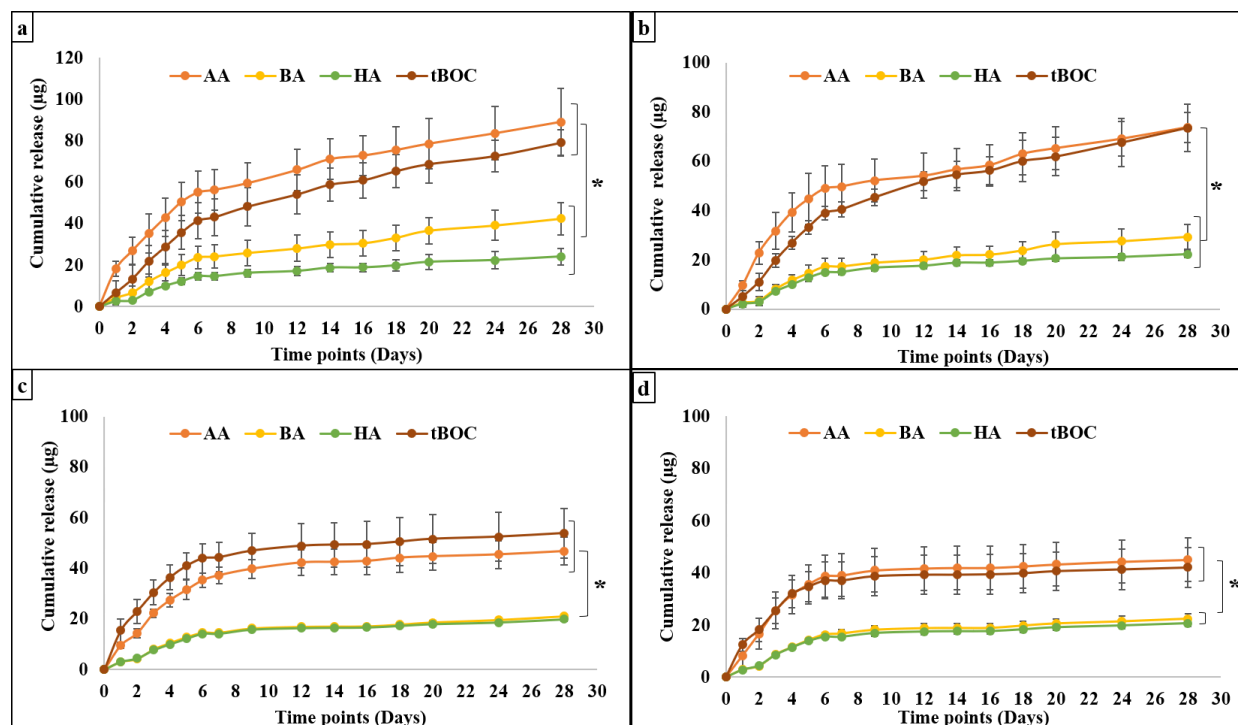


**Figure 2-3:** Graphs show cumulative release over time for thick membranes treated with either fatty acids or tBOC and loaded with (a) 500 $\mu$ g, (b) 250 $\mu$ g, (c) 100 $\mu$ g and (d) 50 $\mu$ g. The AA and tBOC membranes released higher amounts of drug than BA and HA treated membrane. Each value represents the mean  $\pm$  SD (n=6).

Table 2-3 summarizes the percentage release from thick membranes after 28 and 91 days of release. At the end of 28 days, AA and tBOC loaded with 500 $\mu$ g SMV released close to 20% of the drug, whereas the corresponding HA and BA membranes released less than 10%. As the loading amount was halved (250 $\mu$ g), the amount released almost doubled for all the membranes. Similar effects were seen when the membranes were loaded with 100 and 50 $\mu$ g SMV. By the end of 91 days, only the AA and tBOC membranes loaded with 50 $\mu$ g SMV released 100% of the drug. The 100 $\mu$ g loaded membranes released close to 50% of the drug, the 250 $\mu$ g close to 40%

and the 500 $\mu$ g close to 30%. The BA membranes released almost half the amounts released by the AA and tBOC membranes for the corresponding loading amounts. This was also true for HA100 and HA50 membranes. However, HA500 and HA250 released less than 20% of the drug even after 91 days.

**Table 2-3:** Percentage cumulative release of SMV from thick membranes after 28 and 91 days of elution.

	After 28 days				After 91 days			
	500ug	250ug	100ug	50ug	500ug	250ug	100ug	50ug
<b>AA</b>	17.8 $\pm$ 3.2	29.5 $\pm$ 2.4	48.2 $\pm$ 4.8	73 $\pm$ 33.2	32.9 $\pm$ 5.5	42.5 $\pm$ 4.1	53.6 $\pm$ 4.8	104.6 $\pm$ 14
<b>BA</b>	8.5 $\pm$ 1.6	11.7 $\pm$ 2.0	21.1 $\pm$ 0.7	45.0 $\pm$ 3.5	12.3 $\pm$ 1.8	16.8 $\pm$ 1.7	29.6 $\pm$ 1.4	58.5 $\pm$ 4.3
<b>HA</b>	4.8 $\pm$ 0.8	8.9 $\pm$ 0.5	19.9 $\pm$ 0.6	43.0 $\pm$ 3.5	6.8 $\pm$ 1.0	12.0 $\pm$ 0.6	26.8 $\pm$ 1.3	56.5 $\pm$ 3.3
<b>tBOC</b>	15.8 $\pm$ 1.3	29.4 $\pm$ 3.9	53.9 $\pm$ 9.8	88.8 $\pm$ 17.7	27.8 $\pm$ 5.2	10.7	10.9	102.9 $\pm$ 9.3

*2.3.6. Determination of solubility and Flory-Huggins parameter ( $\chi_{1,2}$ ) of SMV with chitosan and differently modified chitosan*

The results for the determination of the HSPs for the differently modified chitosans and different forms of SMV are summarized in Table 2-4. For estimating solubility parameters of chitosan and modified chitosan, we assumed 70% glucosamine and 30% acetylglucosamine and used an average DM = 1 for all the modifications. Results of calculations for Flory-Huggins

interaction parameter ( $\chi_{1,2}$ ) between SMV and polymer using the A<sub>12</sub> assumption for the HSP and  $\Delta\delta_T^2$  parameter are shown in Table 2-4 and 2-5 and figure 2-5.

**Table 2-4:** Estimated Hansen Solubility Parameters for SMV, hydrolyzed SMV and chitosan with different modifications

	$\delta_D$	$\delta_P$	$\delta_H$	$\delta_T$ (MPa <sup>0.5</sup> )
<b>Chitosan</b>	17.77	11.29	15.16	25.94
<b>AA-Chitosan</b>	17.40	9.58	11.33	22.87
<b>BA-Chitosan</b>	17.00	8.67	9.71	21.41
<b>HA-Chitosan</b>	16.89	8.05	9.70	21.07
<b>tBOC-Chitosan</b>	17.21	11.74	12.14	24.11
<b>SMV</b>	16.80	0.42	4.26	17.34
<b>Hydrolyzed SMV</b>	16.99	3.26	7.10	18.70

The schematics of chemical structures for chitosan and differently modified chitosan is represented in Figure 2-4.

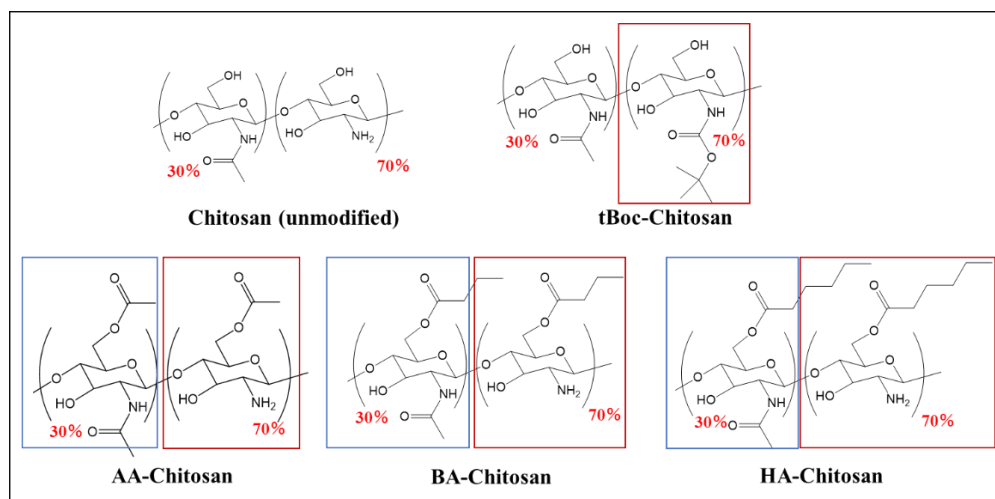


**Figure 2-4:** Schematic of unmodified and modified chitosan after tBOC and fatty acid treatments. The degree of substitution was assumed to be 1 for all the modifications. The tBOC groups attach to amine group of the polymer and the fatty acids react with hydroxyl group.

**Table 2-5:** Hansen solubility differences and polymer-drug interaction parameters at 310K

	$A_{1,2}$		$\chi_{1,2}(310K)$	
	SMV	Hydrolyzed SMV	SMV	Hydrolyzed SMV
<b>Chitosan</b>	60.19	32.97	9.55	5.19
<b>AA-Chitosan</b>	33.85	14.64	5.37	2.31
<b>BA-Chitosan</b>	24.46	9.01	3.88	1.42
<b>HA-Chitosan</b>	21.96	7.44	3.49	1.17
<b>tBOC-Chitosan</b>	47.73	24.38	7.58	3.84

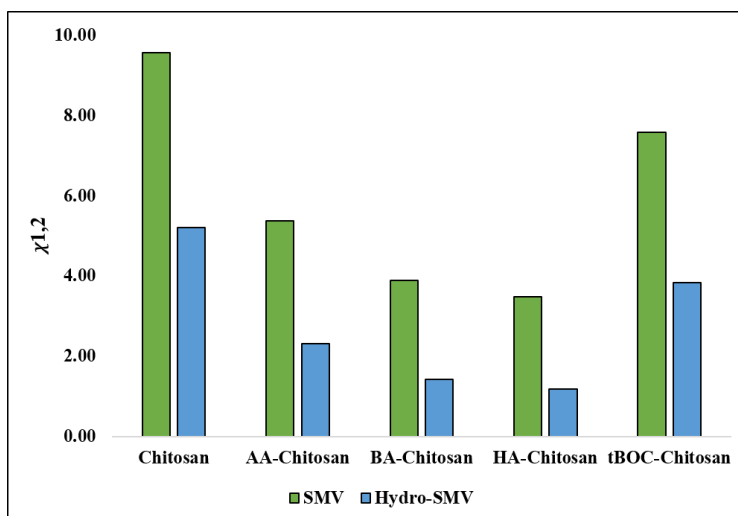


**Figure 2-5:** Flory-Huggins interaction parameter ( $\chi_{1,2}$ ) of SMV and hydrolyzed SMV with chitosan and differently modified chitosan. Hydrolyzed SMV had more interaction with the polymer than the unhydrolyzed lactone form. The drug was more soluble in the BA and HA modified chitosan than the AA and tBOC modified polymer.

It is seen that the solubility and interaction parameters for hydrolyzed SMV is about 2-3 times lower than unhydrolyzed SMV (Figure 2-5). A lower value indicates better compatibility between the drug and polymer. Results also indicate that as the fatty acid chain length increased, the drug became more compatible to the polymer. The BA and HA modified chitosan had lower  $\chi_{1,2}$  values for SMV and hydrolyzed SMV as compared to AA and tBOC modified chitosan

which corresponds to the slower drug release from BA and HA membranes and faster release from the other two.

### 2.3.7. Cytotoxicity evaluation of SMV

The results of the 24 and 72 hour cytotoxicity tests of SMV to the W-20-17 cells based on the Cell Titer glo assay normalized to 0ng/ml SMV, indicated no differences in percent viability of the cells exposed to SMV up to 600ng/ml at either the 24 or 72 hour time points (Figure 2-6). Preliminary studies indicated that concentrations above 600ng/ml showed a dose-dependent toxicity towards the cells.

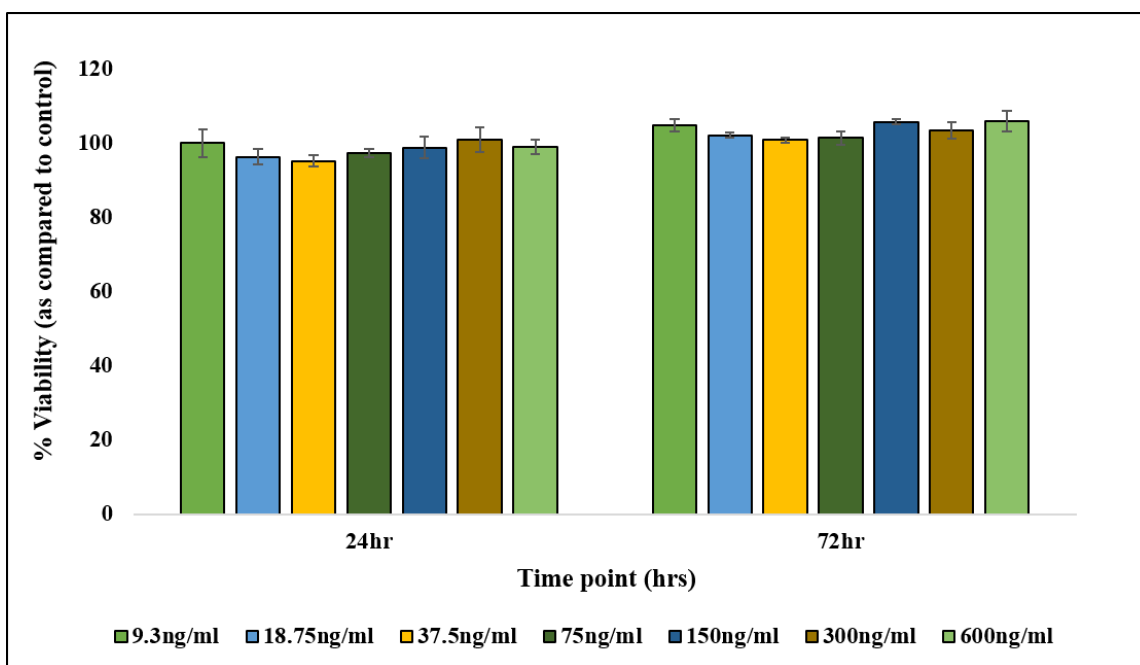


**Figure 2-6:** Graph shows cell viability expressed as a percentage compared to 0ng/ml SMV controls for increasing doses of SMV. Each value represents the mean  $\pm$  SD (n=4).



### *2.3.8. ALP activity and mineralization of W-20-17 cells in the presence of SMV*

W-20-17 cells were cultured for up to 21 days to evaluate the osteogenic potential of SMV. Cells were evaluated for ALP expression as a marker of osteoblastic differentiation and for calcium-phosphate deposition via the o-cresolphthalein reaction, as indicator of terminal differentiation and matrix mineralization. Cells showed a positive dose dependent expression of ALP to increasing concentrations of SMV up to 600ng/ml. (Figure 2-7a). Cells grown in the presence of 600ng/ml SMV showed significantly higher ALP activity as compared to the TCP group on days 7, and 21. By day 21, cells grown with 300ng/ml SMV also exhibited higher ALP activity as compared to TCP groups, though not statistically significant. For cells grown in the BMP-2 media, there was no SMV dose response expression of ALP by the cells, though there was a trend for SMV to enhance the stimulatory effect of BMP-2 on ALP activity in these cells (Figure 2-7b). Only on day 7, 600ng/ml SMV group showed significantly higher ALP activity than the TCP group. Overall, the BMP-2 media groups showed much higher ALP activity as compared to the corresponding regular media groups. All groups showed increase in ALP activity with culture time.

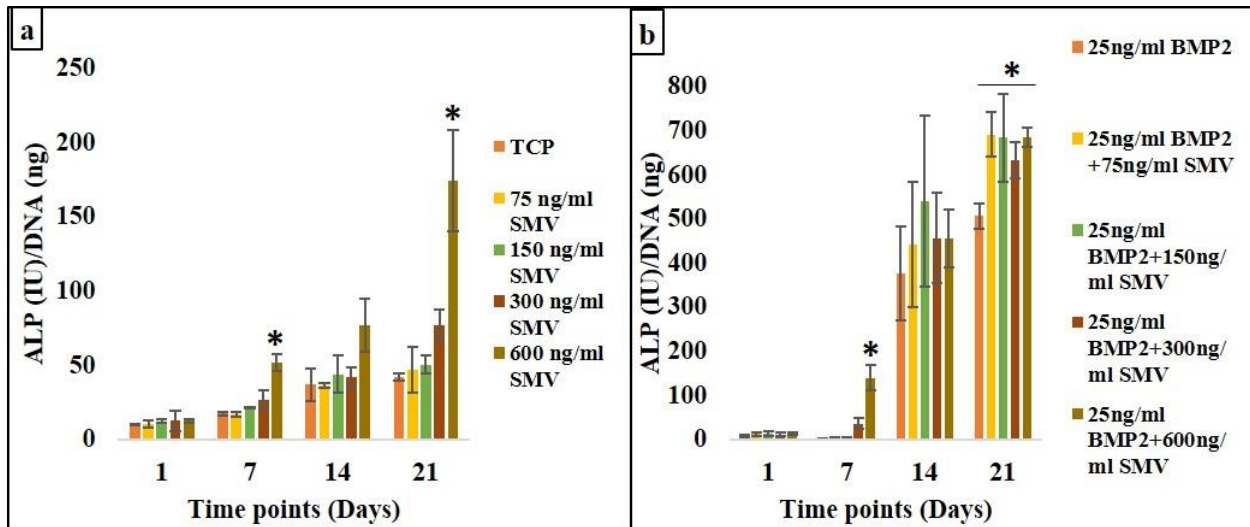


**Figure 2-7:** The effect of SMV on induction of alkaline phosphatase (ALP) activity in W-20-17 cells in regular media (a) and BMP-2 media (b). Each value represents the mean  $\pm$  SD (n=4). \* indicates significant difference between the experimental group and the TCP (tissue culture plastic) group for that time point ( $p < 0.05$ ).

All the groups showed an increase in the amount of calcium deposited from day 14 to day 21 (Figure 2-8). Similar to ALP activity, for the regular media groups, there was a dose-dependent increase in calcium deposition to the increasing SMV concentration. On day 14, 600ng/ml SMV stimulated more calcium deposition than other groups, though not significantly different. By day 21, this effect became significant. Cells cultured with 300ng/ml SMV also showed a trend to stimulate more calcium deposition, though not significantly higher than control group. Among the BMP-2 media groups also there was a trend for increased calcium deposition with increase in SMV concentration, though none of the groups were significantly different. More calcium deposition by the 600ng/ml SMV wells was evident on day 14 and 21 in both media groups. There was no significant difference between levels of calcium deposited by cells grown in control medium and 75ng/ml SMV containing medium, in all the cases.

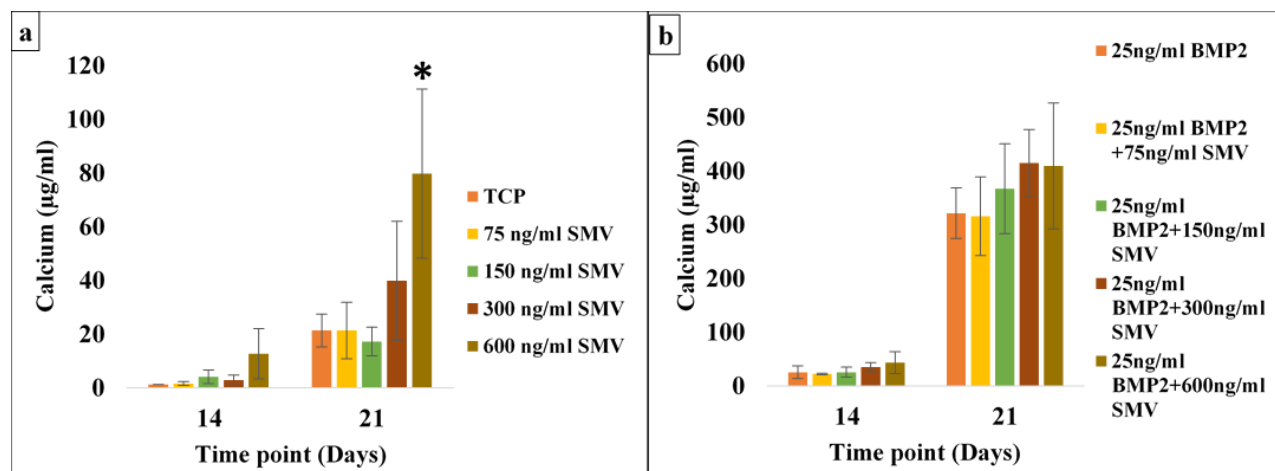


**Figure 2-8:** Calcium assay to determine the amount of calcium deposited by the cells in the presence of different concentrations of SMV in regular media (a) and BMP-2 media (b). Each value represents the mean  $\pm$  SD (n=4). \* indicates significant difference between the experimental group and the control group for that time point ( $p < 0.05$ ).

#### 2.4. Discussion

ESCM modified by capping amine groups with tBOC or by grafting short chain FA to the –OH groups on the polymer maintain their nanofiber structure in aqueous environments and exhibit in vitro and in vivo biocompatibility and degradation properties appropriate for GBR applications [17, 20, 21]. To take advantage of the increased surface area of the nanofibers for local drug delivery, this study showed that membrane modifications can be used to control the release of SMV, an anti-cholesterol drug that also exhibits osteogenic effects and assessed the osteogenic potential of SMV in vitro using a mouse stromal cell line.

The tBOC-modified and BA modified ESCM were prepared following previously reported methods [17, 21]. Protocol reported by Wu et al. to FA modify the membranes with butyric anhydride was modified slightly by using either acetic anhydride or hexanoic anhydride to create the AA- and HA- modified ESCM [20, 21]. FTIR analyses and SEM examinations of

membranes demonstrated that all the treatments were effective in removing the TFA salts without causing significant changes in the size of the nanofiber of the membranes. Relative changes in the intensity of  $-CH_2$  peaks in the FTIR spectra also indicated success in the grafting of acetic anhydride and hexanoic anhydride short chain fatty acids to the chitosan membranes. Similar results were reported by Wu et al. and Su et al., where the treated membranes did not show significant changes in the fiber diameter and the FTIR spectra showed successful grafting of the fatty acid or tBOC groups [17, 20]. Increase in the water contact angles of the membranes in proportion to the fatty acid chains indicated an increase in the hydrophobic nature of the membranes. In another work by Zhang et al., similar increase in water contact angle with increase in the fatty acid chain length was reported [46]. The longer chain fatty acid had larger water contact angle, suggesting their more hydrophobic nature [46]. Su et al, demonstrated an increase in water contact angle of the tBOC membranes as compared to sodium carbonate treated membranes [17].

Removal of TFA salts and addition of functional groups were further confirmed by elemental analysis, which gave an estimate of DM for each membrane modification. DM for the modified membranes was calculated to be close to 1. However, the values varied slightly based on the treatment. tBOC membranes were determined to have a DS of 0.4, whereas a maximum of 0.71 is possible. This may be due to the inability of the bulky tBOC groups to penetrate within the membrane surface to react with more chitosan molecules. The shorter fatty acid modified membranes (AA, BA) had a DM=1 whereas the longer fatty acid modified membranes (HA) on the other hand had a DM of more than 1. The higher DM of HA membranes might also contribute to the more hydrophobic behavior of these membranes. Zhang et al. reported a DS of

more than or equal to 2, for all their fatty acid treated membranes, irrespective of the chain length [46]. Elemental analysis did not detect the presence of fluorine, confirming the removal of TFA salts. Thus, all the treatments were successful in removing the TFA salts and maintaining the porous nanofibrous structure of ESCM by increasing their hydrophobic behavior.

As the treatment procedures were able to retain the porous structure of these membranes and modulate their hydrophobic behavior, their ability to deliver a hydrophobic agent was evaluated using a hydrophobic osteogenic drug- SMV. Generally, drug release from polymer-based systems depends on initial drug loading amount, polymer-drug interactions, polymer degradability and the extent of diffusion [47]. The factors analyzed in this study are (1) initial drug loading amount, (2) hydrophobicity of the membranes (3) thickness of the membranes and (4) polymer-drug interactions. The general concept of like dissolves like were reflected with fatty acid treated membranes. Hydrophobic SMV interacted more with hydrophobic HA and BA membranes, thereby releasing out very slowly. As the hydrophobicity of the membranes decreased, the rate and amount of drug released out of the membranes increased. However, this was not true for the tBOC membranes. Though these membranes were more hydrophobic than HA membranes, based on the water contact angle data, their release was similar to AA membranes. Molecular modeling data using Hansen solubility parameter [45], revealed a high  $\delta_T$  value for tBOC modified chitosan, which indicated a more hydrophilic character of the polymer as compared to the low  $\delta_T$  value of the HA and BA modified polymer. As the  $\delta_T$  value for a compound decreases, it is expected to become more hydrophobic. High water contact angle of tBOC membranes, their high  $\delta_T$  value and low DM suggest that the tBOC treatment might only be a surface phenomenon. The bulky tBOC groups might have attached only to the  $-NH_2$  units

present on the surface and might not have been able to penetrate within the fibers to react throughout the membrane's thickness. From the modeling data it was evident that as the fatty acid chain length increased, the hydrophobic character of the polymer increased. SMV had a low  $\delta_T$  indicating its hydrophobic character. Since the  $\delta_T$  values for tBOC and AA membranes were large, they released SMV at a faster rate as compared to the HA and BA membranes that had lower  $\delta_T$  values.

Further, the large solubility differences ( $A_{1,2}$ ) between SMV (unhydrolyzed) and polymers indicate minimum interaction between the drug and the membranes. Even the most hydrophobic HA membranes seemed to have large  $A_{1,2}$  values with the hydrophobic SMV. However, SMV quickly hydrolyzes within few hours in aqueous environment. This hydrolyzed form had smaller  $\chi_{1,2}$  values with the modified polymers, indicating better polymer-drug interaction. As the interaction parameter,  $\chi_{1,2}$ , decreases, the polymer increasingly becomes a better thermodynamic solvent for the drug, resulting in improved drug solubility. As a result, the drug tended to stay within the membranes, rather than diffuse out. These results confirm our ability to control the release of SMV from chitosan membranes subjected to different modification reactions.

Different concentrations of SMV were evaluated in direct contact with mouse bone-marrow stromal cells to check their cytocompatibility and osteogenic potential. Most papers report a maximum of ~400ng/ml (1 $\mu$ M) SMV as the highest drug concentration tolerated by the cells, however in our work up to 600ng/ml SMV showed no toxicity. The maximum tolerable

level of the drug also depends on the cell type, age of the cells and stage of differentiation. In this study, the osteogenic potential of SMV with and without BMP-2 was evaluated. Additional 25ng/ml BMP-2 was added to the cell culture media to evaluate any adjunctive positive interaction between SMV and BMP-2, since some amount of BMP-2 is always present in the blood stream *in vivo*. This level of BMP-2 was selected because 25ng/ml BMP-2 was the least concentration of BMP-2 which induced noticeably higher ALP activity than the control cells. The W-20-17 cells used for these experiments show a dose-dependent increase in ALP with increase in BMP-2 concentration [48]. ALP is considered to be an early osteogenic marker, which indicates the beginning of differentiation phase. The dose dependent response of ALP and calcium with increasing levels of SMV, and additional enhanced effect in the presence of BMP-2 is similar to previous studies by Park et al. and Shao et al. [49, 50]. MC3T3 cells in the presence of SMV and 60ng/ml BMP-2 showed enhanced osteogenic differentiation, as compared to only SMV group [49], which was similar to the effect shown by the W-20-17 cells. SMV is known to antagonize TNF- $\alpha$  inhibition of BMPs [30]. Since the W-20-17 cells produce ALP in response to BMP-2 in a dose dependent manner, prolonged presence of BMP-2 might have induced higher ALP activity by the cells, leading to better mineralization. This was also evident from the higher ALP activity by the cells that were grown in the presence of BMP-2 and SMV. SMV has also been reported to stimulate the expression of  $\alpha 5$ -integrin and smad molecules, both of which play critical roles in stimulating osteogenesis [49, 50]. SMV is thought to bind to the integrin molecules and induce phosphorylation of FAK, which in turn mediates the BMP-2/smad pathway [51, 52]. In MC3T3 cells, FAK phosphorylation induces the activation of Runx2, which is a key regulator of osteoblast differentiation and also is important in the expression of ALP and

OCN in the differentiation process [53]. The smad molecule is known to mediate the canonical signaling cascade of TGF- $\beta$  superfamily growth factors, of which BMPs are a member [54].

## ***2.5. Conclusion***

Release of SMV from ESCM was controlled by subjecting the membranes to different treatments and by loading different initial drug amounts. Since these membranes have already shown to support and guide bone regeneration, our ability to control the release of a potential osteogenic drug from these membranes would enable us to customize the membranes based on the clinical need. These membranes provide a unique platform to deliver hydrophobic drugs, such as cancer therapeutics, that are difficult to deliver locally in a sustained manner. Preliminary cell studies with SMV and W-20-17 cells confirm the osteogenic potential of this drug, similar to the previous studies. Therefore, next, these cells will be used to investigate the osteogenic potential of SMV loaded modified ESCM.



## *References*

- [1] C. Xu, C. Lei, L. Meng, C. Wang, Y. Song, Chitosan as a barrier membrane material in periodontal tissue regeneration, *Journal of Biomedical Materials Research Part B: Applied Biomaterials*, 100 (2012) 1435-1443.
- [2] P.A. Norowski Jr, T. Fujiwara, W.C. Clem, P.C. Adatrow, E.C. Eckstein, W.O. Haggard, J.D. Bumgardner, Novel naturally cross-linked electrospun nanofibrous chitosan mats for guided bone regeneration membranes: Material characterization and cytocompatibility, *Journal of tissue engineering and regenerative medicine*, 9 (2015) 577-583.
- [3] H. Park, B. Choi, J. Hu, M. Lee, Injectable chitosan hyaluronic acid hydrogels for cartilage tissue engineering, *Acta biomaterialia*, 9 (2013) 4779-4786.
- [4] J.J. Wang, Z.W. Zeng, R.Z. Xiao, T. Xie, G.L. Zhou, X.R. Zhan, S.L. Wang, Recent advances of chitosan nanoparticles as drug carriers, *International journal of nanomedicine*, 6 (2011) 765.
- [5] Z. Chen, P. Wang, B. Wei, X. Mo, F. Cui, Electrospun collagen–chitosan nanofiber: A biomimetic extracellular matrix for endothelial cell and smooth muscle cell, *Acta Biomaterialia*, 6 (2010) 372-382.
- [6] N. Bhattarai, D. Edmondson, O. Veiseh, F.A. Matsen, M. Zhang, Electrospun chitosan-based nanofibers and their cellular compatibility, *Biomaterials*, 26 (2005) 6176-6184.
- [7] R. Jayakumar, M. Prabakaran, S. Nair, H. Tamura, Novel chitin and chitosan nanofibers in biomedical applications, *Biotechnology advances*, 28 (2010) 142-150.

- [8] S.P. Noel, H. Courtney, J.D. Bumgardner, W.O. Haggard, Chitosan films: a potential local drug delivery system for antibiotics, *Clinical orthopaedics and related research*, 466 (2008) 1377-1382.
- [9] A.C. Mendes, C. Gorzelanny, N. Halter, S.W. Schneider, I.S. Chronakis, Hybrid electrospun chitosan-phospholipids nanofibers for transdermal drug delivery, *International journal of pharmaceutics*, 510 (2016) 48-56.
- [10] A. Ali, S. Ahmed, A review on chitosan and its nanocomposites in drug delivery, *International journal of biological macromolecules*, 109 (2018) 273-286.
- [11] P.A. Norowski, J. Babu, P.C. Adatrow, F. Garcia-Godoy, W.O. Haggard, J.D. Bumgardner, Antimicrobial Activity of Minocycline-Loaded Genipin-Cross-linked Nano-Fibrous Chitosan Mats for Guided Tissue Regeneration, *Journal of Biomaterials and Nanobiotechnology*, 3 (2012) 528.
- [12] E.-J. Lee, H.-E. Kim, Accelerated bony defect healing by chitosan/silica hybrid membrane with localized bone morphogenetic protein-2 delivery, *Materials Science and Engineering: C*, 59 (2016) 339-345.
- [13] S.Y. Shin, H.N. Park, K.H. Kim, M.H. Lee, Y.S. Choi, Y.J. Park, Y.M. Lee, Y. Ku, I.C. Rhyu, S.B. Han, Biological evaluation of chitosan nanofiber membrane for guided bone regeneration, *Journal of periodontology*, 76 (2005) 1778-1784.
- [14] Y.J. Yeo, D.W. Jeon, C.S. Kim, S.H. Choi, K.S. Cho, Y.K. Lee, C.K. Kim, Effects of chitosan nonwoven membrane on periodontal healing of surgically created one-wall intrabony defects in beagle dogs, *Journal of Biomedical Materials Research Part B: Applied Biomaterials: An Official Journal of The Society for Biomaterials, The Japanese Society for Biomaterials, and*

The Australian Society for Biomaterials and the Korean Society for Biomaterials, 72 (2005) 86-93.

[15] B.M. Chesnutt, Y. Yuan, K. Buddington, W.O. Haggard, J.D. Bumgardner, Composite chitosan/nano-hydroxyapatite scaffolds induce osteocalcin production by osteoblasts in vitro and support bone formation in vivo, *Tissue Engineering Part A*, 15 (2009) 2571-2579.

[16] S.M. Kuo, S.J. Chang, T.W. Chen, T.C. Kuan, Guided tissue regeneration for using a chitosan membrane: an experimental study in rats, *Journal of Biomedical Materials Research Part A: An Official Journal of The Society for Biomaterials, The Japanese Society for Biomaterials, and The Australian Society for Biomaterials and the Korean Society for Biomaterials*, 76 (2006) 408-415.

[17] H. Su, K.-Y. Liu, A. Karydis, D.G. Abebe, C. Wu, K.M. Anderson, N. Ghadri, P. Adatrow, T. Fujiwara, J.D. Bumgardner, In vitro and in vivo evaluations of a novel post-electrospinning treatment to improve the fibrous structure of chitosan membranes for guided bone regeneration, *Biomedical materials (Bristol, England)*, 12 (2016) 015003-015003.

[18] K. Ohkawa, D. Cha, H. Kim, A. Nishida, H. Yamamoto, Electrospinning of chitosan, *Macromolecular rapid communications*, 25 (2004) 1600-1605.

[19] E.A. EL-HAFIAN, E.S. Elgannoudi, A. Mainal, A.H.B. Yahaya, Characterization of chitosan in acetic acid: Rheological and thermal studies, *Turkish Journal of Chemistry*, 34 (2010) 47-56.

[20] C. Wu, H. Su, S. Tang, J.D. Bumgardner, The stabilization of electrospun chitosan nanofibers by reversible acylation, *Cellulose*, 21 (2014) 2549-2556.

- [21] C. Wu, H. Su, A. Karydis, K.M. Anderson, N. Ghadri, S. Tang, Y. Wang, J.D. Bumgardner, Mechanically stable surface-hydrophobilized chitosan nanofibrous barrier membranes for guided bone regeneration, *Biomedical Materials*, 13 (2017) 015004.
- [22] S.H. Choi, C.K. Kim, K.S. Cho, J.S. Huh, R.G. Sorensen, J.M. Wozney, U.M. Wikesjö, Effect of recombinant human bone morphogenetic protein-2/absorbable collagen sponge (rhBMP-2/ACS) on healing in 3-wall intrabony defects in dogs, *Journal of periodontology*, 73 (2002) 63-72.
- [23] H. Seeherman, J. Wozney, R. Li, Bone morphogenetic protein delivery systems, *Spine*, 27 (2002) S16-S23.
- [24] M. Nyan, J. Hao, T. Miyahara, K. Noritake, R. Rodriguez, S. Kasugai, Accelerated and enhanced bone formation on novel simvastatin-loaded porous titanium oxide surfaces, *Clinical implant dentistry and related research*, 16 (2014) 675-683.
- [25] N. Priyanka, A. Abhilash, S. Saquib, N. Malgaonkar, N. Kudyar, A. Gupta, N. Kalra, A. Pradeep, Clinical Efficacy of Subgingivally Delivered 1.2 mg Simvastatin in the Treatment of Patients with Aggressive Periodontitis: A Randomized Controlled Clinical Trial, *International Journal of Periodontics & Restorative Dentistry*, 37 (2017).
- [26] K.H. Baek, W.Y. Lee, K.W. Oh, H.J. Tae, J.M. Lee, E.J. Lee, J.H. Han, M.I. Kang, B.Y. Cha, K.W. Lee, The effect of simvastatin on the proliferation and differentiation of human bone marrow stromal cells, *Journal of Korean medical science*, 20 (2005) 438-444.
- [27] M.R. Thylin, J.C. McConnell, M.J. Schmid, R.R. Reckling, J. Ojha, I. Bhattacharyya, D.B. Marx, R.A. Reinhardt, Effects of simvastatin gels on murine calvarial bone, *Journal of periodontology*, 73 (2002) 1141-1148.

- [28] M. Nyan, D. Sato, H. Kihara, T. Machida, K. Ohya, S. Kasugai, Effects of the combination with  $\alpha$ -tricalcium phosphate and simvastatin on bone regeneration, *Clinical Oral Implants Research*, 20 (2009) 280-287.
- [29] W.-L. Yu, T.-W. Sun, C. Qi, H.-K. Zhao, Z.-Y. Ding, Z.-W. Zhang, B.-B. Sun, J. Shen, F. Chen, Y.-J. Zhu, Enhanced osteogenesis and angiogenesis by mesoporous hydroxyapatite microspheres-derived simvastatin sustained release system for superior bone regeneration, *Scientific reports*, 7 (2017) 44129.
- [30] M. Yamashita, F. Otsuka, T. Mukai, H. Otani, K. Inagaki, T. Miyoshi, J. Goto, M. Yamamura, H. Makino, Simvastatin antagonizes tumor necrosis factor- $\alpha$  inhibition of bone morphogenetic proteins-2-induced osteoblast differentiation by regulating Smad signaling and Ras/Rho-mitogen-activated protein kinase pathway, *Journal of Endocrinology*, 196 (2008) 601-613.
- [31] K. Sakoda, M. Yamamoto, Y. Negishi, J. Liao, K. Node, Y. Izumi, Simvastatin decreases IL-6 and IL-8 production in epithelial cells, *Journal of dental research*, 85 (2006) 520-523.
- [32] M. Takenaka, K. Hirade, K. Tanabe, S. Akamatsu, S. Dohi, H. Matsuno, O. Kozawa, Simvastatin stimulates VEGF release via p44/p42 MAP kinase in vascular smooth muscle cells, *Biochemical and biophysical research communications*, 301 (2003) 198-203.
- [33] G. Mundy, R. Garrett, S. Harris, J. Chan, D. Chen, G. Rossini, B. Boyce, M. Zhao, G.I. Gutierrez, Stimulation of bone formation in vitro and in rodents by statins, *Science*, 286 (1999) 1946-1949.
- [34] P.S. Wang, D.H. Solomon, H. Mogun, J. Avorn, HMG-CoA reductase inhibitors and the risk of hip fractures in elderly patients, *Jama*, 283 (2000) 3211-3216.

- [35] H.L. Funkhouser, T. Adera, R.A. Adler, Effect of HMG-CoA reductase inhibitors (statins) on bone mineral density, *Journal of Clinical Densitometry*, 5 (2002) 151-158.
- [36] C. Song, Z. Guo, Q. Ma, Z. Chen, Z. Liu, H. Jia, G. Dang, Simvastatin induces osteoblastic differentiation and inhibits adipocytic differentiation in mouse bone marrow stromal cells, *Biochemical and biophysical research communications*, 308 (2003) 458-462.
- [37] Y. Qi, T. Zhao, W. Yan, K. Xu, Z. Shi, J. Wang, Mesenchymal stem cell sheet transplantation combined with locally released simvastatin enhances bone formation in a rat tibia osteotomy model, *Cytotherapy*, 15 (2013) 44-56.
- [38] X. Huang, Z. Huang, W. Li, Highly efficient release of simvastatin from simvastatin-loaded calcium sulphate scaffolds enhances segmental bone regeneration in rabbits, *Molecular medicine reports*, 9 (2014) 2152-2158.
- [39] Y. Zhou, Y. Ni, Y. Liu, B. Zeng, Y. Xu, W. Ge, The role of simvastatin in the osteogenesis of injectable tissue-engineered bone based on human adipose-derived stromal cells and platelet-rich plasma, *Biomaterials*, 31 (2010) 5325-5335.
- [40] S. Jerwood, J. Cohen, Unexpected antimicrobial effect of statins, *Journal of antimicrobial chemotherapy*, 61 (2007) 362-364.
- [41] N. Ghadri, K.M. Anderson, P. Adatrow, S.H. Stein, H. Su, F. Garcia-Godoy, A. Karydis, J.D. Bumgardner, Evaluation of bone regeneration of simvastatin loaded chitosan nanofiber membranes in rodent calvarial defects, *Journal of Biomaterials and Nanobiotechnology*, 9 (2018) 210.

- [42] R. Wong, A. Rabie, Statin collagen grafts used to repair defects in the parietal bone of rabbits, *British Journal of Oral and Maxillofacial Surgery*, 41 (2003) 244-248.
- [43] T. Tanigo, R. Takaoka, Y. Tabata, Sustained release of water-insoluble simvastatin from biodegradable hydrogel augments bone regeneration, *Journal of Controlled Release*, 143 (2010) 201-206.
- [44] T.A. Asafo-Adjei, T.D. Dziubla, D.A. Puleo, Tuning properties of poly (ethylene glycol)-block-poly (simvastatin) copolymers synthesized via triazabicyclodecene, *Reactive and Functional Polymers*, 119 (2017) 37-46.
- [45] C.M. Hansen, Hansen solubility parameters: a user's handbook, CRC press, 2002.
- [46] Z. Zhang, F. Jin, Z. Wu, J. Jin, F. Li, Y. Wang, Z. Wang, S. Tang, C. Wu, Y. Wang, O-acylation of chitosan nanofibers by short-chain and long-chain fatty acids, *Carbohydrate polymers*, 177 (2017) 203-209.
- [47] P.A. Gunatillake, R. Adhikari, Biodegradable synthetic polymers for tissue engineering, *Eur Cell Mater*, 5 (2003) 1-16.
- [48] R.S. Thies, M. Bauduy, B.A. Ashton, L. Kurtzberg, J.M. Wozney, V. Rosen, Recombinant human bone morphogenetic protein-2 induces osteoblastic differentiation in W-20-17 stromal cells, *Endocrinology*, 130 (1992) 1318-1324.
- [49] J.-B. Park, Combination of simvastatin and bone morphogenetic protein-2 enhances the differentiation of osteoblasts by regulating the expression of phospho-Smad1/5/8, *Experimental and therapeutic medicine*, 4 (2012) 303-306.

- [50] P.-L. Shao, S.-C. Wu, Z.-Y. Lin, M.-L. Ho, C.-H. Chen, C.-Z. Wang, Alpha-5 Integrin Mediates Simvastatin-Induced Osteogenesis of Bone Marrow Mesenchymal Stem Cells, *International journal of molecular sciences*, 20 (2019) 506.
- [51] X.-Y. Ma, Y.-F. Feng, T.-S. Wang, W. Lei, X. Li, D.-P. Zhou, X.-X. Wen, H.-L. Yu, L.-B. Xiang, L. Wang, Involvement of FAK-mediated BMP-2/Smad pathway in mediating osteoblast adhesion and differentiation on nano-HA/chitosan composite coated titanium implant under diabetic conditions, *Biomaterials science*, 6 (2018) 225-238.
- [52] Y. Tamura, Y. Takeuchi, M. Suzawa, S. Fukumoto, M. Kato, K. Miyazono, T. Fujita, Focal adhesion kinase activity is required for bone morphogenetic protein—Smad1 signaling and osteoblastic differentiation in murine MC3T3-E1 cells, *Journal of bone and mineral research*, 16 (2001) 1772-1779.
- [53] C. Ge, Q. Yang, G. Zhao, H. Yu, K.L. Kirkwood, R.T. Franceschi, Interactions between extracellular signal-regulated kinase 1/2 and P38 Map kinase pathways in the control of RUNX2 phosphorylation and transcriptional activity, *Journal of Bone and Mineral Research*, 27 (2012) 538-551.
- [54] B. Song, K.D. Estrada, K.M. Lyons, Smad signaling in skeletal development and regeneration, *Cytokine & growth factor reviews*, 20 (2009) 379-388.



## Chapter 3

### Simvastatin Loaded Electrospun Chitosan Guided Bone Regeneration Membranes to Stimulate Osteogenesis

#### *3.1. Introduction*

Nanofibrous chitosan membranes fabricated by electrospinning have shown to have good potential for GBR applications (Kuo et al. 2006; Norowski Jr et al. 2015; Shin et al. 2005). The porous nano fibrous structure mimics the extracellular matrix, provides increased surface area for drug delivery, promotes cell attachment and growth and allows exchange of nutrients between osseous and epithelial tissues, while remaining cell occlusive (Turri et al. 2016; Xu et al. 2012). However, chitosan membranes swell and lose their porous structure when exposed to aqueous environment (Sangsanoh & Supaphol, 2006). Though numerous efforts have been made to overcome this issue, they have had limited success. Recently developed post spinning treatments avoid this issue by using hydrophobic modifications to prevent swelling and maintain the porous nanofibrous structure (Su et al. 2016; Wu et al. 2014). The treatments included acylation reaction using short- chain fatty acids and the addition of tBOC groups (tert-Butyloxycarbonyl protecting group) to the polymer chain (Su et al. 2016; Wu et al. 2014). Membranes treated using these techniques showed good mechanical properties and retained their original morphology even after 4 weeks in aqueous solution (Su et al. 2016; Wu et al. 2017; Wu et al. 2014).

To improve the functionality of these membranes, we investigated the loading and release of a potential osteogenic drug, simvastatin (SMV), which could prove to be an effective alternative to BMP-2. This drug has been used clinically for anti-cholesterol treatment.

Physicians have reported a positive association between the intake of SMV and a decrease in the incidence of fracture among elderly patients (Funkhouser et al. 2002; Wang et al. 2000). Qi et al. investigated the effects of simvastatin locally applied from calcium sulfate (CS) combined with a mesenchymal stem cell (MSC) sheet on fractured tibias healing in rats and reported that SMV loaded group promoted better bone regeneration (Qi et al. 2013). A small but significant amount of bone formation in rabbit parietal bone defects were detected within 14 days when treated with 500 $\mu$ g SMV-loaded collagen sponges (Wong & Rabie, 2003). Xue et al. demonstrated *in vivo* bone formation after 8 weeks, stimulated by locally delivering 4mg SMV via chitosan nanoparticles in rat calvaria (Xue et al. 2019). As the ideal amount and release profile of SMV to stimulate good bone formation is not yet known, we aimed to investigate the effectiveness of different release profiles of SMV from our acylated membranes to stimulate good bone healing in a critical size bone defect.

The amount of drug released from the membranes could be controlled by changing the membrane treatment and or changing the initial loading amounts (Bumgardner, 2019). In this study, acylated (fatty acid treated) electrospun membranes were investigated for the delivery of SMV. Membranes were treated either with acetic anhydride (AA) or hexanoic anhydride (HA). In a previous *in vitro* release study, HA membranes released very low levels of SMV for a long period of time (>90 days), irrespective of the initial drug loading amount. AA membranes on the other hand released SMV at a much faster rate, over a shorter period of time (40 days) in proportion to the initial loading amount (V.P. Murali et al. 2019). These two membrane types were used to evaluate the osteogenic potential of a low sustained release and high rapid release of SMV *in vitro* and *in vivo*. Drug loaded membranes were evaluated with W-20-17 cells with

and without BMP-2 in culture media to evaluate the membrane's ability to stimulate ALP activity and induce mineralization. Critical size rat calvarial defect model was used to evaluate these membranes *in vivo* for 4 and 8 weeks. Retrieved tissue samples were analyzed for new bone formation using micro-computed tomography (micro-CT) analysis, stained with H&E and scored for inflammation.

### **3.2. Materials & Methods**

#### **3.2.1. Materials**

Chitosan with 71% DDA and 311 kDa molecular weight was purchased from Primex. Trifluoroacetic acid (TFA), dichloromethane (DCM), pyridine, and fatty acids were bought from Sigma and Fisher. SMV was purchased from Cayman Chemicals. W-20-17 cells (W-20 clone 17 (ATCC® CRL-2623™)) were obtained from ATCC and cultured as per ATCC instructions. Reagents for cell culture were bought from Fisher. Rh-BMP-2 was obtained from GoldBio.

#### **3.2.2. Electrospinning**

Chitosan membranes were fabricated by electrospinning in an in-house spinning setup, as described previously (Norowski Jr et al. 2015; Norowski et al. 2012; Su et al. 2016; Wu et al. 2014). Briefly, a 5.5% (w/v) chitosan (71% DDA, MW: 311.7kDa) solution was made in 70% TFA and 30% DCM, loaded into 10 ml syringe with a 20-gauge blunt needle and electrospun at 27 kV using a syringe pump onto an aluminum foil covered plate rotating at ~ 8.4 rpm. Three 10ml volumes of chitosan solution were spun consecutively to produce membranes of

approximately  $0.7 \pm 0.1$  mm thickness and 15cm diameters. The electrospinning apparatus was housed inside a ventilated box which was vented to the fume hood. The apparatus was operated at room temperature and at 40-60% humidity.

### *3.2.3. Post-spinning treatment*

The as-spun membrane was punched into small 1cm diameter discs and soaked in a pyridine-fatty acid (v/v) (50-50) solution at 5mg/ml for 1.5 hours (Wu et al. 2014). The fatty acids used were either acetic anhydride (AA) or hexanoic anhydride (HA). Next, the membranes were washed in 1L MQ water ( $18M\Omega@25^\circ$ , Integral 15, Millipore) to remove the unreacted and excess reagents. Water was changed every 24 hours for 3 days, after which the membranes were freeze-dried.

### *3.2.4. SMV loading & release study*

Since AA membranes released SMV at a fast rate, to avoid potential toxicity a release study was performed using AA membranes loaded with  $10\mu\text{g}$  SMV ( $n=4$ ). The release profile of other membranes has been reported elsewhere (Bumgardner, 2019; V.P. Murali et al. 2019). Membranes were made aseptic by rinsing in 70% ethanol and letting them dry under UV light for one hour. AS SMV is very hydrophobic, stock of SMV solution was made in 200 proof ethanol and loaded onto the membranes passively. The volume of SMV stock added onto the membranes was kept to a minimum to ensure complete absorption by the membranes. Membranes were left to dry for 20 to 30 minutes before placing them in 48-well plates and adding 0.5 ml of PBS. PBS was replaced every day for the first week and then every other day for the next 28 days. The

collected samples were stored at -20°C for further analysis. An isocratic HPLC method was used to analyze the amount of SMV released from the membranes. SMV was detected at 236 nm using a UV-VIS detector, a solvent phase of 0.1% TFA: acetonitrile (30:70) and injected at a flow rate of 1ml/min (Asafo-Adjei et al. 2017). The amount of sample injected was 10µl and was detected using a Hypersil GOLD column (dim-150 X 4.6mm) with a particle size of 5µm (ThermoScientific™), heated to 30°C. Since SMV is insoluble in aqueous solvents, standards were made in PBS-ethanol (1:1) solutions. To maintain consistency between samples and standards, the samples were also diluted with ethanol that was spiked with SMV. The spike SMV was added to compensate for any drug loss during dilution, which might result in negative values. SMV readily hydrolyzes when in aqueous environment, giving rise to three separate PLC peaks for hydroxy-acid, lactone, and dimer forms. Area under all these three peaks were added and used to calculate the total concentration of SMV in the eluates. peaks for hydroxy-acid, lactone, and dimer forms. Area under all these three peaks were added and used to calculate the total concentration of SMV in the eluates.

### *3.2.5. Cell culture*

W-20-17, preosteoblast mouse bone marrow stromal cells, were grown and maintained in Dulbecco's Modified Eagle media (DMEM) with 10% FBS and 1% PSN (5 mg of penicillin, 5 mg of streptomycin, and 10 mg of normycin per ml in 0.85% saline, Gibco™, Molecular Probes™). Cells were cultured in T75 flasks (Nunc™ EasyFlask™, vented) and placed in an incubator supplied with 5% CO<sub>2</sub> at 37°C. The culture medium was changed every two days and

the cells were passed when the flask reached 80-90% confluency. Cells used for cell culture experiments were between passage number 4 and 8.

### *3.2.6. Cell viability assay to monitor membrane toxicity*

Membrane toxicity was evaluated by non-contact culture using Falcon™ cell culture inserts (0.45 µm pore size PET membrane, 24 well format). Cells were seeded in 24 well plates at  $5 \times 10^4$  cells/well and allowed to attach overnight. Following day, cell inserts containing non-loaded and SMV loaded membranes were placed in the well plates. AA membranes loaded with 0 (AA0), 10 (AA10) and 50 (AA50) µg SMV and HA membranes loaded with 0 (HA0) and 50 (HA50) µg SMV were evaluated for membrane toxicity. Each membrane was tested in quadruplicates. Cells grown in medium with no membrane was used as the control. After 1, 3, and 7 days, membrane toxicity was analyzed by measuring cell viability using CellTiter-Glo® Luminescent Cell Viability Assay (Promega Corporation).

### *3.2.7. Cell responses to SMV loaded chitosan membranes*

Cells were seeded in 24 well plates at  $1 \times 10^5$  cells/well and left to attach overnight. On the next day, cell inserts containing non-loaded and drug loaded membranes were placed in the 24 well plates. Cells were cultured in DMEM supplemented with 10% FBS, 1% PSN, 5mM beta-glycerophosphate and 50µg/ml ascorbic acid (regular media). To enhance cell response and to see any potential positive effect of SMV on BMP-2, cells were also cultured in regular osteogenic media containing SMV and spiked with 25ng/ml BMP-2 (BMP-2 media). After 1, 7, 14 and 21 days, the supernatant media from all the wells was collected and stored at -20°C for

osteocalcin (OCN) detection. The cells were lysed by adding 300 $\mu$ l of molecular grade water to each well and freeze-thawing the plates three times. These lysates were used to measure double stranded DNA (dsDNA) via the Quant-iT PicoGreen assay kit (Invitrogen) and ALP activity of the cells using the QuantiChrom™ alkaline phosphatase assay kit (DALP-250, BioAssay Systems). ALP activity of cells was normalized to DNA (ng/ml) and expressed as IU/ng. Amount of OCN expressed by the cells was measured using an OCN ELISA kit (eBiosciences, Austria) and expressed as ng/ml. Amount of OCN expressed by the cells was measured using an OCN ELISA kit (eBiosciences, Austria) and expressed as ng/ml.

Additional plates were made for days 14 and 21 to carry out the calcium deposition assay. After the designated time points, medium was completely removed from the wells and the cell layers were carefully washed twice with 500 $\mu$ l of warm PBS. 500 $\mu$ l of 0.5N acetic acid was added to each well and the plates were placed on a rotary shaker (Belly Dancer™, Stroval, life science Inc., Greensboro, NC, USA) at moderate speed for 24 hours to solubilize the deposited calcium. After 24 hours, the entire well content was transferred to labelled microcentrifuge tubes and frozen at -20°C until ready to assay for amount of calcium deposition based on the o-cresolphthalein complexone reaction using the Calcium Reagent Kit (Pointe Scientific, Inc). Amount of calcium ( $\mu$ g/ml) present in the samples was calculated using manufacturer's instructions and normalized to the amount of DNA. The normalized calcium values were expressed as (mg/ng). On day 21, one well from each group was not solubilized for calcium assay and were stained with Alizarin Red S staining to qualitatively determine the amount of

calcium mineral content within the cell layers. The well plates were then imaged using Nikon Eclipse TE300 at 4X magnification.

### 3.2.8. *Experimental animal model*

A calvarial defect model using male Sprague-Dawley rats (~2mon old and ~370 g) was used to evaluate barrier function and the ability of SMV loaded membranes to support bone growth/healing as compared to non-loaded membranes. The *in vivo* study protocol was reviewed and approved by the University of Memphis IACUC committee (protocol #0791). In this study, two 5 mm defects were created on either side of the mid-suture line in each animal. Each defect was covered with either a SMV-loaded membrane or a non-loaded membrane in a paired experimental design. The test membrane groups were AA0-AA10, AA0-AA50 and HA0-HA50. Healing of the defects was evaluated at 4 and 8- week time points. There were eight animals per group per time point for a total of 72 animals. All chitosan membranes were ethylene oxide sterilized for 24 hours at ambient temperature (Anprolene AN 74j, Anderson Products, USA) with 2 hours of degassing process. Endotoxin extraction was performed based on a previously established protocol in which the membranes were incubated in endotoxin free water for 24 hours at 60°C under mild stirring and the extracted water was tested using a Pierce LAL Chromogenic Endotoxin Quantitation kit (Thermo Scientific) (Nakagawa et al. 2003). Test SMV membrane groups were loaded with SMV under aseptic conditions, 2 hours prior to implantation.

For surgery, animals were first anaesthetized with 1% isoflurane gas (in an oxygen carrier) via a mask. Then the surgical site was shaved and cleaned with betadine and 70%



ethanol (Figure 3-1(a)). A midline incision in the skin over the cranium was made from the middle of the nasal bones to the posterior nuchal line (~20 mm) (Figure 3-1(b)). The underlying soft tissue and periosteum were incised and reflected to expose the calvaria (Figure 3-1(c)). Two 5mm circular defects were made diagonally on either side of the mid suture line (Figure 3-1(d)). A trephine burr (5mm diameter, titanium alloy (6Al-4V ELI), Ace surgical supply co, inc.) and a low speed dental drill (NSK Surgic Pro surgery system) with sterile saline irrigation was used to make the defects. After the cranium disks were carefully dissected avoiding dural perforations (Figure 3-1(e)), one SMV loaded and one non-loaded membrane was randomly placed on top of each defect (Figure 3-1(f)). A suture was made on top of the membranes to secure them in place (Figure 3-1(f)). Then the periosteum and skin were closed using resorbable polyglycolic acid (PGA) suture (Butler Schein) (Figure 3-1(g)). 0.5ml carprofen was administered for 2 days postoperatively. After 4 and 8 weeks, 8 rats per group were euthanized by CO<sub>2</sub> inhalation and calvarial tissue along with the membranes was harvested for micro-CT analysis and histological evaluations.



**Figure 3-1:** Surgical procedure for implanting chitosan membranes on rat calvaria. (a) surgical site was shaved and cleaned; (b) a midline incision in the skin over the cranium was made; (c) underlying soft tissue and periosteum were incised and reflected to expose the calvaria; (d & e) two 5mm defects were made diagonally on either side of the mid suture; (f) one drug loaded and

one non-drug loaded membrane was placed on top of each defect and secured in place using a suture; (g) the periosteum and skin were sutured up and the defects left to heal for 4 or 8 weeks.

### *3.2.9. Tissue processing, micro-CT and histologic evaluation*

After euthanasia, the defect site and surrounding bone were carefully dissected and placed in 10% formalin solution and refreshed every 24 hours for 3 days. After fixing, all specimens were scanned on a Scanco  $\mu$ CT40 scanner (Scanco Medical, Bassersdorf, Switzerland) at an energy level of 55 kV, and intensity of 72  $\mu$ A. The data were reconstructed using Scanco Image processing software. Dataviewer software (Bruker AXS Inc.) was used to reorient the reconstructed micro-CT graphs to align the principal axes of the dataset with the principal axes of the calvarial defect along the centronal direction of the cylinder. For each sample, region of interest was identified as a cylinder that corresponded and overlapped with the shape, volume and location of the original defect. Height of cylinder was extended 0.1 - 0.2 mm superior and inferior to the defect to allow for accurate measurements. Analyses for percent volume of new bone formed to total defect volume, was carried out using Bruker Micro-CT Analyser.

Samples were then decalcified and cut in the sagittal direction. Each half of the skull was further cut into two halves through the middle of the defects. The sections were stained by a hematoxylin and eosin (H&E) stain. All the histology slides were graded using a 5-point system for inflammation (0 = absent, 1 = minimum, 2 = mild, and 3 = moderate and 4= severe inflammation) (Macleod et al. 2005). A score of 0 was considered as a total absence of neutrophils, lymphocytes and macrophages. A score of 1 showed primarily very few lymphocytes with very few neutrophils, A score of 2 showed a greater number of lymphocytes

and neutrophils as well as some minor macrophages and focal foreign body reaction. A score of 3 was characterized by greater presence of macrophages, lymphocytes and foreign body reaction, especially the foreign body response. A score 4 was typically determined by even greater numbers of lymphocytes, macrophages and significant foreign body reaction with heavy abscess formation. Histology slides were observed by Nikon Eclipse TE300, and were analyzed for inflammation, bridging of the defect by new bone formation and degradation of membranes by Bioquant Osteo II software (Bioquant Image Analysis Corporation). For samples where membrane could not be seen, the most probable location of the membrane was assumed and the tissues around that region were scored.

#### 3.2.10. Statistical analysis

All data are presented as mean  $\pm$  standard deviation, except where mentioned otherwise. Significant differences in cytotoxicity of membranes, and *in vitro* bioactivity analyses were analyzed by one-way ANOVA followed by Tukey post hoc test. For animal studies, paired t-tests were used to compare differences in percent bone fill in defects between loaded and non-loaded membranes of the same treatment for a given time point. For comparing different membranes over time, one-way ANOVA followed by post hoc analysis was used. The differences in groups and experimental time points at any time were considered significant if  $p < 0.05$ . For inflammatory scores, the 95% confidence intervals were calculated, and groups for which the intervals did not overlap were considered to be significantly different.

### 3.3. Results

#### 3.3.1. SMV release study

Figure 3-2 shows the release of SMV from AA treated membranes loaded with 10 $\mu$ g of SMV. The cumulative release showed 50% of the loaded drug releasing out by day 5 (Figure 3-2(a)). The daily release from these membranes showed a burst release of 4 $\mu$ g/ml SMV on day 1 which reduced to 0.3 $\mu$ g/ml by day 5 (Figure 3-2(b)). After day 7 there was no detectable amount of drug releasing out of the membranes for the rest of the study.

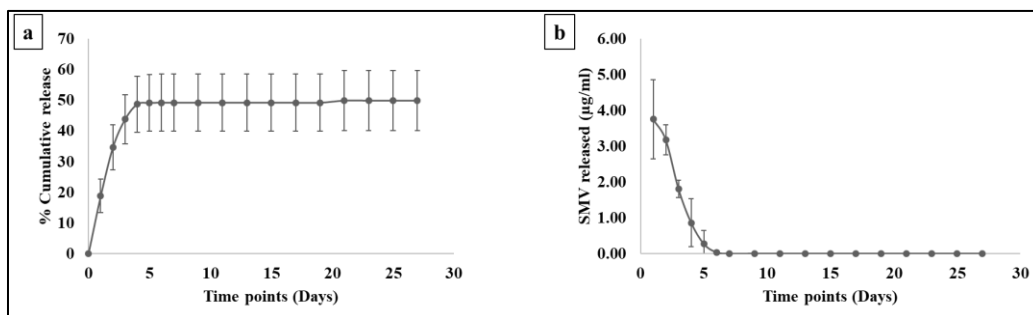


**Figure 3-2:** *In vitro* release profiles of SMV from AA treated chitosan membranes over a 4 week period. The cumulative release (a) and daily release (b) amounts of SMV were determined using a HPLC method at 236nm. Initial amount loaded in the membranes was 10 $\mu$ g. Each value represents the mean  $\pm$  standard deviation (n=4).

#### 3.3.2. Cell viability assay

The results of cell viability and growth over 7 days with the AA (0, 10 & 50) membranes and HA (0 & 50) membranes are shown in figure 3-3. Results are reported as percent of cell in control wells that did not contain membranes. Only cells exposed to AA50 membranes showed a statistically significant reduction in cell viability at each time point ( $p < 0.05$ ). There were no statistical differences in percent viability and growth of cells between the AA0, AA10, HA0 and HA50 membranes ( $p > 0.05$ ).

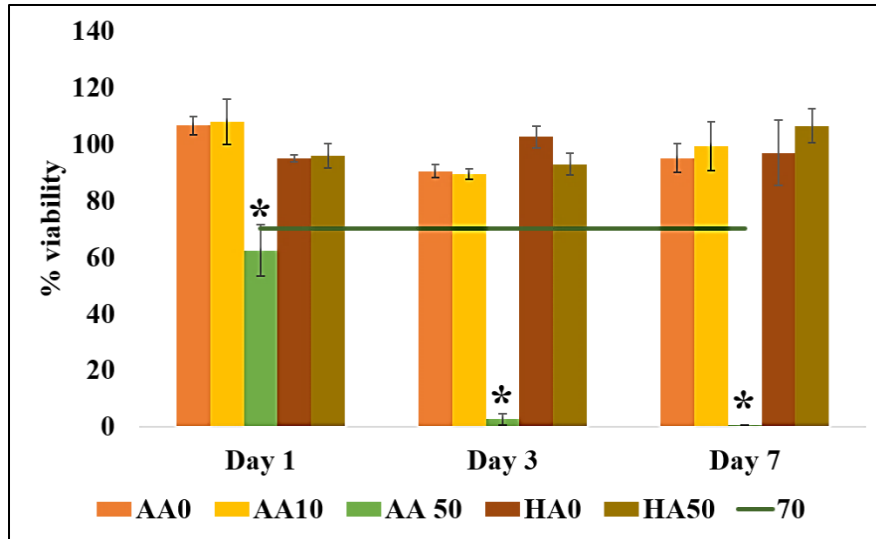


**Figure 3-3:** Cell viability of W-20-17 cells grown in the presence of different membranes and expressed as % viability as compared to cells grown on tissue culture plastic. Each value represents the mean  $\pm$  SD ( $n=4$  per each group). \* denotes significant difference among groups at a given time point ( $p<0.05$ ). The horizontal line represents 70% cell viability, which is the minimum viability required to be supported by a device to be cytocompatible, according to ISO standard

### 3.3.3. *In vitro* osteogenic evaluation of SMV loaded membranes

Since AA50 membranes showed significant toxicity from day 1, they were not included further in the *in vitro* experiments. Results for the evaluation of ALP activity, expression of OCN and terminal mineralization of W-20-17 cells are shown in Figures 4-7. Figure 4 shows that the ALP activity of all the groups increased over the period of 21 days. In regular medium group (Figure 3-4(a)), on day 7, cells grown with HA50 membranes showed significantly higher ALP activity than the control ( $p=0.01$ ). Cells grown with AA10 membranes showed a drop in activity which was recovered by day 14. On days 14 and 21, though the SMV loaded membranes, AA10 and HA50, appeared to stimulate more ALP activity than their corresponding non-loaded membranes, no groups were significantly different from each other and the control. In BMP-2 media group (Figure 3-4(b)), similar to regular media group, on day 7, AA10 membranes

showed lowered ALP activity which was recovered by day 14. On day 14, AA0 and HA0 groups had significantly less ALP activity than the control, whereas the loaded membranes and control had similar activities. By day 21, all the membrane groups showed lowered ALP activity than the control. Different amounts of initial drug loading (10 or 50 $\mu$ g) did not seem to affect the ALP activity significantly.

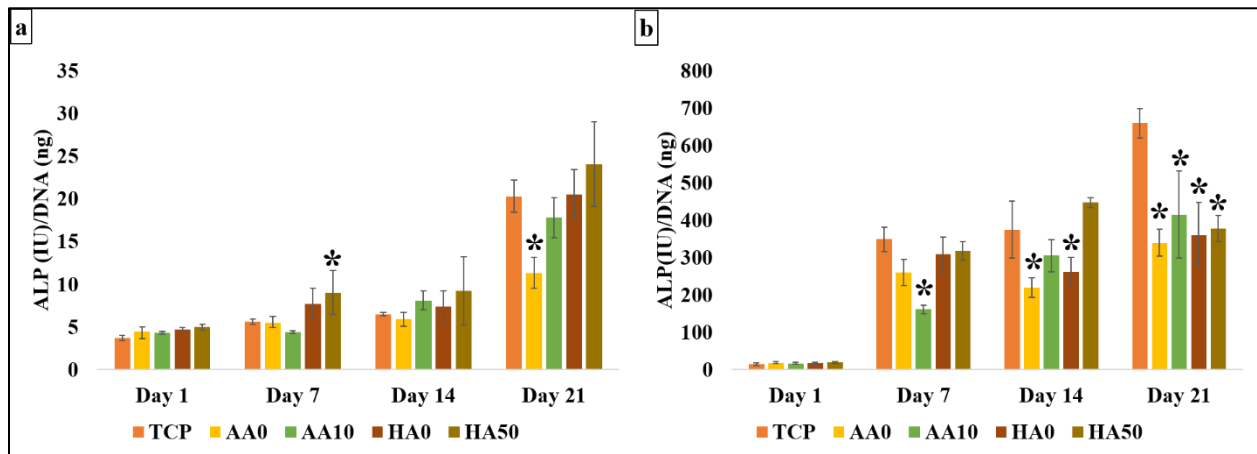


**Figure 3-4:** ALP activity by W-20-17 cells in regular medium (a) and 25ng/ml BMP-2 medium (b). AA0, AA10, HA0 and HA50 membranes were evaluated for their osteogenic potential and compared with controls. Each value represents the mean  $\pm$  SD (n= 4 per each group) \* represents significant difference between membrane group and control.  $p < 0.05$  was considered to be statistically significant.

Measurement of OCN expression by the cells, revealed no significant differences among the groups on day 7 (Figure 3-5). An increase in OCN levels was seen on day 14, which dropped by day 21. On day 14, with the exception of HA50 groups, all regular media groups expressed significantly higher OCN levels than their corresponding BMP-2 media groups. By day 21, even the HA50 regular media group expressed significantly higher OCN than the corresponding BMP-2 media group.

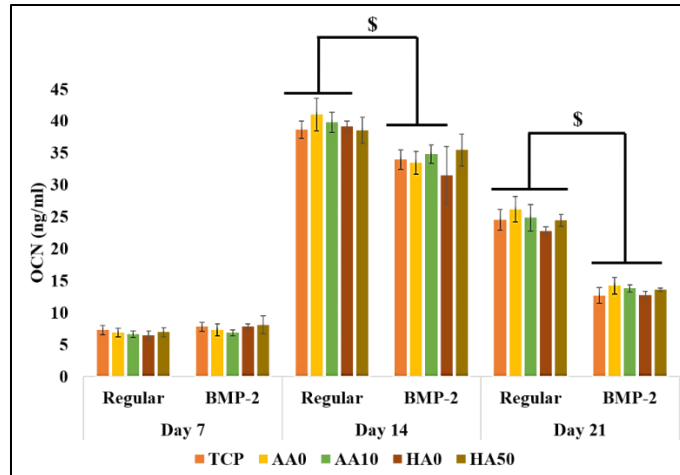


**Figure 3-5:** OCN expression by W-20-17 cells in the presence of AA and HA loaded and non-membranes grown in regular or BMP-2 medium. Each value represents the mean  $\pm$  SD (n= 4 per each group). \$ represents significant difference between regular and BMP-2 media groups.

As a measure of terminal differentiation, amount of calcium deposited by the cells was quantified (Figure 3-6). In regular media groups, on days 14 and 21, AA10 membrane groups deposited less calcium than other groups. On day 21, AA0 membrane groups deposited significantly lower calcium than the control. Only the control and HA50 membrane groups showed statistically significant increase in calcium levels from day 14 to 21. In BMP-2 media groups, similar to ALP activity, AA10 and HA50 groups appeared to stimulate more calcium deposition, but none of the groups were significantly different. All groups showed significantly higher calcium deposition on day 21 than day 14. All the BMP-2 groups showed significantly higher calcium deposition than regular media groups. This was also evident with alizarin red s staining of the well plates (Figure 3-7). All the BMP-2 groups stained much darker than the regular media groups.

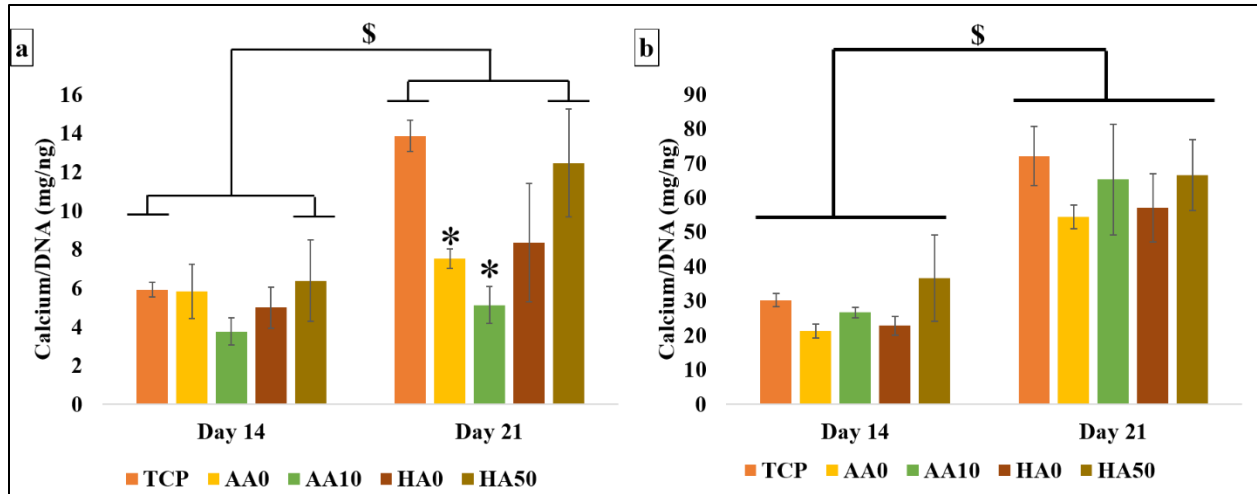


**Figure 3-6:** Calcium assay to quantify the amount of calcium deposited on W-20-17 cells in regular osteogenic media (a) and 25ng/ml BMP-2 supplemented osteogenic media (b). AA0, AA10, HA0 and HA50 membranes were evaluated for their osteogenic potential and compared with controls. Each value represents the mean  $\pm$  SD (n= 4 per each group). \*represents significant difference between membrane group and control; \$ represents significant difference between day 21 vs day 14 for corresponding groups. p<0.05 was considered to be statistically significant.

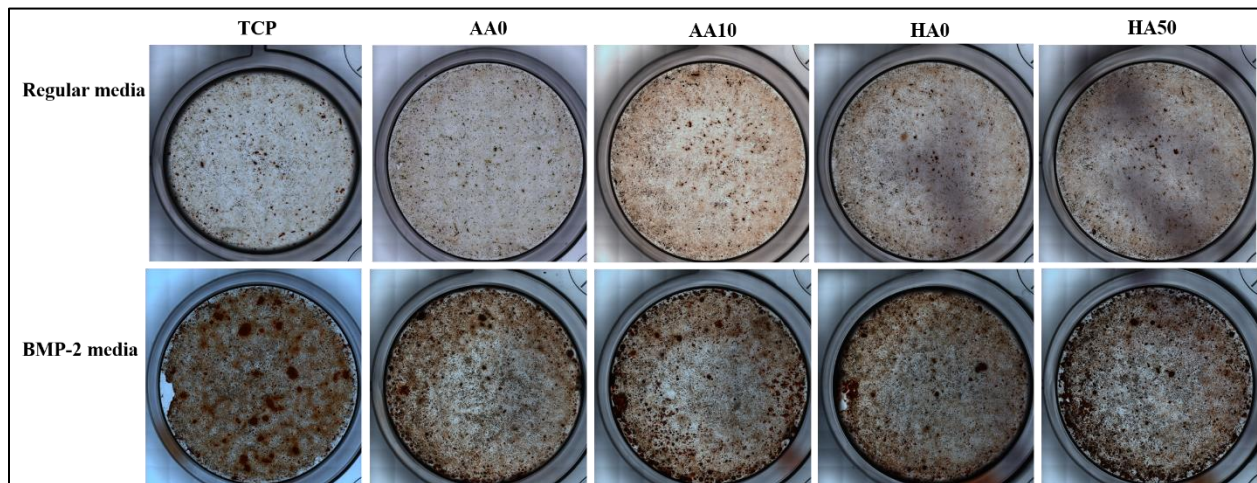


**Figure 3-7:** Representative Alizarin red S staining of the well plates after 21days of mineralization study. All the BMP-2 groups stained darker than the regular media groups.

### 3.3.4. Membrane endotoxin levels, animal surgery and clinical observations

Endotoxin levels of AA and HA membranes were found to be  $0.015 \pm 0.005$  EU/ml and  $0.0004 \pm 0.0002$  EU/ml, respectively, before and after sterilization. This level is much lower than



the FDA approved limit of 0.5EU/ml. Surgeries were uneventful with all animals recovering and defects healing without complications except for two that did not recover due to excessive post-operative bleeding and intra-operative brain damage.

At 4 weeks, sites were well healed in all groups except the AA10-AA0 group which still exhibited some minimal scabbing at the surgical site. Gross examination of retrieved tissue samples did not show any signs of infection or inflammation for any of the test groups. However, two rats with AA10-AA0 membranes, and one rat each of AA50-AA0 and HA50-HA0 membranes had brain swollen into the defect site. HA membranes were still visible over the defects, but none of the AA membranes were noticeable. At the 8 week time point, all rats healed completely with no signs of scabbing. Gross examination of retrieved tissues showed no signs of infection and inflammation. Only one AA0-AA10 membrane rat had the brain swollen into the defect site.

Animals that had either such brain damage/swelling, excessive bleeding during surgery or cracked calvaria during tissue retrievals were excluded from all analysis. Among week 4 animals, two rats with AA10-AA0 membrane, one with AA50-AA0 membrane, and one with HA50-HA0 were excluded due to brain swelling and one rat with AA10-AA0 and one with AA50-AA0 membranes were excluded due to cracked calvaria. From week 8 animals, one AA10-AA0 membrane rat was excluded due to brain swelling and one HA50-HA0 membrane rat was excluded due to excessive bleeding.

### 3.3.5. Histological evaluation of membrane degradation and biocompatibility

At week 4, all samples showed normal wound healing response with mild inflammation (Table 3-1). There were no significant differences in the inflammatory responses towards drug loaded and non-loaded membrane groups. Figure 3-8 shows representative image of a defect covered with AA membrane. Degradation/resorption of AA membranes was observed in all cases. The membranes were infiltrated with fibroblasts and monocytic cells (Figure 3-8(a)). Granulation tissue with monocytic cells were seen at the defect site (Figure 3-8(b)). In some cases, few neutrophils and plasma cells were observed.

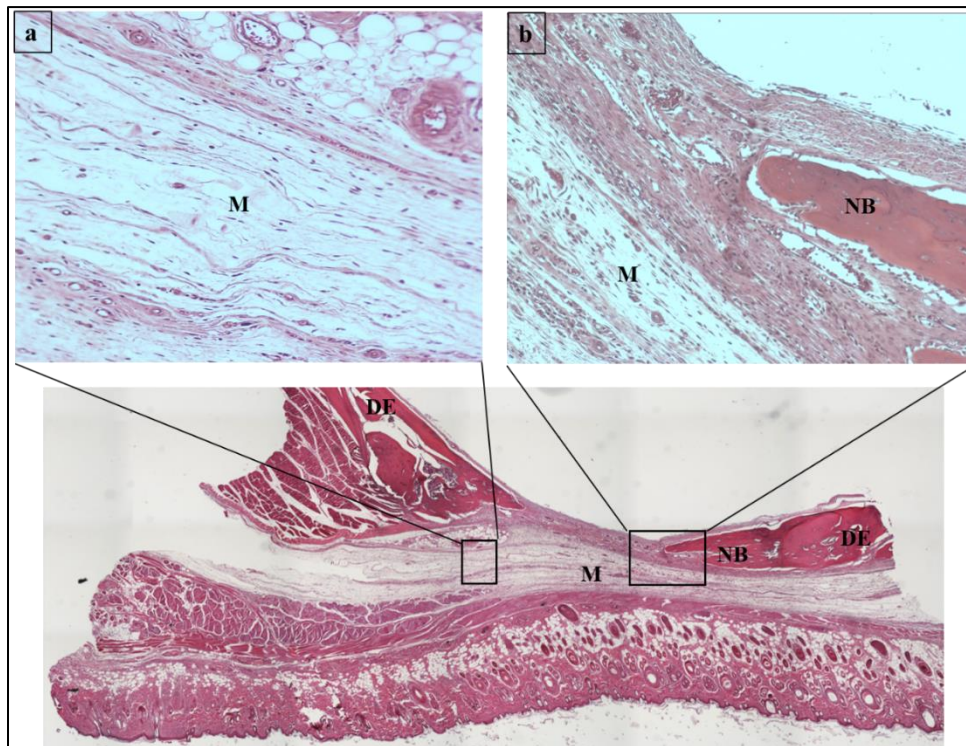


**Figure 3-8:** Representative image of a 4 week defect covered with AA membrane. New bone appeared to grow along the defect edges. Early degradation of AA membranes caused soft tissue infiltration at the defect site. Insets show (a) membrane infiltrated with monocyte and fibroblasts and (b) granulation tissue formation at the defect site. M indicates the membrane region; NB indicates new bone formed; DE indicates defect edge.

HA membranes on the other hand, appeared quite intact with very minimum cellular infiltration into the membranes but were surrounded by monocytic cells (PMNs) (Figure 3-9). There was minimum soft tissue infiltration into the defect site. New bone formed along the membranes, across the defect. Many of the HA membranes showed complete bone bridging.

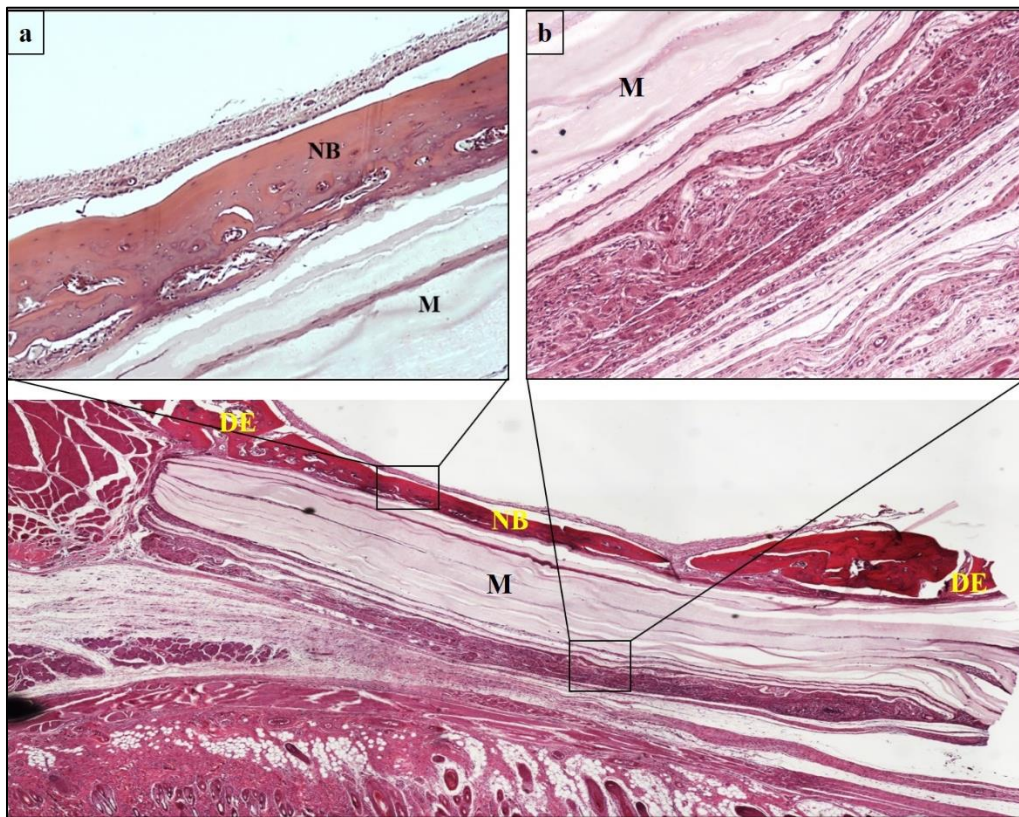


**Figure 3-9:** Representative image of a 4 week defect covered with HA membrane showing bone bridging and minimum soft tissue infiltration at the defect site. Insets show (a) new bone formed across the defect (b) PMNs surrounding the membrane as part of the foreign body response. M indicates the membrane region; NB indicates new bone formed; DE indicates defect edge.

Defects with AA50 membranes showed more bone formation than AA10 and AA0 membranes. Among HA and AA membranes, more bone appeared to form along the HA membranes.



By 8 weeks, the inflammation was further resolved. In rats with AA membranes, dense connective tissue with large number of fibroblastic cells and few monocytic cells was present at the defect sites (Figure 3-10). The membranes were completely resorbed and were replaced by connective tissue with fibroblasts. All the AA membranes showed good amount of bone formation along the defect edges, but none of them resulted in complete defect bridging. No significant differences were noticed in drug loaded and non-loaded membranes.

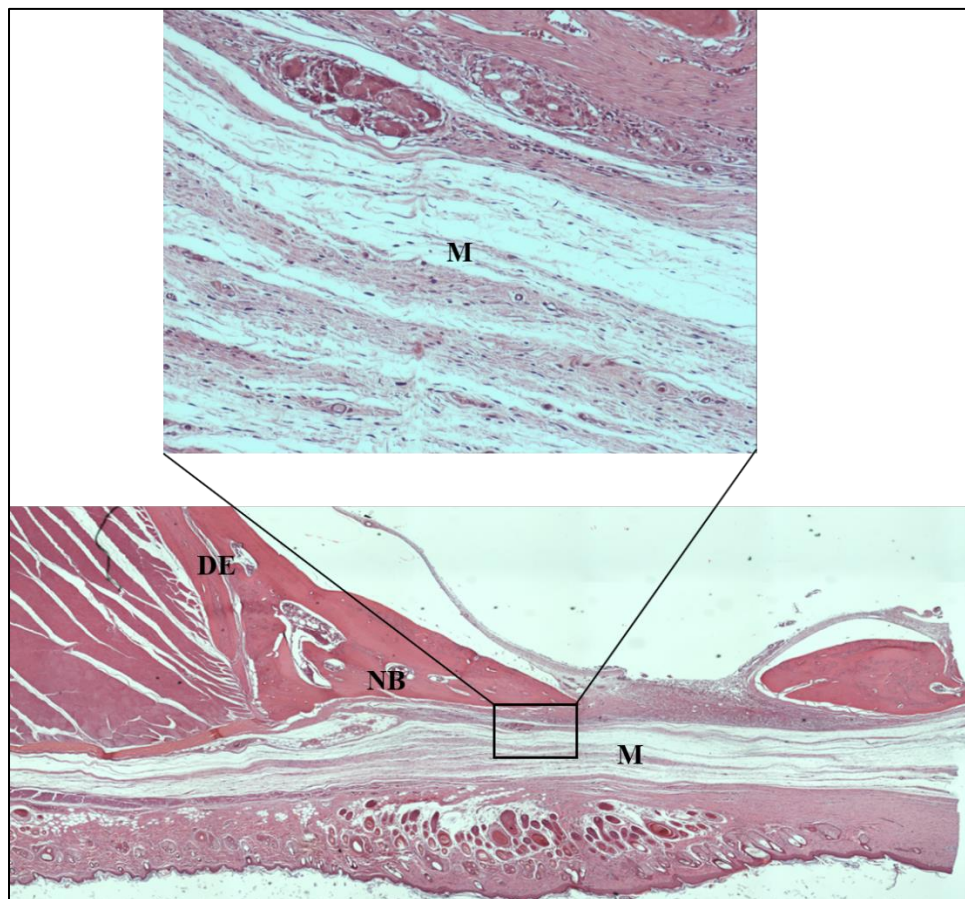


**Figure 3-10:** Representative image of an 8 week defect covered with AA membrane showing new bone formation along the edges and dense connective tissue at the defect site. Inset shows complete resorption of the membrane and presence of connective tissue at the membrane site. M indicates the membrane region; NB indicates new bone formed; DE indicates defect edge.

Drug loaded and non-loaded HA membranes showed signs of resorption with monocytic cells infiltrating them (Figure 3-11). Area around the membranes showed formation of granulation tissue with minimum inflammatory response (Figure 3-11(a)), The defect site however was still protected from soft tissue infiltration (Figure 3-11(b)). All the HA membranes showed bone bridging across the defect site (Figure 3-11((a)). HA50 membranes stimulated more bridging than HA0 membranes.

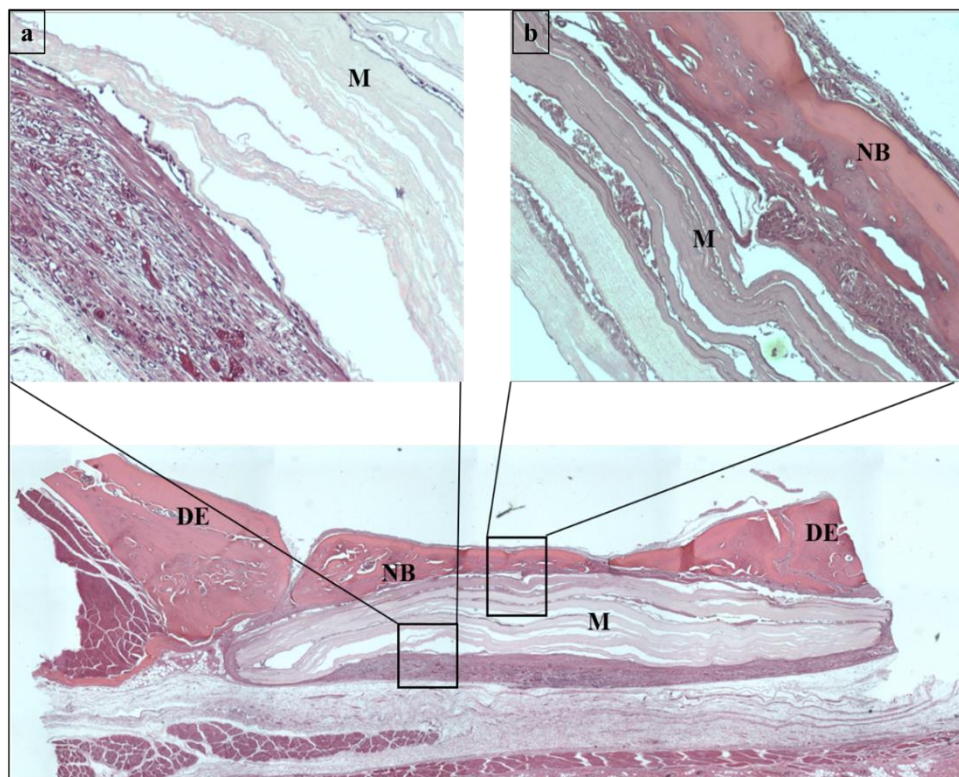


**Figure 3-11:** Representative image of an 8 week defect covered with HA50 membrane showing bone bridging across the defect site. Insets show (a) minimum inflammatory response to HA membranes and (b) monocytic infiltration into the membranes and new bone forming along the membranes. M indicates the membrane; NB indicates new formed; DE indicates defect edges.

All samples were scored on a scale of 0-4 for inflammation. Table 3-1 summarizes the confidence interval range and averages of the inflammatory scores for each membrane type at each time point. At the week 4, all membranes showed very mild inflammatory responses. The

inflammatory scores were not significantly different between loaded and non-loaded membranes for all groups. Three tissue samples (all HA groups) with excessive scabbing received extremely high inflammatory score (>3.5) due to discontinuity in the skin which might have caused the inflammation. These groups were excluded from the analysis. At the end of week 8, inflammation in the tissues resolved. Though the HA membranes were still present, it did not result in a higher inflammatory score. The inflammatory scores between week 4 and 8 were also not significantly different for any group.

**Table 3-1:** The 95% confidence intervals of inflammatory response scores of AA and HA membranes with and without SMV in 5mm rat calvarial defect model. Each value represents the confidence interval and (mean).

<b>Membrane type</b>	<b>Week 4</b>	<b>Week 8</b>
<b>AA0</b>	0.58-1.62 (1.1)	1.00-1.75 (1.75)
<b>AA10</b>	0.29-1.91 (1.1)	0.85-1.44 (1.14)
<b>AA0</b>	0.90-1.44 (1.2)	1.09-1.79 (1.44)
<b>AA50</b>	0.45-1.88 (1.2)	1.06-1.88 (1.47)
<b>HA0</b>	1.09-2.51 (1.8)	0.57-2.07 (1.32)
<b>HA50</b>	0.24-3.36 (1.8)	0.50-2.21 (1.36)

### 3.3.6. Micro-CT analysis for new bone formation

Micro-CT images of reconstructed rat calvaria show bone growing in to and filling defects covered by all membranes at both 4 and 8 weeks (Figure 3-12). At week 4, HA membranes showed signs of bone bridging but were not completely bridged. The AA membranes stimulated more bone growth from the defect edges. Images of week 8 show extensive bone bridging by all of the HA50 membranes and four of the HA0 membranes. Though AA10 and

AA50 membranes showed good amount of healing, the new bone appeared to form along the defect edges. None of the AA groups showed bone bridging. Results of micro-CT analysis for percent bone fill is shown in Table 3-2. Data analyses using paired t-tests indicated significantly more bone formation by AA50 membranes ( $31.01 \pm 5.88$ ) than corresponding AA0 membranes ( $18.53 \pm 13.73$ ) ( $p=0.037$ ) at week 4 time point. Amount of bone formed by AA10 ( $23.91 \pm 10.11\%$ ) and AA0 ( $13.06 \pm 6.95\%$ ) ( $p=0.10$ ) and HA50 ( $31.89 \pm 12.08\%$ ) and HA0 ( $41.84 \pm 18.97\%$ ) ( $p=0.53$ ) were not statistically different between the corresponding loaded and non-loaded membranes. By week 8, HA50 membranes showed more %bone fill than AA50 and AA10 membranes. However, %new bone formed in loaded and non-loaded membranes were similar for all the corresponding loaded and non-loaded groups. Among the HA50-HA0 group, %new bone formed in the presence of HA50 membrane in one of the animals was significantly lower than the other samples of the same group (<than median -1.5IQR). If this value was excluded from the statistical analysis, a significant difference would be detected between the bone formed by HA50 and HA0 membranes ( $p=0.03$ ).

**Table 3-2:** Micro-CT results for bone healing with membranes in 5 mm rat calvarial defects at 4 and 8 weeks. Each value represents mean  $\pm$  standard deviation of % new bone formed in the defect area (new bone volume/total volume). \* represents significantly different from corresponding blank; **a** represents significantly different from week 4. (data within parenthesis shows the mean % bone fill of HA50 membranes at week 8 if one HA50 membrane value that was less than (median -1.5IQR), is neglected from the analysis).

<b>Membrane type</b>	<b>Week 4</b>	<b>Week 8</b>
<b>AA0</b>	13.06 $\pm$ 6.95	37.22 $\pm$ 16.53 <sup>a</sup>
<b>AA10</b>	23.91 $\pm$ 10.11	40.72 $\pm$ 13.03 <sup>a</sup>
<b>AA0</b>	18.53 $\pm$ 13.73	22.95 $\pm$ 16.89
<b>AA50</b>	31.01 $\pm$ 5.88 <sup>*</sup>	38.21 $\pm$ 11.26
<b>HA0</b>	41.84 $\pm$ 18.97	33.94 $\pm$ 29.66 57.00 $\pm$ 14.79 <sup>a</sup>
<b>HA50</b>	31.89 $\pm$ 12.08	(61.68 $\pm$ 8.86 <sup>*,a</sup> )

All the membranes showed an increase in the percent new bone formed over the 8-week period. AA10 and HA50 membranes showed significantly higher bone formation on week 8, compared to week 4. However, this was not seen for the AA50 membranes.



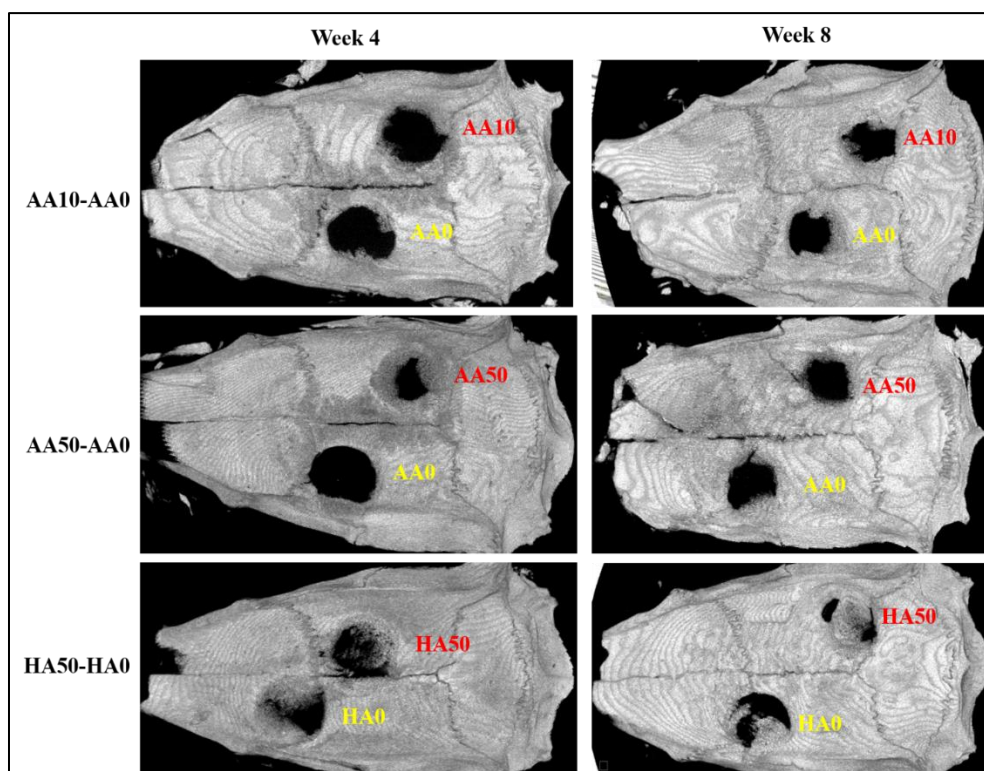


**Figure 3-12:** Representative micro-CT images of 5mm rat calvarial defects after 4 and 8 weeks of membrane implantation.

### 3.4. Discussion

Numerous studies have reported the osteogenic potential of SMV *in vitro* and *in vivo*. In this study, SMV was evaluated as an alternative or for adjunctive therapy with BMP-2. Electrospun chitosan membranes treated with fatty acids possess unique ability to control the release of SMV by modulating their hydrophobic behavior. Previously, more hydrophobic membranes have shown to release the drug in a slow and sustained manner for long time periods and membranes of less hydrophobic nature released the drug faster over a shorter time span (V.P. Murali et al. 2019). This work examined the ability of chitosan membranes to locally deliver SMV in an effort to increase bone healing and regeneration. Since the adequate dosage and

extent of drug release that would stimulate sufficient osteogenesis is not known, membranes with different release profiles were evaluated. Membranes tested in this work provided either fast release of low dose (AA10), fast release of high dose (AA50) or slow release of a high dose (HA50). The fast release of SMV from the AA membranes within one week was similar to the release pattern seen previously with these membranes at other different loadings (V.P. Murali et al. 2019). AA membranes being less hydrophobic, tend to swell more in aqueous environment, as compared to other fatty acid treated membranes, resulting in faster release of the loaded drug (Bumgardner, 2019).

According to ISO standard for biological evaluation of medical devices (Tests for *in vitro* cytotoxicity), membranes are considered non-cytotoxic if they support 70% or more cell growth as compared to the control group. In this study, with the exception of AA50 membranes, all others showed a cell viability of more than 70%, indicating non-toxicity of our membranes. The amount of drug released out of the AA50 membranes on day 1, around 10-12 $\mu$ g, may have been toxic to the cells. Another study where SMV- loaded chitosan nanoparticles were investigated, similar and higher amounts of SMV released from the particles did not show any toxicity to the bone marrow stromal cells tested (Xue et al. 2019). However, the same range of SMV was toxic to rat bone MSCs when delivered from hydroxyapatite (HAP) microspheres (Yu et al. 2017). The toxicity however depends on the cell type, age of cells and stage of cell proliferation. Further, some studies suggested that low amounts of SMV stimulated better bone formation *in vivo* than higher amounts (C.-Z. Wang et al. 2014; Zhou et al. 2010), which motivated the inclusion of an AA10 membrane group in the study.

ALP is an essential enzyme for mineralization and is considered to be an early osteogenic marker (Beck et al. 1998; Golub & Boesze-Battaglia, 2007; Mendes et al. 2004; Weinreb et al. 1990). The increase of ALP activity over the course of 21 days is very typical for the W-20-17 cells and these cells are known to have a dose-dependent response on ALP activity with increasing amounts of BMP-2 (Thies et al. 1992). Since SMV is known to stimulate osteogenesis by antagonizing TNF- $\alpha$  activity on BMP-2 (Yamashita et al. 2008), these cells were thought to be a good model to assess the osteogenic potential of the membranes. While for regular medium groups, ALP activity increased over time, a lowering of ALP activity in AA10 groups on day 7 could be attributed to the fast release of SMV from these membranes which might have had a negative effect on cells. However, further studies need to be carried out to understand the exact mechanism of action of SMV and SMV combined with BMP-2 on these cells. Since after day 7, no SMV remained in the membranes, the negative effect on the cells disappeared and the cells showed ALP activity similar to the control groups, by day 14. By day 21, AA10 and HA50 membranes showed a trend for increased ALP activity over non-loaded membrane groups, indicating the osteogenic potential of SMV. When membranes were combined with media containing BMP-2 to explore any adjunctive effects, the results were similar, in that there were no major differences in ALP activity of drug-loaded and non-loaded membranes. Interestingly in the BMP-2 medium groups, all the membrane groups showed lower ALP activity than the control. This was thought to be because of chitosan's ability to chelate BMP-2, thereby lowering its activity (Park et al. 2006).

OCN is a late osteogenic marker and is expressed by cells towards the later phase of differentiation. Peaking of OCN levels on day 14 and eventual drop by day 21 is typically seen in

bone cells (Kim et al. 2011; Malaval et al. 1999). However, the higher levels of expression by regular media groups than the BMP-2 media groups were contradicting to other *in vitro* experiments. Possibly, the OCN levels of BMP-2 groups might have peaked between days 7 and 14 and was undetectable since the plates were assayed only on these days.

In case of calcium deposition assay, lowered calcium deposition by AA10 membranes in regular media group is thought to be because of the absence of SMV in the culture media. Overall, cells grown with BMP-2 media showed higher mineralization ability which was slightly improved by the presence of SMV. Though the membranes were loaded with and released different drug amounts, their osteogenic potential were not significantly different. In a study reported by Wang et al., cationic polymeric nanoparticles containing SMV released almost 100% of the drug by day 7 but triggered higher ALP activity and calcium deposition by day 4 of incubation in bone marrow MSCs (Wang et al. 2014). These particles released a maximum of 5µg/ml SMV in the first three days, after which less than 500ng/ml of SMV was released (Wang et al. 2014). The amount of drug released out of these particles in the first few days was similar to the amounts releasing out of the AA10 membranes. Yu et al. reported an increased ALP and OCN expression of rat bone marrow MSCs by day 7 when they were incubated with SMV-loaded HAP microspheres (as compared to non-loaded spheres groups and cells alone control). The amount of SMV released from these particles was 1-2µg/ml till day 3, (Yu et al. 2017) which was similar to the amount of SMV released from the HA50 membranes. In another Xue et al. reported SMV loaded chitosan nanoparticles to stimulate significantly higher ALP activity in bone marrow stromal cells, than non-loaded particles only by day 14, since the daily release of SMV was close to only 0.2µg/ml (Xue et al. 2019). However, such low levels of SMV released

from HAP-PLGA particles triggered a higher ALP activity, OCN expression and calcium deposition in mouse MSCs within 3 days of culture (Tai et al. 2013). Because of this wide range of effective SMV dose *in vitro*, the ideal release profile of the drug is still not clear.

Rat calvarial defect model is considered to be an appropriate model for evaluating GBR membranes (Dupoirieux et al. 2001; Hong et al. 2010; J.-H. Kim & Kim, 2013; Song et al. 2014). Though AA50 membranes showed toxicity in cell cultures, the effect was thought to disappear *in vivo*, because of the more dynamic nature of the system, and thus was included in the animal study. Week 4 histological sections of tissue samples showed significant resorption of AA membranes, which can be associated with their less hydrophobic nature. Because AA membranes are more hydrophilic than HA membranes, they are thought to swell more, leading to more cellular infiltration, which could have caused faster membrane resorption. HA membranes were intact but surrounded by monocytic cells as part of the foreign body reaction. None of the membrane groups showed severe inflammation, indicating their biocompatibility. None of the drug loaded membranes showed more inflammation than non-loaded membranes, confirming the release of non-toxic levels of SMV. By week 8, the HA membranes started to show signs of resorption by cellular infiltration by monocytic cells, which may be due the fatty acids hydrolyzing from the polymer chain, thereby making the membranes hydrophilic and susceptible to the foreign body response. These results were similar to the study by Wu et al. and Ghadri et al., where membranes treated with butyric anhydride also showed minimum inflammatory response (Ghadri et al. 2018; Wu et al. 2017). In another study by Su et al. where chitosan membranes were made using a similar process but modified differently, the membranes still showed minimum inflammatory response *in vivo* (Su et al. 2016). Other studies with cross-linked

or neutralized nanofibrous chitosan membranes have also shown to induce a minimal to no inflammatory response when tested in animal (Norowski et al. 2012; Yeo et al. 2005).

From micro-CT analysis, at week 4 AA50 membranes stimulated significantly more bone than their corresponding AA0 membranes, which may be due to the faster release of high SMV dose from these membranes. Since there was no difference between the amount of bone formed by AA10-AA0 and HA50-HA0 membranes, this suggested that a fast release of high SMV dose is more beneficial in early defect healing than a fast release of low dose or slow release of high dose. By week 8, as most of the drug loaded in AA membranes was released by week 4 with almost complete resorption of the membrane, the amount of bone formed by AA50, AA10 and AA0 were not significantly different, though AA50 membranes still showed a trend of higher bone formation. However, since HA membranes released low amounts of SMV for longer time periods, the amount of bone formed by HA50 membranes was higher than HA0 membranes. It was interesting to note that the healing of HA membrane defects resulted in partial bone bridging by week 4 and complete bridging by week 8, whereas such a healing pattern was not observed in any of the AA membrane defects. This is attributed to the presence of intact HA membranes at the defect sites, which are thought to provide scaffolds for the bone cells to proliferate and deposit their bone matrix, thereby guiding bone regeneration all along their length, across the defect. However, in the case of AA membranes, because of early resorption of the membranes, a biomaterial scaffold was not available for the cells to regenerate across the entire defect. These defects followed the natural healing process, where new bone grew around the defect edges and eventually closed in on the defect site. A similar study by Ghadri et al. evaluated 250 $\mu$ g SMV loaded butyric anhydride (another short chain fatty acid) modified chitosan membranes for

guided bone regeneration application (Ghadri et al. 2018). The high dose of SMV did not have significant effect in bone healing, as the loaded and non-loaded groups showed similar bone regeneration, though the loaded membranes released 2-5 $\mu$ g SMV daily for the entire study period of 8 weeks (Ghadri et al. 2018). Similarly, in another study, tricalcium phosphate particles loaded with 100 $\mu$ g of SMV stimulated significantly more bone formation than particles loaded with 250 $\mu$ g SMV, in a rat calvarial defect model by 8 weeks (Nyan et al. 2009). However, the release kinetics of this system are not clear. Several such studies have shown SMV to stimulate bone formation when applied locally at the defect site via a carrier. The effects seem to depend on the carrier and the amount of initial loading. A study investigating SMV microspheres loaded collagen scaffold for bone regeneration, showed improved bone formation in rat calvaria by 8 weeks (Yu et al. 2017). Though the amount of SMV releasing out of these membranes was similar to our HA50 membranes (1-2 $\mu$ g/ml), the defects did not bridge completely, as seen with our membranes because of the resorption of the scaffold material (Yu et al. 2017). Tanigo et al. reported significantly more bone formation in rabbit tooth defect by gelatin hydrogels loaded with 10 $\mu$ g SMV than hydrogels loaded with 67 $\mu$ g SMV by 5 weeks, though most of the drug was released by 3 weeks, *in vitro* (Tanigo et al. 2010).

Overall, in this study, SMV loaded membranes showed higher %bone fill than non-loaded membranes. However, this effect was not significant in all cases and at all time points because of the large variations in the bone formed in each animal. The presence or absence of periosteum seemed to play a crucial role in the extent of bone regeneration. Defects that were covered with partial or intact periosteum after the surgery, showed a trend for more %bone fill than the defects without periosteum covering. Though utmost care was taken to keep the

periosteum intact, this was not possible in all the cases, because of the invasive nature of the surgery.

Typically bone grafts in the oral cavity heal within 3-6 months, depending on the defect size and graft material used. Therefore, membranes used for GBR applications are expected to stay intact for similar time frames. Keeping this in mind, the HA membranes appear to be a better option than the AA membranes. However, since the SMV releasing out of the membranes can stimulate faster bone regeneration, the grafted sites might heal faster and thus the membranes need not be present for so long. In this case, the AA membranes might be a better option, since they release more amount of SMV, leading to faster bone healing, and also resorb faster, not obstructing the bone growth in the defect site. Thus, this study along with other studies suggest that SMV can significantly affect bone formation and promote bone healing if delivered using an appropriate carrier and at appropriate dosing.

### ***3.5. Conclusion***

From this study, it can be concluded that SMV loaded electrospun chitosan membranes seem to have advantages for use as GBR membranes. Rate of bone healing can be controlled by controlling the amount and rate of SMV released from membranes. Fast release of high SMV dosage showed faster initial bone healing, whereas, slower release of high dose stimulated more bone formation in the later time points. Non-loaded membranes by themselves also stimulated and supported good bone formation, which was further enhanced by the addition of SMV. Next,



these membranes need to be tested in higher animal models, to further confirm their efficacy as GBR membranes.

## *References*

- Asafo-Adjei TA, Dziubla TD, Puleo DA. 2017. Tuning properties of poly (ethylene glycol)-block-poly (simvastatin) copolymers synthesized via triazabicyclodecene. *Reactive and Functional Polymers*. 119:37-46.
- Beck GR, Sullivan EC, Moran E, Zerler B. 1998. Relationship between alkaline phosphatase levels, osteopontin expression, and mineralization in differentiating mc3t3-e1 osteoblasts. *Journal of cellular biochemistry*. 68(2):269-280.
- . Development of electrospun chitosan membranes for guided bone regeneration. *International Association for Dental Research*; 2019; Vancouver, Canada.
- Dupoirieux L, Pourquier D, Picot M, Neves M. 2001. Comparative study of three different membranes for guided bone regeneration of rat cranial defects. *International journal of oral and maxillofacial surgery*. 30(1):58-62.
- Funkhouser HL, Adera T, Adler RA. 2002. Effect of hmg-coa reductase inhibitors (statins) on bone mineral density. *Journal of Clinical Densitometry*. 5(2):151-158.
- Ghadri N, Anderson KM, Adatrow P, Stein SH, Su H, Garcia-Godoy F, Karydis A, Bumgardner JD. 2018. Evaluation of bone regeneration of simvastatin loaded chitosan nanofiber membranes in rodent calvarial defects. *Journal of Biomaterials and Nanobiotechnology*. 9(02):210.
- Golub EE, Boesze-Battaglia K. 2007. The role of alkaline phosphatase in mineralization. *Current opinion in Orthopaedics*. 18(5):444-448.

Hong KS, Kim EC, Bang SH, Chung CH, Lee YI, Hyun JK, Lee HH, Jang JH, Kim TI, Kim HW. 2010. Bone regeneration by bioactive hybrid membrane containing fgf2 within rat calvarium. *Journal of Biomedical Materials Research Part A*. 94(4):1187-1194.

Kim J-H, Kim H-W. 2013. Rat defect models for bone grafts and tissue engineered bone constructs. *Tissue engineering and regenerative medicine*. 10(6):310-316.

Kim S, Tsao H, Kang Y, Young DA, Sen M, Wenke JC, Yang Y. 2011. In vitro evaluation of an injectable chitosan gel for sustained local delivery of bmp-2 for osteoblastic differentiation. *Journal of Biomedical Materials Research Part B: Applied Biomaterials*. 99(2):380-390.

Kuo SM, Chang SJ, Chen TW, Kuan TC. 2006. Guided tissue regeneration for using a chitosan membrane: An experimental study in rats. *Journal of Biomedical Materials Research Part A: An Official Journal of The Society for Biomaterials, The Japanese Society for Biomaterials, and The Australian Society for Biomaterials and the Korean Society for Biomaterials*. 76(2):408-415.

Macleod T, Williams G, Sanders R, Green C. 2005. Histological evaluation of permacol™ as a subcutaneous implant over a 20-week period in the rat model. *British journal of plastic surgery*. 58(4):518-532.

Malaval L, Liu F, Roche P, Aubin JE. 1999. Kinetics of osteoprogenitor proliferation and osteoblast differentiation in vitro. *Journal of cellular biochemistry*. 74(4):616-627.

Mendes SC, Tibbe J, Veenhof M, Both S, Oner F, Van Blitterswijk C, De Bruijn J. 2004. Relation between in vitro and in vivo osteogenic potential of cultured human bone marrow stromal cells. *Journal of Materials Science: Materials in Medicine*. 15(10):1123-1128.

Nakagawa Y, Murai T, Hasegawa C, Hirata M, Tsuchiya T, Yagami T, Haishima Y. 2003. Endotoxin contamination in wound dressings made of natural biomaterials. *Journal of Biomedical Materials Research Part B: Applied Biomaterials: An Official Journal of The Society for Biomaterials, The Japanese Society for Biomaterials, and The Australian Society for Biomaterials and the Korean Society for Biomaterials.* 66(1):347-355.

Norowski Jr PA, Fujiwara T, Clem WC, Adatrow PC, Eckstein EC, Haggard WO, Bumgardner JD. 2015. Novel naturally cross-linked electrospun nanofibrous chitosan mats for guided bone regeneration membranes: Material characterization and cytocompatibility. *Journal of tissue engineering and regenerative medicine.* 9(5):577-583.

Norowski PA, Babu J, Adatrow PC, Garcia-Godoy F, Haggard WO, Bumgardner JD. 2012. Antimicrobial activity of minocycline-loaded genipin-cross-linked nano-fibrous chitosan mats for guided tissue regeneration. *Journal of Biomaterials and Nanobiotechnology.* 3(04):528.

Nyan M, Sato D, Kihara H, Machida T, Ohya K, Kasugai S. 2009. Effects of the combination with  $\alpha$ -tricalcium phosphate and simvastatin on bone regeneration. *Clinical Oral Implants Research.* 20(3):280-287.

Park YJ, Kim KH, Lee JY, Ku Y, Lee SJ, Min BM, Chung CP. 2006. Immobilization of bone morphogenetic protein-2 on a nanofibrous chitosan membrane for enhanced guided bone regeneration. *Biotechnology and applied biochemistry.* 43(1):17-24.

Qi Y, Zhao T, Yan W, Xu K, Shi Z, Wang J. 2013. Mesenchymal stem cell sheet transplantation combined with locally released simvastatin enhances bone formation in a rat tibia osteotomy model. *Cytotherapy.* 15(1):44-56.

Sangsanoh P, Supaphol P. 2006. Stability improvement of electrospun chitosan nanofibrous membranes in neutral or weak basic aqueous solutions. *Biomacromolecules*. 7(10):2710-2714.

Shin SY, Park HN, Kim KH, Lee MH, Choi YS, Park YJ, Lee YM, Ku Y, Rhyu IC, Han SB. 2005. Biological evaluation of chitosan nanofiber membrane for guided bone regeneration. *Journal of periodontology*. 76(10):1778-1784.

Song JM, Shin SH, Kim YD, Lee JY, Baek YJ, Yoon SY, Kim HS. 2014. Comparative study of chitosan/fibroin–hydroxyapatite and collagen membranes for guided bone regeneration in rat calvarial defects: Micro-computed tomography analysis. *International journal of oral science*. 6(2):87.

Su H, Liu K-Y, Karydis A, Abebe DG, Wu C, Anderson KM, Ghadri N, Adatrow P, Fujiwara T, Bumgardner JD. 2016. In vitro and in vivo evaluations of a novel post-electrospinning treatment to improve the fibrous structure of chitosan membranes for guided bone regeneration. *Biomedical materials (Bristol, England)*. 12(1):015003-015003.

Tai I-c, Fu Y-C, Wang C-K, Chang J-K, Ho M-L. 2013. Local delivery of controlled-release simvastatin/plga/hap microspheres enhances bone repair. *International journal of nanomedicine*. 8:3895.

Tanigo T, Takaoka R, Tabata Y. 2010. Sustained release of water-insoluble simvastatin from biodegradable hydrogel augments bone regeneration. *Journal of Controlled Release*. 143(2):201-206.

Thies RS, Bauduy M, Ashton BA, Kurtzberg L, Wozney JM, Rosen V. 1992. Recombinant human bone morphogenetic protein-2 induces osteoblastic differentiation in w-20-17 stromal cells. *Endocrinology*. 130(3):1318-1324.

Turri A, Elgali I, Vazirisani F, Johansson A, Emanuelsson L, Dahlin C, Thomsen P, Omar O. 2016. Guided bone regeneration is promoted by the molecular events in the membrane compartment. *Biomaterials*. 84:167-183.

. Electrospun chitosan guided bone regeneration membranes for delivery of simvastatin to stimulate osteogenesis. Society for Biomaterials; 2019; Seattle, Washington, USA

Wang C-Z, Fu Y-C, Jian S-C, Wang Y-H, Liu P-L, Ho M-L, Wang C-K. 2014. Synthesis and characterization of cationic polymeric nanoparticles as simvastatin carriers for enhancing the osteogenesis of bone marrow mesenchymal stem cells. *Journal of colloid and interface science*. 432:190-199.

Wang PS, Solomon DH, Mogun H, Avorn J. 2000. Hmg-coa reductase inhibitors and the risk of hip fractures in elderly patients. *Jama*. 283(24):3211-3216.

Weinreb M, Shinar D, Rodan GA. 1990. Different pattern of alkaline phosphatase, osteopontin, and osteocalcin expression in developing rat bone visualized by in situ hybridization. *Journal of Bone and Mineral Research*. 5(8):831-842.

Wong R, Rabie A. 2003. Statin collagen grafts used to repair defects in the parietal bone of rabbits. *British Journal of Oral and Maxillofacial Surgery*. 41(4):244-248.

Wu C, Su H, Karydis A, Anderson KM, Ghadri N, Tang S, Wang Y, Bumgardner JD. 2017. Mechanically stable surface-hydrophobilized chitosan nanofibrous barrier membranes for guided bone regeneration. *Biomedical Materials*. 13(1):015004.

Wu C, Su H, Tang S, Bumgardner JD. 2014. The stabilization of electrospun chitosan nanofibers by reversible acylation. *Cellulose*. 21(4):2549-2556.

Xu C, Lei C, Meng L, Wang C, Song Y. 2012. Chitosan as a barrier membrane material in periodontal tissue regeneration. *Journal of Biomedical Materials Research Part B: Applied Biomaterials*. 100(5):1435-1443.

Xue Y, Wu M, Liu Z, Song J, Luo S, Li H, Li Y, Jin L, Guan B, Lin M. 2019. In vitro and in vivo evaluation of chitosan scaffolds combined with simvastatin-loaded nanoparticles for guided bone regeneration. *Journal of Materials Science: Materials in Medicine*. 30(4):47.

Yamashita M, Otsuka F, Mukai T, Otani H, Inagaki K, Miyoshi T, Goto J, Yamamura M, Makino H. 2008. Simvastatin antagonizes tumor necrosis factor- $\alpha$  inhibition of bone morphogenetic proteins-2-induced osteoblast differentiation by regulating smad signaling and ras/rho-mitogen-activated protein kinase pathway. *Journal of Endocrinology*. 196(3):601-613.

Yeo YJ, Jeon DW, Kim CS, Choi SH, Cho KS, Lee YK, Kim CK. 2005. Effects of chitosan nonwoven membrane on periodontal healing of surgically created one-wall intrabony defects in beagle dogs. *Journal of Biomedical Materials Research Part B: Applied Biomaterials: An Official Journal of The Society for Biomaterials, The Japanese Society for Biomaterials, and The Australian Society for Biomaterials and the Korean Society for Biomaterials*. 72(1):86-93.

Yu W-L, Sun T-W, Qi C, Zhao H-K, Ding Z-Y, Zhang Z-W, Sun B-B, Shen J, Chen F, Zhu Y-J. 2017. Enhanced osteogenesis and angiogenesis by mesoporous hydroxyapatite microspheres-derived simvastatin sustained release system for superior bone regeneration. *Scientific reports*. 7:44129.

Zhou Y, Ni Y, Liu Y, Zeng B, Xu Y, Ge W. 2010. The role of simvastatin in the osteogenesis of injectable tissue-engineered bone based on human adipose-derived stromal cells and platelet-rich plasma. *Biomaterials*. 31(20):5325-5335.

## Chapter 4

### Evaluating Angiogenic And Osteogenic Potential of Magnesium Incorporated Chitosan Membranes for Promoting Bone Growth: Preliminary Study

#### *4.1. Introduction*

Bone graft materials used for treating large bone defects are frequently susceptible to failure due to high incidence of delayed and/or non-union of the defect site. This is commonly caused by poor vascularization of the grafted implant (Dimitriou, Jones, McGonagle, & Giannoudis, 2011). Vascularization is critical in bone healing not only for the transport of oxygen and nutrients to the defect site but also to transport cells to facilitate bone regeneration (Stegen, van Gastel, & Carmeliet, 2015). There is a close connection between angiogenesis and osteogenesis in the process of bone repair (Carano & Filvaroff, 2003; Street et al., 2002). Therefore, a need to develop biomaterials with angiogenic and osteogenic potential has been growing in recent years.

Electrospun chitosan nanofibrous membranes (ESCM) used for GBR and bone tissue engineering applications are biocompatible and biodegradable and are known to promote bone healing (Kuo, Chang, Chen, & Kuan, 2006; Norowski Jr et al., 2015; Shin et al., 2005; Yeo et al., 2005). The porous nanofibrous membranes mimic the fibers in the extracellular matrix and provide increased surface area for the cells to attach and proliferate (Xu, Lei, Meng, Wang, & Song, 2012). The increased surface area of these membranes also allows for greater adsorption and or provide more reaction sites for loading and releasing therapeutic agents, making them an attractive option for drug delivery. These membranes have been loaded with growth factors and



drugs to promote tissue regeneration (Ghadri et al., 2018; Ji et al., 2013; Lee & Kim, 2016; Norowski et al., 2012). However, very few studies have explored specifically loading and releasing angiogenic agents from chitosan membranes. In one such study, Liu et al. reported enhanced *in vitro* angiogenic potential of chitosan based membranes by loading and releasing two therapeutic agents- icariin and deferoxamine-known to have angiogenic potential (H. Liu, Wen, Chen, Zhou, & Luo, 2018).

Incorporating an angiogenic agent into these membranes is thought to improve its functionality in promoting bone healing. The currently used gold standard for promoting angiogenesis is the use of Vascular endothelial growth factor (VEGF). Polyethylene glycol based nanofibrous membranes loaded with VEGF showed improved proliferation of vascular endothelial cells *in vitro* (Zhang et al., 2013). *In vivo*, these membrane constructs permitted good adhesion and proliferation of endothelial and smooth muscle cells (Zhang et al., 2013). Controlled release of VEGF from collagen-hyaluronic acid based membranes promoted enhanced tube formation by HUVECs as compared to non-loaded membranes (Lai et al., 2014). These membranes showed complete wound closure in diabetic rats within four weeks of implantation as compared to 6 weeks' time by non-loaded membrane wounds and empty wounds (Lai et al., 2014). Though these studies showed good angiogenic potential of VEGF loaded biomaterial constructs, this growth factor has disadvantages like supra-physiological dosing required to elicit the sought effect, short term bioactivity, unintended side effects and high therapeutic costs (H. Liu et al., 2018).

Magnesium (Mg) has potential to overcome the disadvantages of VEGF due to its angiogenic and osteogenic potential (Kim et al., 2017; Y. Liu, Yang, Tan, Li, & Zhang, 2014; Maier, Bernardini, Rayssiguier, & Mazur, 2004; Wang et al., 2014). Magnesium has shown to stimulate endothelial proliferation and migration in a dose-dependent manner (Maier et al., 2004). Mg doped bioglass has shown to promote angiogenesis *in vitro* (Priya et al., 2016). Mg stimulates the production of nitric oxide in endothelial cells and promotes angiogenesis in a mechanism similar to VEGF induced angiogenesis (Cooke & Losordo, 2002; Maier et al., 2004). Mg alloys are being increasingly used in biomedical applications due to their improved mechanical and biological activities. Magnesium based alloys demonstrate positive osteogenic responses *in vivo* (N. Li & Zheng, 2013; Y. Liu et al., 2014; Staiger, Pietak, Huadmai, & Dias, 2006; Wang et al., 2014). Magnesium based particles and bioglass have shown potential to stimulate mineralization of mesenchymal stem cells (Priya et al., 2016; Yegappan et al., 2019). Thus, incorporating magnesium into ESCMs is thought to increase the bioactivity of membranes and lead to increased healing via enhanced angiogenesis and osteogenesis.

The aim of this study is to investigate two different methods to incorporate Mg into fatty acid (FA) modified ESCM. The FA-modified ESCM are advantageous in bone healing applications, since they maintain biomimetic nanofiber structure, are biocompatible and biodegradable, and have promoted bone healing in critical size bone defects in as early as 4 weeks (Ghadri et al., 2018) The first method involves manufacturing magnesium phosphate nanoparticles (MgP-NP) and cospinning them with chitosan. The second method involves physical adsorption of magnesium salts onto chitosan membranes. These membranes were characterized by scanning electron microscopy (SEM) and energy dispersive spectroscopy (EDS)

and evaluated for release of Mg. Membranes were evaluated to analyze their potential in stimulating endothelial tube formation by HUVECs and alkaline phosphate (ALP) activity by bone cells to assess their *in vitro* angiogenic and osteogenic, respectively. The hypothesis of this work is that Mg incorporated chitosan membranes will promote tube formation in endothelial cells and increase ALP activity in mouse stromal cells.

## **4.2. Materials & Methods**

### **4.2.1. Materials**

Chitosan with 71% DDA and 311 kDa was purchased from Primex. Chemicals and salts for fabricating membranes and nanoparticles were bought from Sigma and Fisher. Iscove's modified Dulbecco's medium (IMDM), large vessel endothelial supplement (LVES), Alamar Blue, and Geltrex™ were purchased from Invitrogen. W-20-17 cells and HUVECs were obtained from ATCC and cultured as per ATCC instructions. All other reagents for cell culture were bought from Fisher.

### **4.2.2. Synthesizing MgP-NP**

MgP-NPs were manufactured using a previously established protocol (Zhou, Luchini, & Bhaduri, 2012). Magnesium chloride hexahydrate and monopotassium phosphate were used as the source of  $Mg^{2+}$  and  $PO_4^{4-}$ . Briefly, 3.12g of magnesium chloride hexahydrate, 2.27g of sodium bicarbonate and 1.36g monopotassium phosphate were dissolved in 1L MQ water, pH adjusted to 6.8 and solution microwaved at 800-900W for 5mins. To get particles of uniform morphology, the solution was left undisturbed until it completely cooled down to room

temperature. Once the solution containing the particles was cooled to room temperature, it was added to dialysis bags, and subjected to dialysis for 3 days with the water being changed every day. The dialyzed solution was then lyophilized to separate out the nanoparticles.

#### *4.2.3. Fabricating Mg incorporated chitosan membranes*

Two methods were employed to incorporate Mg into the membranes. In the first method, MgP-NPs were cospun with the chitosan membranes with polyvinyl alcohol (PVA) as the carrier and in the second method, membranes were immersed in simulated body fluid (SBF) containing elevated Mg concentrations. SBF was made using a previously established protocol (Zhou et al., 2012). The composition of SBF is summarized in Table 4-1. Membranes were fabricated by electrospinning a 5.5% (w/v) chitosan in 70% Trifluoroacetic acid and 30% dichloromethane solution at 27kV using a custom spinning setup, as previously described (Ghadri et al., 2018; Norowski et al., 2012; Su et al., 2016; C. Wu, Su, Tang, & Bumgardner, 2014). For incorporating MgP-NPs, a three stage electrospinning process was used. First, a 10ml volume of the chitosan solution was electrospun on to a collector plate covered with aluminum foil. Then a second 10ml volume of chitosan solution was cospun with 5ml of 10% (w/v) PVA containing 10% (w/w of chitosan) MgP-NPs, directly on top of the first layer. For cospinning MgP-NP dispersed PVA, the voltage was set to 30kV and the flow rate at 0.004ml/min to obtain uniform nanofibrous membranes. Then a third layer of 10ml of the chitosan solution was-spun at 27k on top of the MgP-NP layer. Discs, 0.5cm in diameter, were punched out and subjected to acylation modifications using either acetic anhydride (AA cospun) or hexanoic anhydride (HA cospun) (C. Wu et al., 2017; C. Wu et al., 2014).

In the second method for incorporating Mg into the membranes, plain chitosan membranes were fabricated by electrospinning three 10 ml volumes of the chitosan solution at 27kV, punched into 0.5cm discs and then modified using acetic anhydride (AA) or hexanoic anhydride (HA) (C. Wu et al., 2017; C. Wu et al., 2014). The modified discs were then placed in SBF (2mg membrane/ml SBF) containing five times more magnesium salts (AA-SBF and HA-SBF) and incubated with gentle agitation for one week with solution change every 48 hours. After one week, the membrane discs were removed from the solution and dried at 60°C overnight.

**Table 4-1:** Composition of 1L test SBF containing 5X more Mg ions

Order	Reagent	Amount (g)
1	Sodium chloride	6.55
2	Sodium bicarbonate	2.27
3	Potassium chloride	0.37
4	Sodium phosphate dibasic	0.14
5	Magnesium chloride hexahydrate	1.52
6	1M HCl	10 ml
7	Calcium chloride dihydrate	0.39
8	Sodium sulfate	0.072
9	Tris-Base	6.06
10	1M HCl	33.3 ml

#### 4.2.4. Characterization of MgP-NP and membranes

The size and morphology of the MgP-NP and membrane fibers were examined under SEM (Nova NANOSEM 650 FEI™) at 10kV and 10,000X magnification. EDS was used to evaluate the composition of the synthesized MgP-NP and the incorporation of Mg into the membranes. Four different samples of particles and membranes, fabricated separately were analyzed. In case of membrane samples, each sample was analyzed at five different regions. The Aztec software (version 3.0) attached to the SEM was used to do the EDS analysis.

#### 4.2.5. *In vitro* Mg release profile

The *in vitro* release of Mg ions from the membranes was evaluated over 5-days. The membranes were placed in 500µl of phosphate buffer saline (PBS) and kept at 37°C. The PBS was collected and refreshed every day. The collected PBS was stored at -20°C until ready for analysis. Eluates (n=4) were analyzed using QuantiChrom™ Magnesium assay kit (DIMG-250).

#### 4.2.6. Endothelial cell cultures

Compatibility of the particles and membranes was first evaluated using HUVECs. To evaluate the cytotoxicity of the particles, HUVECs were seeded in 96 well plates at 10,000 cells/well and allowed to attach at 37°C. MgP-NP were first sterilized by exposure to UV light for 30 minutes, and then dispersed at 10 to 1000µg particles/ml of IMDM medium. The medium with the particles was incubated with agitation for 24hrs at 37°C, and then centrifuged to remove the particles. The HUVECs were exposed to the conditioned medium for 24 and

48hrs and evaluated for viability using Alamar blue assay. Each concentration was tested in quadruplicates.

To assess the angiogenic potential, *in vitro* tube formation assay was performed. 96 well plates were coated with 50  $\mu$ L of Geltrex® and incubated at 37 °C for 1 hour. Briefly, 40,000 cells were added to Geltrex® coated wells. To each well, conditioned basal media (as described above) was added. After 4 hours of incubation, presence of capillary tube-like structure was observed under inverted phase contrast microscope. Bright field images of well plates were quantified for tube formation using angiogenesis analyzer plugin in ImageJ (Carpentier, Martinelli, Courty, & Cascone, 2012). Number of meshes formed was used as the indicator for angiogenic potential of the samples. Each sample was tested in quadruplicates and each well was imaged in 5 different fields. GS4012, a VEGF inducer, was used as the positive control and cells alone were used as the negative control.

#### 4.2.7. Bone cell cultures

The growth and ALP expression of W-20-17 cells were used to evaluate osteogenic potential of the Mg membranes using indirect culture method. W-20-17 cells were seeded at 50,000 cells/well in 24 well plate and allowed to attach for 24 hours at 37°C. Membranes were gas sterilized using ethylene oxide. A test Mg- or control (no Mg)- chitosan membrane was placed into a transwell insert (0.45  $\mu$ m pore size PET membrane, 24 well format, Falcon™) and the inserts then placed in cell seeded well plates. The media was changed every other day. After 1, 5 and 7 days of culture, the cells were lysed and analyzed for growth by measuring the double stranded DNA using picogreen assay (Quant-iT Picogreen assay kit, Invitrogen)

according to the manufacturer's protocol. ALP activity was measured using QuantiChrom™ alkaline phosphatase assay kit (DALP-250) from BioAssay Systems. Each membrane group was analyzed in quadruplicates. Cells grown on tissue culture plastic (TCP) were used as the control.

#### *4.2.8. Statistical analysis*

Results are represented as mean  $\pm$  standard deviation,  $n = 4$ . Tube formation assay and cell viability results were analyzed using one-way ANOVA followed by Tukey's post hoc comparisons. For evaluating significant differences between a given sample at two time points, t-test was performed.  $p < 0.05$  was considered as statistically significant.

### **4.3. Results**

#### *4.3.1. Characterization of MgP-NP and Mg incorporated chitosan membranes*

SEM examination revealed that the particles had a uniform spherical morphology with a diameter of  $237.2 \pm 51.6$ nm (Figure 4-1(A)). EDS analysis of the particles confirmed the presence of magnesium ( $22.9 \pm 0.4$  wt%), phosphorous ( $25.6 \pm 0.5$  wt%) and oxygen ( $51.4 \pm 0.5$  wt%) in the particles (Table 4-2).

SEM revealed uniform nanofibrous structure of the AA and HA cospun membranes with fiber diameters of  $227.8 \pm 19.3$ nm and  $245.4 \pm 31.6$ nm, respectively (Figure 4-1(B) & (C)). Though no distinct MgP-NPs were visible, EDS detected Mg ions in the membranes (Table 4-2).



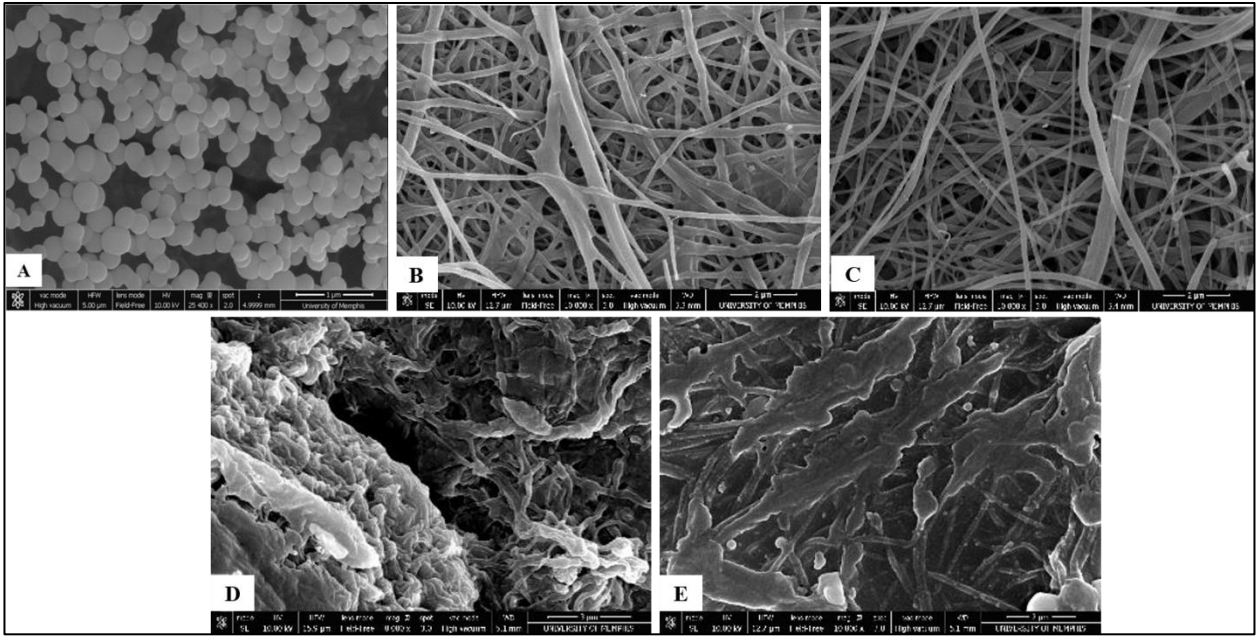


**Figure 4-1:** Representative SEM images of particles (A) showing uniform spherical morphology; AA cospun and HA cospun (B & C) showing nanofibrous structure and AA-SBF and HA-SBF (D & E) showing the salt deposits on the membrane surface.

SEM images of membranes soaked in SBF with 5X Mg revealed salt deposition on the membranes, along the fiber length, especially in case of HA membranes (Figure 4-1(E)). EDS spectra revealed that these salts were largely made of magnesium and calcium ions.

**Table 4-2:** EDS results showing the weight percent of magnesium and phosphorous in the particles and membranes. Each value represents mean  $\pm$  std dev (n=4)

Sample	%Mg	%P
MgP-NP	22.9 $\pm$ 0.4	25.6 $\pm$ 0.5
AA cospun	0.5 $\pm$ 0.3	0
HA cospun	0.5 $\pm$ 0.2	0
AA-SBF	10.5 $\pm$ 0.4	0
HA-SBF	15.3 $\pm$ 1.3	0

### 4.3.2. Mg release from membranes

In case of cospun membranes, AA and HA membranes released very small amounts of Mg through-out the study period (Figure 4-2(A)). However, these membranes revealed the presence of Mg in them after 5 days in PBS upon EDS analysis (Table 4-3).

AA-SBF and HA-SBF membranes showed a burst release profile, with most Mg release occurring by day 3 (Figure 4-2(B)). AA-SBF membranes released more Mg than HA-SBF membranes at day 1. When these membranes were evaluated by EDS after 5 days in PBS, there was still significant amount of Mg detected in these membranes (Table 4-3). Almost 5 and 3% of Mg was detected in AA cospun and HA cospun, respectively.

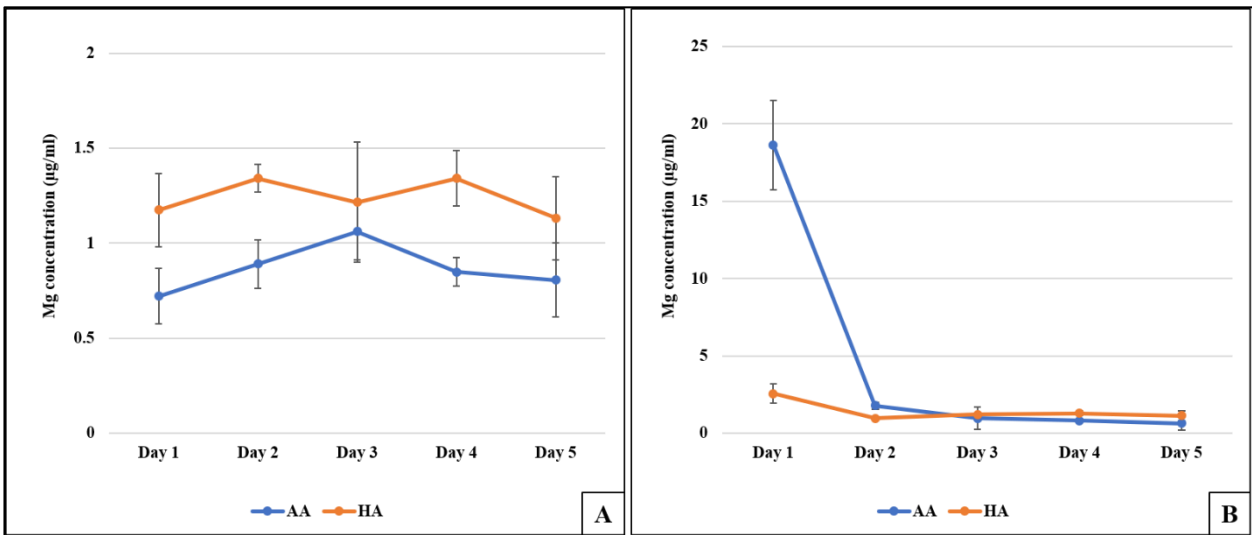


**Figure 4-2:** Release of Mg from (A) Cospun membranes and (B) SBF treated membranes. Low levels of magnesium were detected in the cospun membranes. AA-SBF membranes released much higher Mg than HA-SBF membranes on day 1. Each value represents mean  $\pm$  std dev (n=4).

**Table 4-3:** EDS results of membranes after 5 days of elution showing weight percent of magnesium left in the membranes.

Sample	% Mg
AA cospun	4.7±0.7
HA cospun	3.0±0.9
AA-SBF	7.2±0.7
HA-SBF	10.5±0.9

4.3.3. Cell viability and tube formation assay using HUVECs

Cell proliferation was evaluated for 24 and 72 hours with HUVECs and quantified using Alamar Blue assay. No significant difference was found between cells treated with different concentrations of MgP-NPs (Figure 4-3(a)) and different membranes (Figure 4-3(b)). All the groups had similar viability as the control. These results indicate that the levels of magnesium releasing out of these particles are not toxic to the cells.

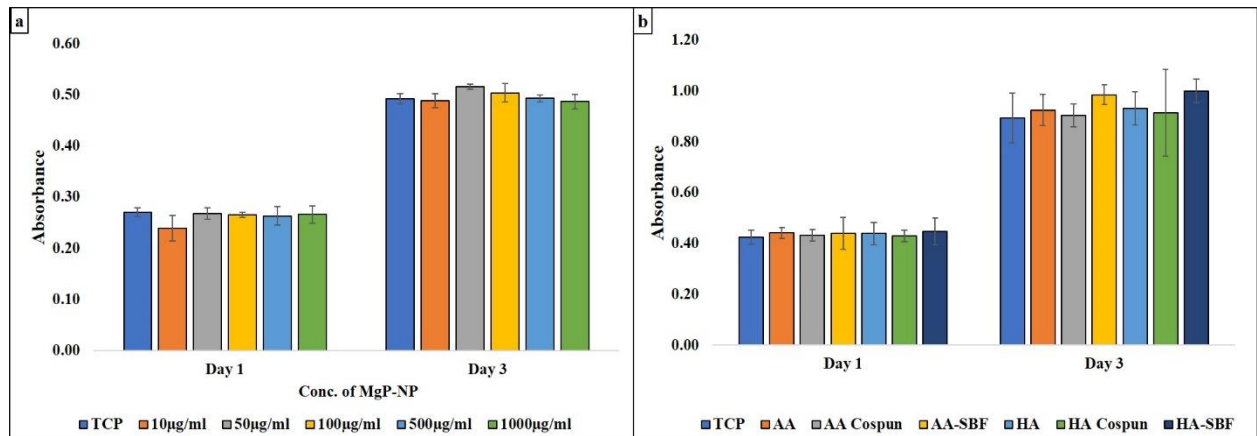


**Figure 4-3:** Cell viability assay with MgP-NPs (a) and Mg membranes (b) showed no cytotoxicity to the cells. Each value represents mean ± standard deviation with n=4.

Results of tubule formation by HUVECs exposed to MgP-NP extracts are shown in Figure 4-4. Negative control, HUVECs in basal medium did not show any tube-like morphology. Cells grown with GS4012 showed significant amount of tube-like structures. All concentrations showed significantly higher number of tube-like structures than the negative control group ( $p < 0.001$ ) (Figure 4-4(A)). Cells exposed to extracts from 500 and 1000  $\mu\text{g/ml}$  MgP-NPs exhibited similar amount of tubule formation as the positive control ( $p = 0.98$  for 500  $\mu\text{g/ml}$  and  $p = 0.77$  for 1000  $\mu\text{g/ml}$ ), with very well-developed mesh formations (Figure 4-4(B)). Number of mesh formed increased with increase in the concentrations of particles (Figure 4-4(B)).

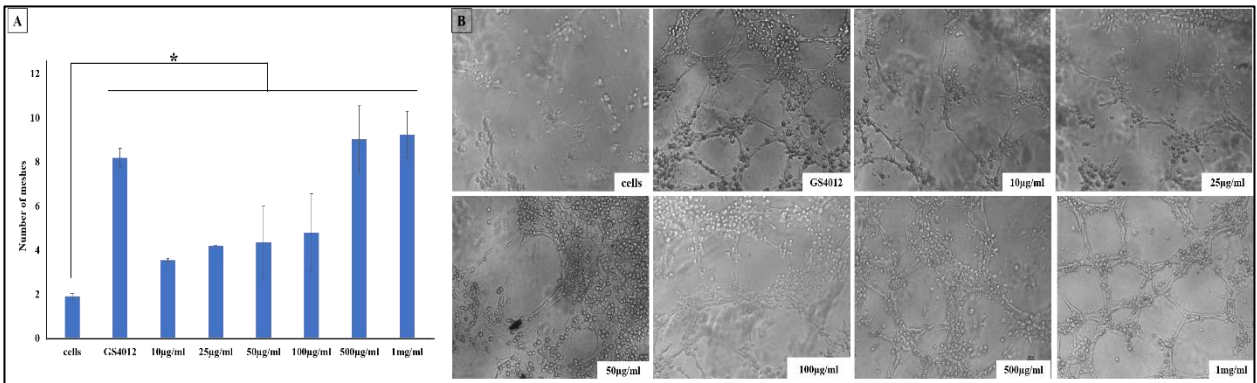


**Figure 4-4:** Quantifying the number of meshes formed by HUVECs in the presence of different MgP-NP concentrations (A). Each value represents mean  $\pm$  standard deviation with  $n = 4$ . Representative images of in vitro tube formation by different MgP-NP concentrations (B). Increased particle concentration demonstrated increased angiogenic potential. \* indicates significantly different than cells ( $p < 0.05$ )

All membrane groups exhibited greater tube formation than the negative control cells group ( $p < 0.001$ ) (Figure 4-5(A)). Mg incorporated membranes showed significantly higher tube formation than the non-loaded membranes and cells alone groups. AA copun and AA-SBF showed higher tube formation than HA copun and HA-SBF. There was no statistical difference between the AA-SBF and AA copun groups. The HA copun membrane group stimulated significantly more tube formation than HA-SBF.

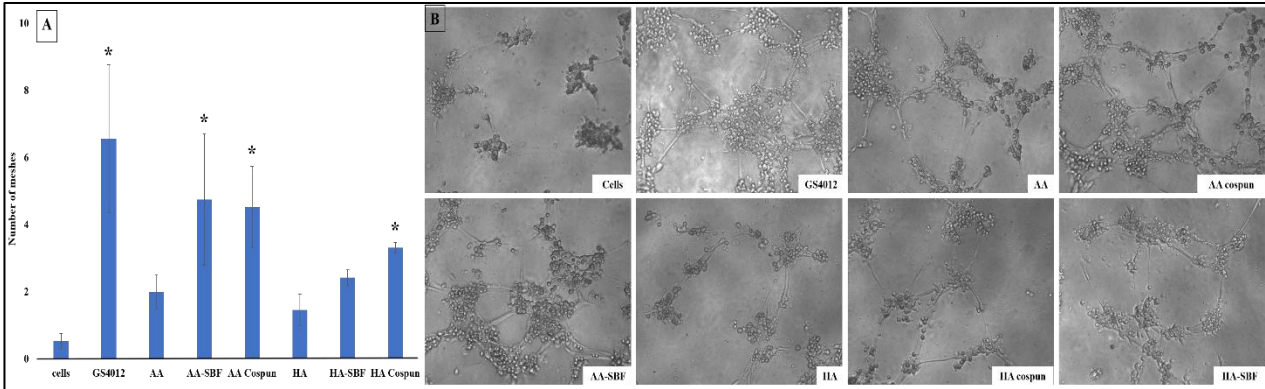


**Figure 4-5:** Quantifying the number of meshes in each membrane groups (A)). Each value represents mean  $\pm$  standard deviation with n= 4. Representative images of *in vitro* tube formation by different membranes (A). Mg incorporated AA membranes showed more angiogenic potential than HA membranes. \* indicates significantly different than cells (p<0.05)

4.3.4. *Cytocompatibility and osteogenic potential of membranes*

Cytocompatibility of the membranes was assessed for 1, 5 and 7 days with W-20-17 cells using Picogreen assay (Figure 4-6)). AA and HA membranes without Mg or MgP-NP were used as membrane controls. On day 1, none of the groups showed significant toxicity towards the cells as compared to the control. By day 5, all the groups showed cell proliferation and the membrane groups showed higher viability than the control. On day 7, AA-SBF showed significantly higher cell viability than the control, but all other groups showed viability similar to the control.

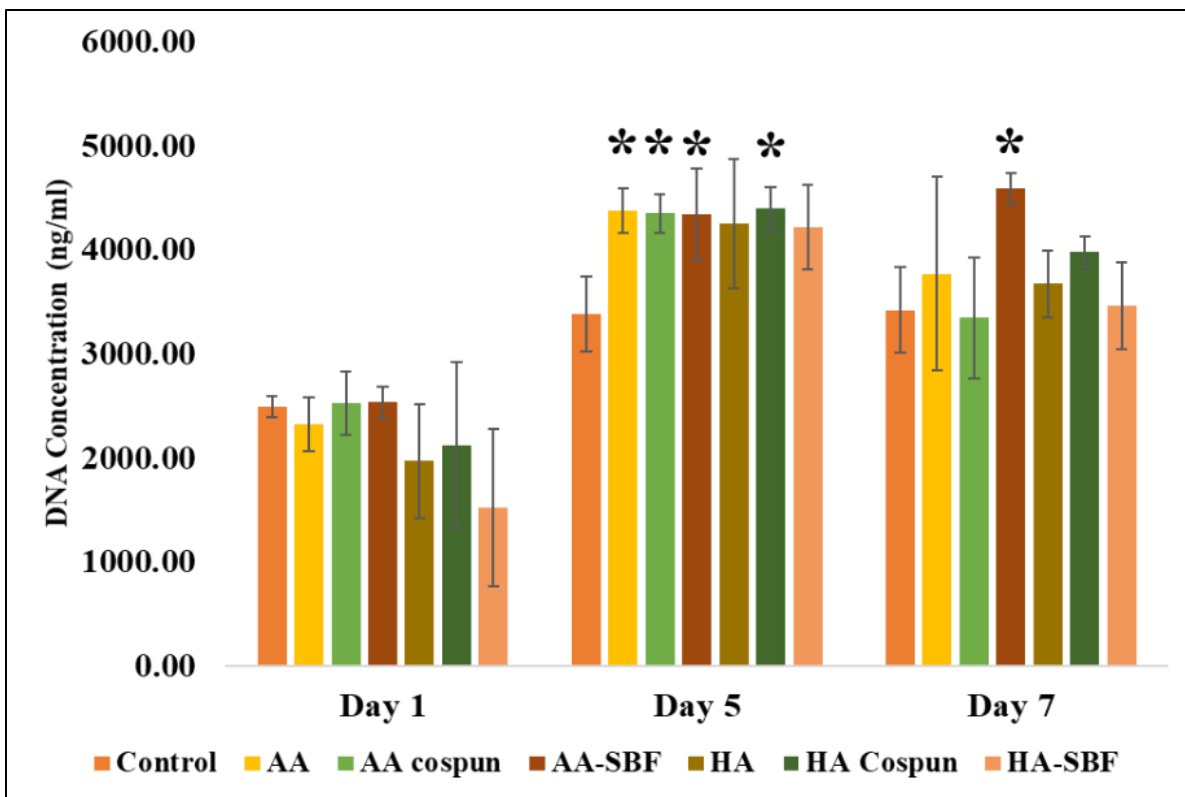


**Figure 4-6:** Cytocompatibility of Mg loaded membranes with W-20-17 cells in indirect culture. None of the groups showed any toxic effects towards the cells. Each value represents mean  $\pm$  std dev (n=4). \* indicates significantly different from control at the given time point.

Osteogenic potential of the membranes was evaluated with W-20-17 cells and quantified using ALP assay kit (Figure 4-7). ALP expression by cells exposed to Mg-containing and control membranes were not significantly different from controls (cells not exposed to any membrane) at the 1, 5 and 7 day time points. All the groups showed an increase in ALP activity by day 5 as compared to day 1, however the ALP levels were not very significantly different for day 5 and 7.

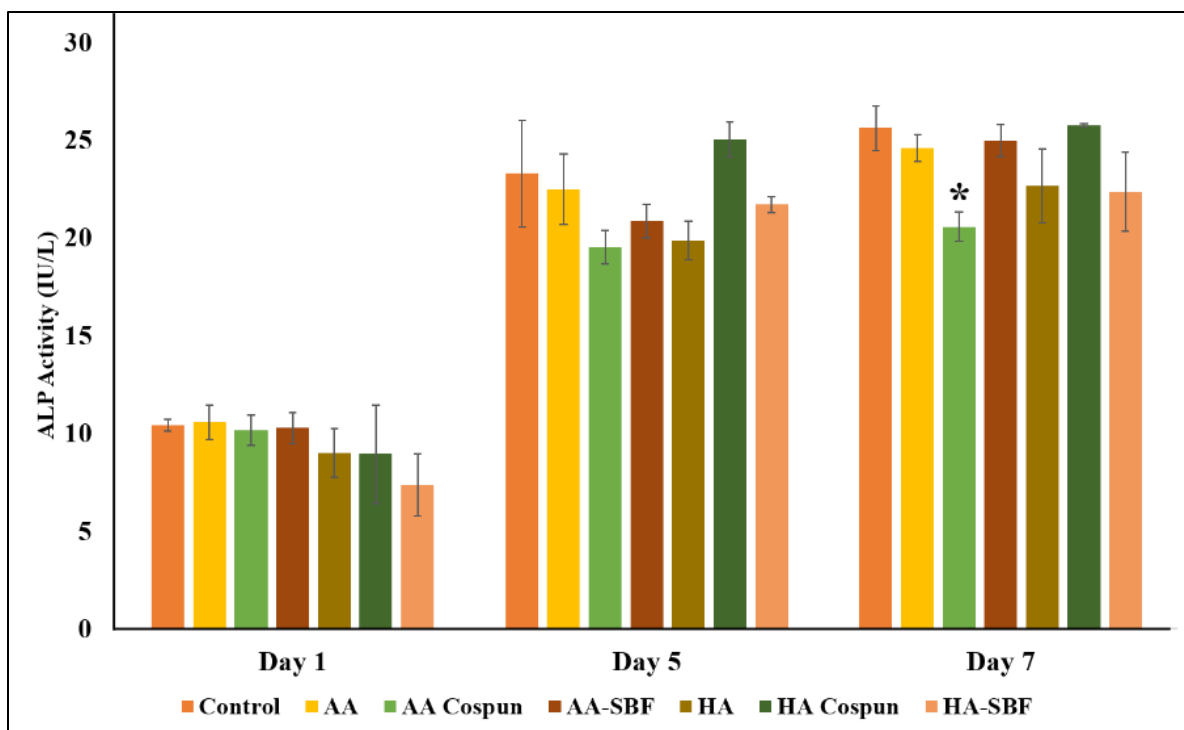


**Figure 4-7:** ALP activity of W-20-17 cells in the presence of conditioned media from different membrane groups. ALP activity of membrane groups was not significantly different from the control group. Each value represents mean  $\pm$  standard deviation with  $n = 4$ . \* indicates significantly different from control at the given time point.

#### 4.4. Discussion

The importance of angiogenesis in bone healing has motivated researchers to develop biomaterials that promote angiogenesis as well as osteogenesis. Chitosan nanofibrous membranes have previously shown good osteogenic potential *in vivo* (Ghadri et al., 2018; Lee & Kim, 2016; Norowski Jr et al., 2015; Shin et al., 2005). To further improve their functionality, we hypothesized that the incorporation of magnesium in these membranes would promote angiogenesis. Magnesium based particles and magnesium incorporated membranes were able to stimulate tube formation in endothelial cells, indicating their angiogenic capability.

MgP-NP originally developed by Zhou et al. (Zhou et al., 2012) showed good angiogenic potential in this work. The particles synthesized had morphology and diameters similar to previously reported study (Zhou et al., 2012). Particles reported by Zhou et al. had a wide range of diameter, whereas particles synthesized in this study had a more uniform size distribution. HUVECs when exposed to angiogenic environment, tend to form capillary-like tubular structures (tube formation), which eventually grow and form mesh like networks. The greater the angiogenic stimulus, the higher number of meshes will be formed. As the concentrations of particles increased, the HUVECs produced increased number of meshes confirming the angiogenic potential of the particles. Particles as low as 10 $\mu$ g/ml stimulated significantly higher number of mesh formation than the cells alone.

In order to deliver these particles locally to defect sites, they were incorporated into ESCMs by co-electrospinning the particle and polymer solutions to obtain Mg membranes that were subjected to acylation reaction to preserve the nanofibrous structure upon exposure to aqueous environment (C. Wu et al., 2017; C. Wu et al., 2014). The reaction procedure involves several washing steps, which are thought to wash away the particles to some extent. EDS evaluation showed very low amount of magnesium present in the membranes after the treatment and accordingly the release study also detected low levels of Mg from these membranes. Thus, as an alternative, we compared physical adsorption of magnesium and magnesium salts to the modified (acylated) chitosan membranes. Higher amount of Mg ion deposition on SBF treated membranes resulted in greater release of Mg from these membranes as compared to the cospun membranes.



Higher release of Mg from AA-SBF membranes than HA-SBF membranes could be attributed to the different hydrophobic behavior of the membranes. From previous work, AA membranes are less hydrophobic than HA membranes (Bumgardner, 2019). The less hydrophobic nature might have caused the membranes to swell more than the HA membranes, thereby releasing more magnesium. However, it was interesting to note that EDS evaluation of the membranes after 5 days of elution, still detected magnesium ions on the membranes, for both the groups, though no Mg was detected in the eluates from the release study. This could be because of the detection limit of the kit used, which was close to 1 $\mu$ g/ml. The membranes might still be releasing some low levels of Mg, which could not be detected by the kit. The presence of Mg in the membranes even after 5 days in aqueous solution was thought to be partly because of chitosan's ability to chelate metal ions (Ali, Hassan, & Elnashar, 2017). Previous research on chitosan resins have shown the polymer's ability to chelate metal ions including magnesium, for hard water softening applications (Ali et al., 2017). The mechanism of chelation is beyond the scope of this paper.

Tube formation by HUVECs showed a dose response to the increasing concentrations of the particle. Particles at 500 and 1000 $\mu$ g/ml showed an angiogenic response similar to the positive control, which is a potent VEGF inducer (Y. Li, Zhao, Sang, & Leung, 2019; Y.-C. Wu et al., 2015). Both types of membranes (Cospun and SBF-treated) were shown to stimulate mesh formation in HUVECs, though the cospun membranes released very low levels of magnesium. AA membranes (AA cospun & AA-SBF) stimulated more mesh formation than HA membranes, which was thought to be because of more swelling of AA membranes, releasing more magnesium and thus stimulating more angiogenesis. It was interesting to note

that similar tube formation response was seen in membranes releasing as high as 20 $\mu$ g/ml Mg (AA-SBF) and as low as less than 1 $\mu$ g/ml (AA cospun). Previously, carrageenan hydrogels loaded with 600 $\mu$ g of Mg based nanoparticles stimulated significant tube formation in HUVECs as compared to cells alone and non-loaded carrageenan hydrogel groups (Yegappan et al., 2019). In another report, chitin hydrogels loaded with 1mg of Mg doped bioglass promoted angiogenesis in mouse aortic ring assay (Priya et al., 2016). Though these scaffolds showed good angiogenic potential, the amount of magnesium releasing from them has not been reported. The exact amount of magnesium required to stimulate angiogenesis *in vivo* is unknown. Though in a regular wound healing process, new capillaries were seen to form within the initial three to five days, a prolonged release of angiogenic agents is thought to be beneficial because of their stimulatory effects on bone cell differentiation as well (De la Riva et al., 2010; Wernike et al., 2010). Angiogenic growth factors like VEGF and platelet-derived growth factor have been targeted to release for at least two to three weeks to stimulate bone formation *in vivo* (De la Riva et al., 2010; Kanczler et al., 2008; Leach, Kaigler, Wang, Krebsbach, & Mooney, 2006). The ability of chitosan to chelate magnesium ions is thought to entrap these ions in the membranes for longer time and thereby maintain its angiogenic potential for an extended time period. However, this needs to be investigated further in more elaborate *in vitro* and *in vivo* models.

Magnesium supplementation is gaining importance as adjuvant treatment to improve osteogenesis. Magnesium-based alloys and biomaterials are being actively investigated for bone tissue regeneration (Brar, Platt, Sarntinoranont, Martin, & Manuel, 2009; Kim et al., 2017; Y. Liu et al., 2014; Staiger et al., 2006; Wang et al., 2014). In order to evaluate the

osteogenic potential of these magnesium incorporated membranes, mouse bone marrow stromal W-20-17 cells were used. ALP is an early osteogenic marker, and preosteoblastic cells produce ALP at the beginning of their osteogenic differentiation phase. Though previous reports have shown the osteogenic potential of magnesium and magnesium-based biomaterials (Bondarenko et al., 2014; Kim et al., 2017; Y. Liu et al., 2014; Staiger et al., 2006; Wang et al., 2014), such an effect was not seen in this study. The magnesium membranes did not stimulate higher ALP activity in the cells, as compared to cells by themselves. The amount of magnesium released by the membranes might not have been sufficient to stimulate osteogenic differentiation of the cells in a span of 7 days. Hydrogels containing Mg-doped bioglass stimulated higher ALP expression than non-loaded hydrogels in rabbit-adipose derived mesenchymal stem cells by day 7 without osteogenic media (Priya et al., 2016). Mg-calcium phosphate nanoparticles stimulated increased ALP activity in rabbit mesenchymal stem cells only at day 14 even in the presence of osteogenic media (Yegappan et al., 2019). However, the release profile of magnesium from these constructs have not been reported and thus the levels of magnesium required to stimulate osteogenesis is still not clear. Longer mineralization studies with osteogenic media need to be conducted to thoroughly explore the osteogenic potential of these membranes.

#### ***4.5. Conclusion***

In this study, MgP-NP and Mg incorporated membranes were successfully fabricated. MgP-NPs showed good cytocompatibility and angiogenic potential. Mg was incorporated into chitosan membranes using two different techniques to produce Mg cospun membranes and Mg-SBF membranes. Incorporation of Mg did not affect the cytocompatibility of the membranes and both the membranes showed good angiogenic potential. The membranes did not have significant effect on preosteoblasts' ability to form bone cells in the initial 7 days of culture. Further investigation of these membranes to stimulate angiogenesis and osteogenesis in more elaborate *in vitro* and *in vivo* systems need to be carried out to further confirm the ability of these membranes to stimulate better bone healing in defect sites.

## *References*

- Ali, K., Hassan, M., & Elnashar, M. (2017). Development of functionalized carrageenan, chitosan and alginate as polymeric chelating ligands for water softening. *International Journal of Environmental Science and Technology*, 14(9), 2009-2014.
- Bondarenko, A., Angrisani, N., Meyer-Lindenberg, A., Seitz, J., Waizy, H., & Reifenrath, J. (2014). Magnesium-based bone implants: Immunohistochemical analysis of peri-implant osteogenesis by evaluation of osteopontin and osteocalcin expression. *Journal of biomedical materials research Part A*, 102(5), 1449-1457.
- Brar, H. S., Platt, M. O., Sarntinoranont, M., Martin, P. I., & Manuel, M. V. (2009). Magnesium as a biodegradable and bioabsorbable material for medical implants. *Jom*, 61(9), 31-34.
- Bumgardner, J. D. (2019). Development of Electrospun Chitosan Membranes for Guided Bone Regeneration. Paper presented at the International Association for Dental Research, Vancouver, Canada.
- Carano, R. A., & Filvaroff, E. H. (2003). Angiogenesis and bone repair. *Drug discovery today*, 8(21), 980-989.
- Carpentier, G., Martinelli, M., Courty, J., & Cascone, I. (2012). Angiogenesis analyzer for ImageJ. Paper presented at the 4th ImageJ User and Developer Conference proceedings.
- Cooke, J. P., & Losordo, D. W. (2002). Nitric oxide and angiogenesis. In: *Am Heart Assoc.*
- De la Riva, B., Sánchez, E., Hernández, A., Reyes, R., Tamimi, F., López-Cabarcos, E., . . . Évora, C. (2010). Local controlled release of VEGF and PDGF from a combined brushite–chitosan system enhances bone regeneration. *Journal of Controlled Release*, 143(1), 45-52.
- Dimitriou, R., Jones, E., McGonagle, D., & Giannoudis, P. V. (2011). Bone regeneration:

current concepts and future directions. *BMC medicine*, 9(1), 66.

Ghadri, N., Anderson, K. M., Adatrow, P., Stein, S. H., Su, H., Garcia-Godoy, F., . . .

Bumgardner, J. D. (2018). Evaluation of bone regeneration of simvastatin loaded chitosan nanofiber membranes in rodent calvarial defects. *Journal of Biomaterials and Nanobiotechnology*, 9(02), 210.

Ji, X., Yang, W., Wang, T., Mao, C., Guo, L., Xiao, J., & He, N. (2013). Coaxially electrospun core/shell structured poly (L-lactide) acid/chitosan nanofibers for potential drug carrier in tissue engineering. *Journal of biomedical nanotechnology*, 9(10), 1672-1678.

Kanczler, J. M., Ginty, P. J., Barry, J. J., Clarke, N. M., Howdle, S. M., Shakesheff, K. M., & Oreffo, R. O. (2008). The effect of mesenchymal populations and vascular endothelial growth factor delivered from biodegradable polymer scaffolds on bone formation. *Biomaterials*, 29(12), 1892-1900.

Kim, K.-J., Choi, S., Cho, Y. S., Yang, S.-J., Cho, Y.-S., & Kim, K. K. (2017). Magnesium ions enhance infiltration of osteoblasts in scaffolds via increasing cell motility. *Journal of Materials Science: Materials in Medicine*, 28(6), 96.

Kuo, S. M., Chang, S. J., Chen, T. W., & Kuan, T. C. (2006). Guided tissue regeneration for using a chitosan membrane: an experimental study in rats. *Journal of Biomedical Materials Research Part A: An Official Journal of The Society for Biomaterials, The Japanese Society for Biomaterials, and The Australian Society for Biomaterials and the Korean Society for Biomaterials*, 76(2), 408-415.

Lai, H.-J., Kuan, C.-H., Wu, H.-C., Tsai, J.-C., Chen, T.-M., Hsieh, D.-J., & Wang, T.-W. (2014). Tailored design of electrospun composite nanofibers with staged release of multiple angiogenic growth factors for chronic wound healing. *Acta biomaterialia*, 10(10), 4156-4166.

- Leach, J. K., Kaigler, D., Wang, Z., Krebsbach, P. H., & Mooney, D. J. (2006). Coating of VEGF-releasing scaffolds with bioactive glass for angiogenesis and bone regeneration. *Biomaterials*, 27(17), 3249-3255.
- Lee, E.-J., & Kim, H.-E. (2016). Accelerated bony defect healing by chitosan/silica hybrid membrane with localized bone morphogenetic protein-2 delivery. *Materials Science and Engineering: C*, 59, 339-345.
- Li, N., & Zheng, Y. (2013). Novel magnesium alloys developed for biomedical application: a review. *Journal of Materials Science & Technology*, 29(6), 489-502.
- Li, Y., Zhao, Y., Sang, S., & Leung, T. (2019). Methylglyoxal-Induced Retinal Angiogenesis in Zebrafish Embryo: A Potential Animal Model of Neovascular Retinopathy. *Journal of ophthalmology*, 2019.
- Liu, H., Wen, W., Chen, S., Zhou, C., & Luo, B. (2018). Preparation of Icariin and Deferoxamine Functionalized Poly (l-lactide)/chitosan Micro/Nanofibrous Membranes with Synergistic Enhanced Osteogenesis and Angiogenesis. *ACS Applied Bio Materials*, 1(2), 389-402.
- Liu, Y., Yang, Z., Tan, L., Li, H., & Zhang, Y. (2014). An animal experimental study of porous magnesium scaffold degradation and osteogenesis. *Brazilian Journal of Medical and Biological Research*, 47(8), 715-720.
- Maier, J. A., Bernardini, D., Rayssiguier, Y., & Mazur, A. (2004). High concentrations of magnesium modulate vascular endothelial cell behaviour *in vitro*. *Biochimica et Biophysica Acta (BBA)-Molecular Basis of Disease*, 1689(1), 6-12.
- Norowski Jr, P. A., Fujiwara, T., Clem, W. C., Adatrow, P. C., Eckstein, E. C., Haggard, W. O., & Bumgardner, J. D. (2015). Novel naturally cross-linked electrospun nanofibrous chitosan

mats for guided bone regeneration membranes: Material characterization and cytocompatibility. *Journal of tissue engineering and regenerative medicine*, 9(5), 577-583.

Norowski, P. A., Babu, J., Adatrow, P. C., Garcia-Godoy, F., Haggard, W. O., & Bumgardner, J. D. (2012). Antimicrobial Activity of Minocycline-Loaded Genipin-Cross-linked Nano-Fibrous Chitosan Mats for Guided Tissue Regeneration. *Journal of Biomaterials and Nanobiotechnology*, 3(04), 528.

Priya, M. V., Sivshanmugam, A., Boccaccini, A., Goudouri, O., Sun, W., Hwang, N., . . . Jayakumar, R. (2016). Injectable osteogenic and angiogenic nanocomposite hydrogels for irregular bone defects. *Biomedical Materials*, 11(3), 035017.

Shin, S. Y., Park, H. N., Kim, K. H., Lee, M. H., Choi, Y. S., Park, Y. J., . . . Han, S. B. (2005). Biological evaluation of chitosan nanofiber membrane for guided bone regeneration. *Journal of periodontology*, 76(10), 1778-1784.

Staiger, M. P., Pietak, A. M., Huadmai, J., & Dias, G. (2006). Magnesium and its alloys as orthopedic biomaterials: a review. *Biomaterials*, 27(9), 1728-1734.

Stegen, S., van Gastel, N., & Carmeliet, G. (2015). Bringing new life to damaged bone: the importance of angiogenesis in bone repair and regeneration. *Bone*, 70, 19-27.

Street, J., Bao, M., deGuzman, L., Bunting, S., Peale, F. V., Ferrara, N., . . . Daugherty, A. (2002). Vascular endothelial growth factor stimulates bone repair by promoting angiogenesis and bone turnover. *Proceedings of the National Academy of Sciences*, 99(15), 9656-9661.

Su, H., Liu, K.-Y., Karydis, A., Abebe, D. G., Wu, C., Anderson, K. M., . . . Bumgardner, J. D. (2016). *In vitro* and *in vivo* evaluations of a novel post-electrospinning treatment to improve the fibrous structure of chitosan membranes for guided bone regeneration. *Biomedical materials (Bristol, England)*, 12(1), 015003-015003.



Wang, G., Li, J., Zhang, W., Xu, L., Pan, H., Wen, J., . . . Liu, X. (2014). Magnesium ion implantation on a micro/nanostructured titanium surface promotes its bioactivity and osteogenic differentiation function. *International journal of nanomedicine*, 9, 2387.

Wernike, E., Montjovent, M.-O., Liu, Y., Wismeijer, D., Hunziker, E. B., Siebenrock, K.-A., . . . Klenke, F. M. (2010). VEGF incorporated into calcium phosphate ceramics promotes vascularisation and bone formation *in vivo*. *Eur Cell Mater*, 19(3).

Wu, C., Su, H., Karydis, A., Anderson, K. M., Ghadri, N., Tang, S., . . . Bumgardner, J. D. (2017). Mechanically stable surface-hydrophobilized chitosan nanofibrous barrier membranes for guided bone regeneration. *Biomedical Materials*, 13(1), 015004.

Wu, C., Su, H., Tang, S., & Bumgardner, J. D. (2014). The stabilization of electrospun chitosan nanofibers by reversible acylation. *Cellulose*, 21(4), 2549-2556.

Wu, Y.-C., Chang, C.-Y., Kao, A., Hsi, B., Lee, S.-H., Chen, Y.-H., & Wang, I.-J. (2015). Hypoxia-induced retinal neovascularization in zebrafish embryos: a potential model of retinopathy of prematurity. *PloS one*, 10(5), e0126750.

Xu, C., Lei, C., Meng, L., Wang, C., & Song, Y. (2012). Chitosan as a barrier membrane material in periodontal tissue regeneration. *Journal of Biomedical Materials Research Part B: Applied Biomaterials*, 100(5), 1435-1443.

Yegappan, R., Selvaprithiviraj, V., Amirthalingam, S., Mohandas, A., Hwang, N. S., & Jayakumar, R. (2019). Injectable angiogenic and osteogenic carrageenan nanocomposite hydrogel for bone tissue engineering. *International journal of biological macromolecules*, 122, 320-328.

Yeo, Y. J., Jeon, D. W., Kim, C. S., Choi, S. H., Cho, K. S., Lee, Y. K., & Kim, C. K. (2005). Effects of chitosan nonwoven membrane on periodontal healing of surgically created one-wall

intrabony defects in beagle dogs. *Journal of Biomedical Materials Research Part B: Applied Biomaterials: An Official Journal of The Society for Biomaterials, The Japanese Society for Biomaterials, and The Australian Society for Biomaterials and the Korean Society for Biomaterials*, 72(1), 86-93.

Zhang, H., Jia, X., Han, F., Zhao, J., Zhao, Y., Fan, Y., & Yuan, X. (2013). Dual-delivery of VEGF and PDGF by double-layered electrospun membranes for blood vessel regeneration. *Biomaterials*, 34(9), 2202-2212.

Zhou, H., Luchini, T. J., & Bhaduri, S. B. (2012). Microwave assisted synthesis of amorphous magnesium phosphate nanospheres. *Journal of Materials Science: Materials in Medicine*, 23(12), 2831-2837.

## **Chapter 5**

### **Conclusions**

The results presented in this dissertation indicate the ability of our modified electrospun chitosan GBR membranes to stimulate osteogenesis and angiogenesis, by the controlled and sustained delivery of loaded/incorporated therapeutics. The need for effective GBR membranes is increasing with the rise in the number of grafting procedures. Drawbacks of currently used GBR membranes have led to the development of newer alternatives. Electrospun chitosan membranes have previously been investigated for GBR applications but needed improvement in maintaining their nanofibrous structure, which is thought to play a critical role in GBR applications. Our ability to better preserve the nanofibrous structure and stimulate better osteogenesis by providing a sustained release of loaded SMV is thought to improve the effectiveness of these membranes. The ability of these membranes to incorporate and release magnesium for stimulating angiogenesis may further enhance their bone healing capabilities and expand their application to the treatment of long segmental bone defects. This control over the amount and duration of drug release, would enable surgeons to customize these membranes based on the clinical need.

Modification of chitosan membranes using fatty acids and/or tBOC groups allowed us to control the amount of drug being released out of the membranes. SMV was investigated as an economical but effective alternative to BMP-2. AA and tBOC membranes released higher levels of SMV at a faster rate as compared to HA and BA membranes which released lower levels, at slower rate. Drug release levels were influenced by initial drug loading amounts only for AA and tBOC membranes. Chitosan modifications employed in this work, influenced the hydrophobic

behavior of the membranes. Among the fatty acid treated membranes, the BA and HA membranes were more hydrophobic than AA membranes. Since like dissolves like, hydrophobic membranes were thought to retain the hydrophobic SMV within themselves and prevent it from releasing out early. This was further confirmed by molecular modeling, which showed a stronger interaction between BA and HA modified membranes and SMV. Though tBOC membranes had hydrophobicity similar to HA membranes, their release profile was similar to AA membranes. Molecular modeling also showed similar interaction of tBOC and AA membranes with SMV. The ability of our membranes to control the release of a passively loaded drug, confers an additional advantage to them. These membranes can be packaged, sterilized and delivered to the clinics without the loaded drug. The drug can later be added to the membranes at the point of care, depending on the clinical need. This would give flexibility to the surgeons to either use a drug-loaded or non-loaded membrane at the defect site, since the non-loaded membranes have also shown good bone healing in previous studies. Loading the drug at the point of care would also enable the clinicians to control the amount of drug that is thought to be appropriate for healing the defect. Advantages of such a system also include, increased shelf-life, ease of sterilization and ease in FDA approval.

Though numerous studies have investigated the osteogenic potential of locally delivered SMV, the dosage and extent of release is not clear. Effectiveness of the drug appeared to depend on the type of carrier and the defect and cell type used. Since we were able to modulate the release pattern from a single carrier type, membranes with different loadings and release pattern were investigated here. AA membranes loaded with either 250 $\mu$ g (AA250) or 50 $\mu$ g (AA50) and HA membranes loaded with 50 $\mu$ g (HA50) of SMV were considered for further biological

evaluation. These membranes represented a fast release of high dose, fast release of low dose and slow release of low dose of SMV, respectively. However, the amount of SMV released from AA250 and AA50 were toxic to the cells. Also, from previous studies, lower amount of SMV was found to be more effective in bone healing. Thus, an AA10 group was included in the study. *In vitro*, AA10 membranes showed a 100% release of SMV by day 5. AA50 membranes released most of the drug by day 28, whereas HA50 membranes released less than 50% of the loaded drug during the same time period. Since AA membranes released SMV at a faster rate within a shorter time period, they could be used in treating small defect areas, which would heal relatively soon. In the *in vivo* studies using critical size defects, SMV-loaded AA membranes had stimulated significantly more bone than the non-loaded membranes by week 4 which improved by week 8. The membranes started to show signs of degradation at week 4 and were completely resorbed in the next four weeks. Since the bone had significantly healed by week 8, the resorption of the membranes by this time point was considered advantageous. The HA membranes on the other hand, released low amount of SMV over longer time periods. These membranes can be used in larger defect areas, which might take longer to heal. *In vivo* evaluation of SMV-loaded HA membranes showed signs of bone bridging by week 4 and complete bone bridging by week 8. These membranes prevented soft tissue infiltration into the defect and remained intact with very minimum degradation/dissolution even after two months of implantation. The prolonged presence of these membranes is thought to be advantageous in healing larger defects, since such defects would need to be protected from soft tissue infiltration for a longer period and would require the osteogenic stimulation for extended time. However, AA membranes can also be advantageous in such cases, since the faster release of SMV from these membranes might help in

faster bone healing, thereby doing away with the need of using a GBR membrane for longer time periods.

The importance of angiogenesis in bone healing led to the investigation of magnesium, as an alternative to VEGF, to stimulate vascularization. Presence of magnesium in the membranes enabled them to possess angiogenic property which was shown by tube formation assays in HUVECs. Initially MgP-NPs were thought to be a good option and were tested successfully for stimulating angiogenesis. However, when they were cospun into the membranes, the fatty acid modification steps washed away most of the magnesium from them. Nevertheless, these membranes still showed good angiogenic potential *in vitro*, and trace amounts of magnesium was still detected in these membranes after 5 days of elution. As an alternative, the fatty acid treated membranes were soaked in simulated body fluid with increased magnesium ions, as an attempt to physically deposit/adsorb these ions onto the membranes. Elution studies with these membranes showed an increased release of magnesium from AA membranes as compared to HA membranes, which attributed to the more hydrophilic nature of AA membranes, causing them to swell more and release higher amounts of the deposited/adsorbed ions. Accordingly, though both the membrane groups showed good angiogenic property, the AA membranes stimulated better angiogenesis (more tube formation) than HA membranes. Experiments performed in this work provide preliminary evidence about the angiogenic property of these membranes. More elaborate *in vitro* and *in vivo* experiments need to be performed to confirm their bioactivity. Further, dual loaded membranes that are incorporated with magnesium and loaded with SMV need to be evaluated for their angiogenic and osteogenic properties, to help better understand their ability to stimulate better/faster bone healing. Since most of the large bone defects fail due to non-unions or delayed unions caused by lack of sufficient vascularization, developing membranes that would

stimulate angiogenesis and osteogenesis could help overcome this issue. Apart from GBR applications, such membranes can be used in treating long segmental bone defects which have received extensive bone grafting. The GBR property of the membranes would prevent any soft tissue infiltration into the grafted site, and their angiogenic and osteogenic potential would further enhance the bone healing capabilities of the graft material, leading to better defect healing.

## Chapter 6

### Future Work

The following evaluations are recommended in order to provide a more thorough assessment of the potential use of chitosan membranes in delivering an osteogenic and angiogenic agent to promote bone regeneration for various bone tissue engineering applications:

- *In vivo* evaluation of SMV loaded chitosan membranes in larger animal model, like porcine segmental mandibular defect model, and compare their bone healing ability with commercially available collagen-based GBR membranes.
- Evaluate angiogenic potential of SMV loaded chitosan membranes in promoting angiogenesis *in vitro*, since statins have reported to possess angiogenic potential as well.
- Test angiogenic potential of Mg membranes for longer time periods with HUVECs and in animal models.
- Examine the osteogenic potential of Mg membranes *in vitro* with osteogenic culture medium.
- Evaluate the angiogenic and osteogenic potential of dual loaded membranes *in vitro* and *in vivo*.
- Explore the bone healing potential of dual loaded membranes in treating long bone defects.
- Continue research in loading and releasing other therapeutics (especially hydrophobic molecules) from these modified chitosan membranes for other tissue engineering and drug delivery applications.



## BIBLIOGRAPHY

Aini, N., Yahya, M., Lepit, A., Jaafar, N., Harun, M., & Ali, A. (2012). Preparation and characterization of UV irradiated SPEEK/chitosan membranes. *Int. J. Electrochem. Sci*, 7, 8226-8235.

Ali, A., & Ahmed, S. (2018). A review on chitosan and its nanocomposites in drug delivery. *International journal of biological macromolecules*, 109, 273-286.

Aurer, A., & Jorgić-Srdjak, K. (2005). Membranes for periodontal regeneration. *Acta Stomatologica Croatica*, 39(1), 107-112.

Austero, M. S., Donius, A. E., Wegst, U. G., & Schauer, C. L. (2012). New crosslinkers for electrospun chitosan fibre mats. I. Chemical analysis. *Journal of the Royal Society Interface*, 9(75), 2551-2562.

Balagangadharan, K., Dhivya, S., & Selvamurugan, N. (2017). Chitosan based nanofibers in bone tissue engineering. *International journal of biological macromolecules*, 104, 1372-1382.

Bartee, B. K. (1995). The use of high-density polytetrafluoroethylene membrane to treat osseous defects: clinical reports. *Implant dentistry*, 4(1), 21-26.

Bartee, B. K., & Carr, J. (1995). Evaluation of a high-density polytetrafluoroethylene (n-PTFE) membrane as a barrier material to facilitate guided bone regeneration in the rat mandible. *The Journal of oral implantology*, 21(2), 88-95.

Bavariya, A. J., Andrew Norowski Jr, P., Mark Anderson, K., Adatrow, P. C., Garcia-Godoy, F., Stein, S. H., & Bumgardner, J. D. (2014). Evaluation of biocompatibility and

degradation of chitosan nanofiber membrane cross-linked with genipin. *Journal of Biomedical Materials Research Part B: Applied Biomaterials*, 102(5), 1084-1092.

Beachley, V., & Wen, X. (2009). Effect of electrospinning parameters on the nanofiber diameter and length. *Materials Science and Engineering: C*, 29(3), 663-668.

Becker, W., Becker, B. E., Handelsman, M., Ochsenein, C., & Albrektsson, T. (1991). Guided tissue regeneration for implants placed into extraction sockets: A study in dogs. *Journal of periodontology*, 62(11), 703-709.

Bhattarai, N., Edmondson, D., Veiseh, O., Matsen, F. A., & Zhang, M. (2005). Electrospun chitosan-based nanofibers and their cellular compatibility. *Biomaterials*, 26(31), 6176-6184.

Bondarenko, A., Angrisani, N., Meyer-Lindenberg, A., Seitz, J., Waizy, H., & Reifenrath, J. (2014). Magnesium-based bone implants: Immunohistochemical analysis of peri-implant osteogenesis by evaluation of osteopontin and osteocalcin expression. *Journal of biomedical materials research Part A*, 102(5), 1449-1457.

Buser, D., Brägger, U., Lang, N., & Nyman, S. (1990). Regeneration and enlargement of jaw bone using guided tissue regeneration. *Clinical Oral Implants Research*, 1(1), 22-32.

Carano, R. A., & Filvaroff, E. H. (2003). Angiogenesis and bone repair. *Drug discovery today*, 8(21), 980-989.

Chen, C.-H., Chen, S.-H., Shalumon, K., & Chen, J.-P. (2015). Dual functional core–sheath electrospun hyaluronic acid/polycaprolactone nanofibrous membranes embedded with silver nanoparticles for prevention of peritendinous adhesion. *Acta biomaterialia*, 26, 225-235.

Chen, D. W., Hsu, Y.-H., Liao, J.-Y., Liu, S.-J., Chen, J.-K., & Ueng, S. W.-N. (2012). Sustainable release of vancomycin, gentamicin and lidocaine from novel electrospun sandwich-structured PLGA/collagen nanofibrous membranes. *International journal of pharmaceutics*, 430(1-2), 335-341.

Chen, Z., Wang, P., Wei, B., Mo, X., & Cui, F. (2010). Electrospun collagen–chitosan nanofiber: A biomimetic extracellular matrix for endothelial cell and smooth muscle cell. *Acta biomaterialia*, 6(2), 372-382.

Choi, S. H., Kim, C. K., Cho, K. S., Huh, J. S., Sorensen, R. G., Wozney, J. M., & Wikesjö, U. M. (2002). Effect of recombinant human bone morphogenetic protein-2/absorbable collagen sponge (rhBMP-2/ACS) on healing in 3-wall intrabony defects in dogs. *Journal of periodontology*, 73(1), 63-72.

Cooke, J. P., & Losordo, D. W. (2002). Nitric oxide and angiogenesis. In: *Am Heart Assoc.*

Correia, D. M., Gámiz-González, M., Botelho, G., Vidaurre, A., Ribelles, J. G., Lanceros-Méndez, S., & Sencadas, V. (2014). Effect of neutralization and cross-linking on the thermal degradation of chitosan electrospun membranes. *Journal of Thermal Analysis and Calorimetry*, 117(1), 123-130.

De Long Jr, W. G., Einhorn, T. A., Koval, K., McKee, M., Smith, W., Sanders, R., & Watson, T. (2007). Bone grafts and bone graft substitutes in orthopaedic trauma surgery. A critical analysis. *The Journal of bone and joint surgery. American volume*, 89(3), 649.

Demir, M. M., Yilgor, I., Yilgor, E., & Erman, B. (2002). Electrospinning of polyurethane fibers. *Polymer*, 43(11), 3303-3309.

Duan, B., Yuan, X., Zhu, Y., Zhang, Y., Li, X., Zhang, Y., & Yao, K. (2006). A nanofibrous composite membrane of PLGA–chitosan/PVA prepared by electrospinning. *European Polymer Journal*, 42(9), 2013-2022.

Finkemeier, C. G. (2002). Bone-grafting and bone-graft substitutes. *JBJS*, 84(3), 454-464.

Funkhouser, H. L., Adera, T., & Adler, R. A. (2002). Effect of HMG-CoA reductase inhibitors (statins) on bone mineral density. *Journal of Clinical Densitometry*, 5(2), 151-158.

Gaviria, L., Salcido, J. P., Guda, T., & Ong, J. L. (2014). Current trends in dental implants. *Journal of the Korean Association of Oral and Maxillofacial Surgeons*, 40(2), 50-60.

Gentile, P., Chiono, V., Tonda-Turo, C., Ferreira, A. M., & Ciardelli, G. (2011). Polymeric membranes for guided bone regeneration. *Biotechnology Journal*, 6(10), 1187-1197.

Gouda, A., Helal, E., Ali, S., Bakry, S., & Yassin, S. (2018). Maxillary sinus lift using osteoinductive simvastatin combined with  $\beta$ -TCP versus  $\beta$ -TCP—a comparative pilot study to evaluate simvastatin enhanced and accelerated bone formation. *Acta Odontologica Scandinavica*, 76(1), 39-47.

Haider, A., Haider, S., & Kang, I.-K. (2018). A comprehensive review summarizing the effect of electrospinning parameters and potential applications of nanofibers in biomedical and biotechnology. *Arabian Journal of Chemistry*, 11(8), 1165-1188.

Hung, Y., & Yeung, V. (2000). Hypothyroidism presenting as hypercholesterolaemia and simvastatin-induced myositis. *HONG KONG MEDICAL JOURNAL*, 6(4), 423-424.

Jayakumar, R., Prabakaran, M., Nair, S., & Tamura, H. (2010). Novel chitin and chitosan nanofibers in biomedical applications. *Biotechnology advances*, 28(1), 142-150.

Jerwood, S., & Cohen, J. (2007). Unexpected antimicrobial effect of statins. *Journal of antimicrobial chemotherapy*, 61(2), 362-364.

Jiang, L., Sun, H., Yuan, A., Zhang, K., Li, D., Li, C., . . . Zheng, C. (2013). Enhancement of osteoinduction by continual simvastatin release from poly (lactic-co-glycolic acid)-hydroxyapatite-simvastatin nano-fibrous scaffold. *Journal of biomedical nanotechnology*, 9(11), 1921-1928.

Jo, J.-Y., Jeong, S.-I., Shin, Y.-M., Kang, S.-S., Kim, S.-E., Jeong, C.-M., & Huh, J.-B. (2015). Sequential delivery of BMP-2 and BMP-7 for bone regeneration using a heparinized collagen membrane. *International journal of oral and maxillofacial surgery*, 44(7), 921-928.

Jody, D. N. (1997). Myositis and Rhabdomyolysis Associated With Concurrent Use of Simvastatin and Nefazodone-Reply. *Jama*, 277(4), 296-297.

Jovanovic, S. A., & Nevins, M. (1995). Bone formation utilizing titanium-reinforced barrier membranes. *International Journal of Periodontics & Restorative Dentistry*, 15(1).

Khor, E. (2001). Chitin, Fulfilling a Biomaterials Promise, Dept. Of Chemistry, National University of Singapore, Rep. Of Singapore.

Kuo, S. M., Chang, S. J., Chen, T. W., & Kuan, T. C. (2006). Guided tissue regeneration for using a chitosan membrane: an experimental study in rats. *Journal of Biomedical Materials Research Part A: An Official Journal of The Society for Biomaterials, The Japanese Society for*

Biomaterials, and The Australian Society for Biomaterials and the Korean Society for Biomaterials, 76(2), 408-415.

Laurant, P., & Touyz, R. M. (2000). Physiological and pathophysiological role of magnesium in the cardiovascular system: implications in hypertension. *Journal of hypertension*, 18(9), 1177-1191.

Lee, E.-J., & Kim, H.-E. (2016). Accelerated bony defect healing by chitosan/silica hybrid membrane with localized bone morphogenetic protein-2 delivery. *Materials Science and Engineering: C*, 59, 339-345.

Lew, T. A., Walker, J. A., Wenke, J. C., Blackbourne, L. H., & Hale, R. G. (2010). Characterization of craniomaxillofacial battle injuries sustained by United States service members in the current conflicts of Iraq and Afghanistan. *Journal of Oral and Maxillofacial Surgery*, 68(1), 3-7.

Li, N., & Zheng, Y. (2013). Novel magnesium alloys developed for biomedical application: a review. *Journal of Materials Science & Technology*, 29(6), 489-502.

Li, X., Kanjwal, M. A., Lin, L., & Chronakis, I. S. (2013). Electrospun polyvinyl-alcohol nanofibers as oral fast-dissolving delivery system of caffeine and riboflavin. *Colloids and Surfaces B: Biointerfaces*, 103, 182-188.

Lindfors, L. T., Tervonen, E. A., Sándor, G. K., & Ylikontiola, L. P. (2010). Guided bone regeneration using a titanium-reinforced ePTFE membrane and particulate autogenous bone: the effect of smoking and membrane exposure. *Oral Surgery, Oral Medicine, Oral Pathology, Oral Radiology, and Endodontology*, 109(6), 825-830.

Liu, Y., Yang, Z., Tan, L., Li, H., & Zhang, Y. (2014). An animal experimental study of porous magnesium scaffold degradation and osteogenesis. *Brazilian Journal of Medical and Biological Research*, 47(8), 715-720.

Ma, S., Adayi, A., Liu, Z., Li, M., Wu, M., Xiao, L., . . . Zhang, X. (2016). Asymmetric collagen/chitosan membrane containing minocycline-loaded chitosan nanoparticles for guided bone regeneration. *Scientific reports*, 6, 31822.

Maeda, T., Kawane, T., & Horiuchi, N. (2003). Statins augment vascular endothelial growth factor expression in osteoblastic cells via inhibition of protein prenylation. *Endocrinology*, 144(2), 681-692.

Maier, J. A., Bernardini, D., Rayssiguier, Y., & Mazur, A. (2004). High concentrations of magnesium modulate vascular endothelial cell behaviour *in vitro*. *Biochimica et Biophysica Acta (BBA)-Molecular Basis of Disease*, 1689(1), 6-12.

Maksoud, M. A. (2001). Immediate implants in fresh posterior extraction sockets: report of two cases. *Journal of Oral Implantology*, 27(3), 123-126.

Mauffrey, C., Barlow, B. T., & Smith, W. (2015). Management of segmental bone defects. *JAAOS-Journal of the American Academy of Orthopaedic Surgeons*, 23(3), 143-153.

Meinig, R. P. (2010). Clinical use of resorbable polymeric membranes in the treatment of bone defects. *Orthopedic Clinics*, 41(1), 39-47.

Mi, F.-L., Tan, Y.-C., Liang, H.-C., Huang, R.-N., & Sung, H.-W. (2001). *In vitro* evaluation of a chitosan membrane cross-linked with genipin. *Journal of Biomaterials Science, Polymer Edition*, 12(8), 835-850.

Mundy, G., Garrett, R., Harris, S., Chan, J., Chen, D., Rossini, G., . . . Gutierrez, G. I. (1999). Stimulation of bone formation *in vitro* and in rodents by statins. *Science*, 286(5446), 1946-1949.

Noel, S. P., Courtney, H., Bumgardner, J. D., & Haggard, W. O. (2008). Chitosan films: a potential local drug delivery system for antibiotics. *Clinical orthopaedics and related research*, 466(6), 1377-1382.

Norowski Jr, P. A., Fujiwara, T., Clem, W. C., Adatrow, P. C., Eckstein, E. C., Haggard, W. O., & Bumgardner, J. D. (2015). Novel naturally cross-linked electrospun nanofibrous chitosan mats for guided bone regeneration membranes: Material characterization and cytocompatibility. *Journal of tissue engineering and regenerative medicine*, 9(5), 577-583.

Norowski, P., Mishra, S., Adatrow, P., Haggard, W., & Bumgardner, J. (2012). Suture pullout strength and *in vitro* fibroblast and RAW 264.7 monocyte biocompatibility of genipin cross-linked nanofibrous chitosan mats for guided tissue regeneration. *Journal of biomedical materials research Part A*, 100(11), 2890-2896.

Norowski, P. A., Babu, J., Adatrow, P. C., Garcia-Godoy, F., Haggard, W. O., & Bumgardner, J. D. (2012). Antimicrobial Activity of Minocycline-Loaded Genipin-Cross-linked Nano-Fibrous Chitosan Mats for Guided Tissue Regeneration. *Journal of Biomaterials and Nanobiotechnology*, 3(04), 528.

Nyan, M., Hao, J., Miyahara, T., Noritake, K., Rodriguez, R., & Kasugai, S. (2014). Accelerated and enhanced bone formation on novel simvastatin-loaded porous titanium oxide surfaces. *Clinical implant dentistry and related research*, 16(5), 675-683.



Nyan, M., Sato, D., Kihara, H., Machida, T., Ohya, K., & Kasugai, S. (2009). Effects of the combination with  $\alpha$ -tricalcium phosphate and simvastatin on bone regeneration. *Clinical Oral Implants Research*, 20(3), 280-287.

Ohkawa, K., Cha, D., Kim, H., Nishida, A., & Yamamoto, H. (2004). Electrospinning of chitosan. *Macromolecular rapid communications*, 25(18), 1600-1605.

Park, Y. J., Kim, K. H., Lee, J. Y., Ku, Y., Lee, S. J., Min, B. M., & Chung, C. P. (2006). Immobilization of bone morphogenetic protein-2 on a nanofibrous chitosan membrane for enhanced guided bone regeneration. *Biotechnology and applied biochemistry*, 43(1), 17-24.

Park, Y. J., Lee, Y. M., Park, S. N., Sheen, S. Y., Chung, C. P., & Lee, S. J. (2000). Platelet derived growth factor releasing chitosan sponge for periodontal bone regeneration. *Biomaterials*, 21(2), 153-159.

Park, Y. J., Nam, K. H., Ha, S. J., Pai, C. M., Chung, C. P., & Lee, S. J. (1997). Porous poly (L-lactide) membranes for guided tissue regeneration and controlled drug delivery: membrane fabrication and characterization. *Journal of Controlled Release*, 43(2-3), 151-160.

Pradeep, A., Priyanka, N., Kalra, N., Naik, S. B., Singh, S. P., & Martande, S. (2012). Clinical efficacy of subgingivally delivered 1.2-mg simvastatin in the treatment of individuals with Class II furcation defects: a randomized controlled clinical trial. *Journal of periodontology*, 83(12), 1472-1479.

Pradeep, A. R., & Thorat, M. S. (2010). Clinical effect of subgingivally delivered simvastatin in the treatment of patients with chronic periodontitis: a randomized clinical trial. *Journal of periodontology*, 81(2), 214-222.

Priya, M. V., Sivshanmugam, A., Boccaccini, A., Goudouri, O., Sun, W., Hwang, N., . . . Jayakumar, R. (2016). Injectable osteogenic and angiogenic nanocomposite hydrogels for irregular bone defects. *Biomedical Materials*, 11(3), 035017.

Priyanka, N., Abhilash, A., Saquib, S., Malgaonkar, N., Kudyar, N., Gupta, A., . . . Pradeep, A. (2017). Clinical Efficacy of Subgingivally Delivered 1.2 mg Simvastatin in the Treatment of Patients with Aggressive Periodontitis: A Randomized Controlled Clinical Trial. *International Journal of Periodontics & Restorative Dentistry*, 37(2).

Qi, Y., Zhao, T., Yan, W., Xu, K., Shi, Z., & Wang, J. (2013). Mesenchymal stem cell sheet transplantation combined with locally released simvastatin enhances bone formation in a rat tibia osteotomy model. *Cytotherapy*, 15(1), 44-56.

Sakoda, K., Yamamoto, M., Negishi, Y., Liao, J., Node, K., & Izumi, Y. (2006). Simvastatin decreases IL-6 and IL-8 production in epithelial cells. *Journal of dental research*, 85(6), 520-523.

Sangsanoh, P., & Supaphol, P. (2006). Stability improvement of electrospun chitosan nanofibrous membranes in neutral or weak basic aqueous solutions. *Biomacromolecules*, 7(10), 2710-2714.

Schiffman, J. D., & Schauer, C. L. (2007). Cross-linking chitosan nanofibers. *Biomacromolecules*, 8(2), 594-601.

Seeherman, H., Wozney, J., & Li, R. (2002). Bone morphogenetic protein delivery systems. *Spine*, 27(16S), S16-S23.

Sela, M. N., Kohavi, D., Krausz, E., Steinberg, D., & Rosen, G. (2003). Enzymatic degradation of collagen-guided tissue regeneration membranes by periodontal bacteria. *Clinical Oral Implants Research*, 14(3), 263-268.

Sencadas, V., Correia, D. M., Areias, A., Botelho, G., Fonseca, A., Neves, I., . . . Mendez, S. L. (2012). Determination of the parameters affecting electrospun chitosan fiber size distribution and morphology. *Carbohydrate Polymers*, 87(2), 1295-1301.

Sencadas, V., Correia, D. M., Ribeiro, C., Moreira, S., Botelho, G., Ribelles, J. G., & Lanceros-Méndez, S. (2012). Physical-chemical properties of cross-linked chitosan electrospun fiber mats. *Polymer Testing*, 31(8), 1062-1069.

Shin, S. Y., Park, H. N., Kim, K. H., Lee, M. H., Choi, Y. S., Park, Y. J., . . . Han, S. B. (2005). Biological evaluation of chitosan nanofiber membrane for guided bone regeneration. *Journal of periodontology*, 76(10), 1778-1784.

Staiger, M. P., Pietak, A. M., Huadmai, J., & Dias, G. (2006). Magnesium and its alloys as orthopedic biomaterials: a review. *Biomaterials*, 27(9), 1728-1734.

Stegen, S., van Gastel, N., & Carmeliet, G. (2015). Bringing new life to damaged bone: the importance of angiogenesis in bone repair and regeneration. *Bone*, 70, 19-27.

Stein, D., Lee, Y., Schmid, M. J., Killpack, B., Genrich, M. A., Narayana, N., . . . Marx, D. B. (2005). Local simvastatin effects on mandibular bone growth and inflammation. *Journal of periodontology*, 76(11), 1861-1870.

Su, H., Liu, K.-Y., Karydis, A., Abebe, D. G., Wu, C., Anderson, K. M., . . . Bumgardner, J. D. (2016). *In vitro* and *in vivo* evaluations of a novel post-electrospinning treatment to improve

the fibrous structure of chitosan membranes for guided bone regeneration. *Biomedical materials* (Bristol, England), 12(1), 015003-015003.

Subbiah, T., Bhat, G. S., Tock, R. W., Parameswaran, S., & Ramkumar, S. S. (2005). Electrospinning of nanofibers. *Journal of applied polymer science*, 96(2), 557-569.

Taba Jr, M., Jin, Q., Sugai, J., & Giannobile, W. (2005). Current concepts in periodontal bioengineering. *Orthodontics & craniofacial research*, 8(4), 292-302.

Taguchi, Y., Amizuka, N., Nakadate, M., Ohnishi, H., Fujii, N., Oda, K., . . . Maeda, T. (2005). A histological evaluation for guided bone regeneration induced by a collagenous membrane. *Biomaterials*, 26(31), 6158-6166.

Takenaka, M., Hirade, K., Tanabe, K., Akamatsu, S., Dohi, S., Matsuno, H., & Kozawa, O. (2003). Simvastatin stimulates VEGF release via p44/p42 MAP kinase in vascular smooth muscle cells. *Biochemical and biophysical research communications*, 301(1), 198-203.

Tal, H., Kozlovsky, A., Artzi, Z., Nemcovsky, C. E., & Moses, O. (2008). Long-term biodegradation of cross-linked and non-cross-linked collagen barriers in human guided bone regeneration. *Clinical Oral Implants Research*, 19(3), 295-302.

Tempro, P. J., & Nalbandian, J. (1993). Colonization of retrieved polytetrafluoroethylene membranes: morphological and microbiological observations. *Journal of periodontology*, 64(3), 162-168.

Thacharodi, D., & Rao, K. P. (1996). Collagen-chitosan composite membranes controlled transdermal delivery of nifedipine and propranolol hydrochloride. *International journal of pharmaceutics*, 134(1-2), 239-241.

- Thaller, S., & McDonald, W. S. (2004). Facial trauma: CRC Press.
- Tsai, W.-B., Chen, Y.-R., Li, W.-T., Lai, J.-Y., & Liu, H.-L. (2012). RGD-conjugated UV-cross-linked chitosan scaffolds inoculated with mesenchymal stem cells for bone tissue engineering. *Carbohydrate Polymers*, 89(2), 379-387.
- Turri, A., Elgali, I., Vazirisani, F., Johansson, A., Emanuelsson, L., Dahlin, C., . . . Omar, O. (2016). Guided bone regeneration is promoted by the molecular events in the membrane compartment. *Biomaterials*, 84, 167-183.
- Wang, J. J., Zeng, Z. W., Xiao, R. Z., Xie, T., Zhou, G. L., Zhan, X. R., & Wang, S. L. (2011). Recent advances of chitosan nanoparticles as drug carriers. *International journal of nanomedicine*, 6, 765.
- Wang, P. S., Solomon, D. H., Mogun, H., & Avorn, J. (2000). HMG-CoA reductase inhibitors and the risk of hip fractures in elderly patients. *Jama*, 283(24), 3211-3216.
- Wong, R., & Rabie, A. (2003). Statin collagen grafts used to repair defects in the parietal bone of rabbits. *British Journal of Oral and Maxillofacial Surgery*, 41(4), 244-248.
- Wu, C., Su, H., Karydis, A., Anderson, K. M., Ghadri, N., Tang, S., . . . Bumgardner, J. D. (2017). Mechanically stable surface-hydrophobilized chitosan nanofibrous barrier membranes for guided bone regeneration. *Biomedical Materials*, 13(1), 015004.
- Wu, C., Su, H., Tang, S., & Bumgardner, J. D. (2014). The stabilization of electrospun chitosan nanofibers by reversible acylation. *Cellulose*, 21(4), 2549-2556.

Xu, C., Lei, C., Meng, L., Wang, C., & Song, Y. (2012). Chitosan as a barrier membrane material in periodontal tissue regeneration. *Journal of Biomedical Materials Research Part B: Applied Biomaterials*, 100(5), 1435-1443.

Xue, Y., Wu, M., Liu, Z., Song, J., Luo, S., Li, H., . . . Lin, M. (2019). *In vitro* and *in vivo* evaluation of chitosan scaffolds combined with simvastatin-loaded nanoparticles for guided bone regeneration. *Journal of Materials Science: Materials in Medicine*, 30(4), 47.

Yamashita, M., Otsuka, F., Mukai, T., Otani, H., Inagaki, K., Miyoshi, T., . . . Makino, H. (2008). Simvastatin antagonizes tumor necrosis factor- $\alpha$  inhibition of bone morphogenetic proteins-2-induced osteoblast differentiation by regulating Smad signaling and Ras/Rho-mitogen-activated protein kinase pathway. *Journal of Endocrinology*, 196(3), 601-613.

Yang, E., Qin, X., & Wang, S. (2008). Electrospun cross-linked polyvinyl alcohol membrane. *Materials Letters*, 62(20), 3555-3557.

Yegappan, R., Selvaprithiviraj, V., Amirthalingam, S., Mohandas, A., Hwang, N. S., & Jayakumar, R. (2019). Injectable angiogenic and osteogenic carrageenan nanocomposite hydrogel for bone tissue engineering. *International journal of biological macromolecules*, 122, 320-328.

Yeo, Y. J., Jeon, D. W., Kim, C. S., Choi, S. H., Cho, K. S., Lee, Y. K., & Kim, C. K. (2005). Effects of chitosan nonwoven membrane on periodontal healing of surgically created one-wall intrabony defects in beagle dogs. *Journal of Biomedical Materials Research Part B: Applied Biomaterials: An Official Journal of The Society for Biomaterials, The Japanese Society for Biomaterials, and The Australian Society for Biomaterials and the Korean Society for Biomaterials*, 72(1), 86-93.

Zachar, M. R., Labella, C., Kittle, C. P., Baer, P. B., Hale, R. G., & Chan, R. K. (2013). Characterization of mandibular fractures incurred from battle injuries in Iraq and Afghanistan from 2001-2010. *Journal of Oral and Maxillofacial Surgery*, 71(4), 734-742.

Zhang, Q. G., Hu, W. W., Zhu, A. M., & Liu, Q. L. (2013). UV-cross-linked chitosan/polyvinylpyrrolidone blended membranes for pervaporation. *Rsc Advances*, 3(6), 1855-1861.

Zhao, B. j., & Liu, Y. h. (2014). Simvastatin induces the osteogenic differentiation of human periodontal ligament stem cells. *Fundamental & clinical pharmacology*, 28(5), 583-592.

Zhao, N., & Zhu, D. (2015). Endothelial responses of magnesium and other alloying elements in magnesium-based stent materials. *Metallomics*, 7(1), 118-128.

Zhao, S., Pinholt, E. M., Madsen, J. E., & Donath, K. (2000). Histological evaluation of different biodegradable and non-biodegradable membranes implanted subcutaneously in rats. *Journal of Cranio-Maxillofacial Surgery*, 28(2), 116-122.

Zwahlen, R. A., Cheung, L. K., Zheng, L. W., Chow, R. L., Li, T., Schuknecht, B., . . . Weber, F. E. (2009). Comparison of two resorbable membrane systems in bone regeneration after removal of wisdom teeth: a randomized-controlled clinical pilot study. *Clinical Oral Implants Research*, 20(10), 1084-1091.

## APPENDIX 1

### *Computation of Hansen solubility and Flory-Huggins parameter ( $\chi_{1,2}$ ) of SMV with chitosan and differently modified chitosan*

The solubility parameter ( $\delta_T$ ), first suggested by Hildebrand, is defined as square-root of the cohesive energy density (1), where the cohesive energy  $E_{coh} = \Delta H_{vap} - RT$ ,  $V_m$  is the molar volume of the substance, and  $\Delta H_{vap}$  is the heat of vaporization. Hildebrand predicted that non-polar substances with similar solubility parameters,  $\Delta\delta_T = |\delta_{T2} - \delta_{T1}| \approx 0$ , are generally more miscible with each other. Hansen proposed splitting the solubility parameter into three components to improve miscibility predictions for a wider range of substances. These three parameters, referred to as Hansen solubility parameters (HSPs), account for dispersion forces ( $\delta_D$ ), dipolar intermolecular forces ( $\delta_P$ ) and hydrogen bonding ( $\delta_H$ ) [45]. The sum of these squared parameters is the squared total solubility parameter  $\delta_T$  (2).

$$\delta_T^2 = \sqrt{\frac{E_{coh}}{V_m}} \quad (1)$$

$$\delta_T^2 = \delta_D^2 + \delta_P^2 + \delta_H^2 \quad (2)$$

The solubility parameters for any two chemical species (i.e., drug and polymer) can be used to calculate the Flory-Huggins interaction parameter ( $\chi_{1,2}$ ) according to Equation 3, where  $V_{m,1}$  is the molar volume of the drug,  $R$  is the ideal gas constant and  $T$  is the absolute temperature [45]. The subscripts 1 and 2 represent the drug and polymer, respectively. It is interpreted that the drug is more compatible with a polymer for lower values of  $\chi_{1,2}$ . The interaction parameter  $\chi_{1,2}$  decreases as the difference between two solubility parameters  $\Delta\delta_T$  decreases. Therefore, lower values of  $\Delta\delta_T$  make the drug more compatible with the polymer.



$$\chi_{1,2} = \frac{V_{m,1}}{RT}(\delta_{T2} - \delta_{T1})^2 = \frac{V_{m,1}}{RT}\Delta\delta_T^2 \quad (3)$$

However, chitosan is far from non-polar and  $\Delta\delta_T^2$  is not the best descriptor for drug-polymer incompatibility. Hansen proposed using  $A_{1,2}$  (4) in place of  $\Delta\delta_T^2$ , which was generally found to provide more accurate predictions of  $\chi_{1,2}$  for a wider range of systems [45]. The value  $A_{1,2}$  is the sum of squared differences of each parameter with weights of  $\frac{1}{4}$  applied on the polar and hydrogen bond parameters. By using  $A_{1,2}$  in place of  $\Delta\delta_T^2$ , Equation 3 can be rewritten as Equation 5. Therefore, the Flory-Interaction parameter between SMV and polymer are calculated using Equation 7 [45].

$$A_{1,2} = (\delta_{D2} - \delta_{D1})^2 + \frac{1}{4}(\delta_{P2} - \delta_{P1})^2 + \frac{1}{4}(\delta_{H2} - \delta_{H1})^2 \quad (4)$$

$$\chi_{1,2} = \frac{V_{m,1}}{RT}A_{1,2} \quad (5)$$

The Hansen Solubility Parameters (HSPs) were calculated using Hansen Solubility Parameters in Practice (HSPiP) software version 5.1.08. The SMILES (Simplified Molecular Input Line Entry Syntax) representations of each compound are used as inputs. For the monomeric units of chitosan, the polymer format for SMILES was used. The software predicts the HSPs parameters using group contribution method based on Yamamoto-molecular break method (Y-MB) that splits the input structure to functional groups. Furthermore, the HSPs for chitosan, AA-chitosan, BA-chitosan, HA-chitosan and tBOC-chitosan were estimated by taking weighted root-mean-squares of the HSPs for N-acetylglucosamine (D, NAc) and glucosamine (D, Glu) monomeric units (Equations 6a,b,c,d) with their respective modifications. The weights are 0.3 for N-acetylglucosamine and 0.7 for glucosamine monomeric units since chitosan with ~70% DDA is

used in this work. The weighted averages were taken this way to ensure that the squared sum of the HSPs always equals the squared total solubility parameter as shown in Equation 6d.

$$\delta_{D2} = (0.3 \cdot \delta_{D, \text{NAC}}^2 + 0.7 \cdot \delta_{D, \text{Glu}}^2)^{1/2} \quad (6a)$$

$$\delta_{P2} = (0.3 \cdot \delta_{P, \text{NAC}}^2 + 0.7 \cdot \delta_{P, \text{Glu}}^2)^{1/2} \quad (6b)$$

$$\delta_{H2} = (0.3 \cdot \delta_{H, \text{NAC}}^2 + 0.7 \cdot \delta_{H, \text{Glu}}^2)^{1/2} \quad (6c)$$

$$\delta_{T2}^2 = \delta_{D2}^2 + \delta_{P2}^2 + \delta_{H2}^2 = 0.3 \cdot \delta_{T, \text{NAC}}^2 + 0.7 \cdot \delta_{T, \text{Glu}}^2 \quad (6d)$$

## APPENDIX 2

The fiber diameters of modified membranes did not change significantly when loaded with ethanol containing SMV. Figure A2 shows representative images of HA and AA membranes loaded with 10 $\mu$ l of ethanol containing 50 $\mu$ g of SMV. The AA membranes showed some fiber swelling which could be because of its less hydrophobic character.

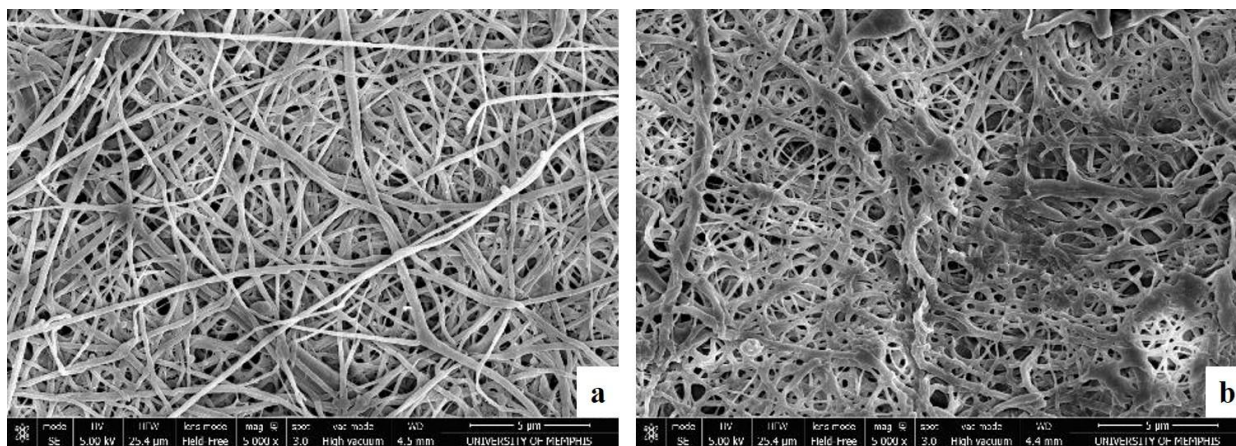


**Figure A2:** SEM images of HA (a) and AA (b) membranes loaded with 50 $\mu$ g SMV.



## IACUC PROTOCOL ACTION FORM

<b>To:</b>	Joel Bumgardner
<b>From</b>	Institutional Animal Care and Use Committee
<b>Subject</b>	Animal Research Protocol
<b>Date</b>	November 1, 2016

**The institutional Animal Care and Use Committee (IACUC) has taken the following action concerning your Animal Research Protocol No. 0791** In vivo evaluations of guided bone regeneration membranes and bone graft materials

Your protocol is approved for the following period:

From:  To:

Your protocol is not approved for the following reasons (see attached memo).


Your protocol is renewed without changes for the following period:

From:  To:


Your protocol is renewed with the changes described in your IACUC Animal Research Protocol Update/Amendment Memorandum dated  for the following period:

From:  To:

Your protocol is not renewed and the animals have been properly disposed of as described in your IACUC Animal Research Protocol Update/Amendment Memorandum dated

  
\_\_\_\_\_

Amy L. de Jongh Curry, PhD, Chair of the IACUC

  
\_\_\_\_\_

Dr. Karyl Buddington, University Veterinarian and Director of the Animal Care Facilities